C O N T E N T S

Production and Characterization of N-Halamine Based Polyvinyl Chloride (PVC) Nanowebs

Batuhan ÇOBANOĞLU[1,2] 🆔 0000-0002-5508-1739
Fatma Nur PARIN[1*] 🆔 0000-0003-2048-2951
Kenan YILDIRIM[1*] 🆔 0000-0002-1591-1988

[1]Bursa Technical University / Department of Polymer Materials Engineering / Yildirim, Bursa, Turkey
[2]RB Karesi Textile, Yildirim, Bursa, Turkey

Corresponding Author: Fatma Nur Parın, nur.parin@btu.edu.tr

ABSTRACT

Antibacterial agent N-halamine, 7,7,9,9-tetramethyl-1,3,8-triazaspiro [4.5]-decane-2,4-dione (TTDD), was synthesized, and it was added into the polyvinyl chloride (PVC) nanoweb. A versatile, and relatively simple method, electrospinning, was used to fabricate continuous and uniform nanowebs. 7,7,9,9-tetramethyl-1,3,8-triazaspiro [4.5]-decane-2,4-dione (TTDD) is a cyclic N-halamine that can be chlorinated easily due to three functional groups (imide, amide, and amine). Therefore, TTDD was preferred for PVC regarding having high stability, non-toxic, non-irritant for skin, and renewable. The rechargeable chlorination process was applied to webs using dilute hypochlorite solution. The antibacterial activity of the webs were evaluated using the ASTM 2149 procedure. FTIR, TGA, and SEM were used to investigate the morphology, thermal characteristics, and chemical structures of PVC webs. Scanning electron microscopy (SEM) displayed that the average diameter of the fibers increased with TTDD concentration. The thermal properties of the PVC webs did not changed significantly. All chlorinated webs indicated highly effective antibacterial activities against both *Staphylococcus aureus* and *Escherichia coli* with increased inactivation. Furthermore, the antibacterial efficacy of nanowebs is reformed again by the rechargeable process. The rechargeable chlorination capacity of obtained PVC non-wovens is over > 60% (within 6 hours, in pH 5), for four rechargeable chlorine cycles. The new antibacterial PVC nanowebs have the potential for especially useful in medical applications.

1. INTRODUCTION

Microbes are the smallest microorganisms that are a part of daily life and can be found all over the environment and in our bodies [1]. The spread of microorganisms such as bacteria, fungus, algae, and viruses is becoming an increasingly serious problem for healthcare organizations [1, 2]. They are infectious and can cause nosocomial infections in the community if humidity and temperature are optimum [1, 3-5]. Nosocomial infections are usually dangerous to people, and they can be present in everyday products, particularly hospital equipment [6]. Furthermore,

washing and disinfection may not be enough to prevent infections, as resistant strains have emerged in recent decades. Antimicrobial agents are being employed in various medical equipment and hospital workers to overcome pathogen-caused hygiene deficiencies [7-10].

In compared to other agents, N-halamines have showed excellent antibacterial activity against Gram-positive and Gram-negative bacteria, fungi, protozoa, and viruses [10-12]. N-halamines can be utilized as biocides due to their long-lasting and rechargeable antibacterial characteristics.

To cite this article: *Çobanoğlu B, Parın FN, Yıldırım K. 2021. Production and characterization of n-halamine based polyvinyl chloride (PVC) nanowebs. Tekstil ve Konfeksiyon, 31(3), 147-155.*

N-halamine structures have one or more nitrogen-halogen covalent bonds and possess unique properties such as high stability over a wide temperature and humidity range, long-term usage, and the ability to be repeatedly regenerated in a chlorine solution [10, 13-19]. As a result, N-halamines could be used in water purification systems, food packaging, coatings, medical devices, the textile industry, hospitals, hygienic products, dental office equipment, and household sanitation.

Electrospinning is regarding a versatile method for fabricating fibrous structures with diameters from micrometers to nanometers [20-24]. Because of the unique properties of electrospun webs like a high specific surface area, high porosity, and low diameter, they need potential use in sterilization applications with fast response behavior [25].

To fabricate protective medical garments, textiles in the form of fibrous structures- non-wovens with antibacterial agents have been widely used for over 20 years [26]. There are several strategies to antibacterial agents such as essential oils, boric acid, chitosan, triclosan, quaternary ammonium salts, and N-halamines addition to non-wovens [21, 27-30]. In this regard, Parın et al. synthesized gelatin nanofibers containing essential orange oil (EOO) and reported antibacterial efficacy against S. aureus bacteria due to the D-limonene component found in orange oil [28]. Chen et al. synthesized and functionalized poly-hexamethylene guanidine (PHMG) using chitosan nanofibers. The resulting nanofibers exhibit a better antibacterial impact against S. aureus and P. aeruginosa bacteria [31]. In another study, Ullah et al. produced fibrous structures by adding silver sulfadiazine (AgSD) to polyacrylonitrile (PAN) [32]. The structures indicated good antibacterial activity against both Escherichia coli and Bacillus. Moreover, Zhang et al. prepared polyurethane/ triclosan coated polylactic acid nonwovens, which were reported to have high antibacterial activity against Staphylococcus aureus and Escherichia coli in a zone test [30]. Zhang et al. reported electrospun PVA fibers modified with quaternary ammonium salt and zwitterionic sulfopropylbetaine showed 99.9% antibacterial efficiency against both gram-positive and gram-negative bacteria [33]. Lv et al. developed antibacterial mats based on AgNPs-loaded starch/PEO nanofibers for medical care. The obtained NFs indicated limited antibacterial activity [34]. So far, studies have revealed that antibacterial agents other than N-halamine compounds have a considerable decrease in bactericidal activity, which is one of the technology's major drawbacks [35].

N-halamine modified electrospun poly(vinyl alcohol) (PVA) membranes for food packaging applications were investigated by Liu et al. The antibacterial activity of the resulting surfaces has been found to be 99.99 percent [36]. In a similar study reported by Tian et al. that PS/PU modified with 5, 5-dimethyl hydantoin which is a N-halamine compound and their study showed high antibacterial efficiency (99.77%) against both E. coli and S. aureus [37]. Ma et al. also developed rechargeable N-halamine based nanofibrous sulfonated-polyethyleneimine (PEI-S) surfaces that exhibited almost 100 % biocidal activity and high disinfection efficiency with 99.9% [38]. 7,7,9,9-tetramethyl-1,3,8-triazaspiro [4.5]-decane-2,4-dione (TTDD) is a cyclic N-halamine. Song mentioned in his PhD thesis that cyclic N-halamines are very efficient, which can last relatively long. Besides, N-halamines with imide functionality exhibit higher biocidal activity than those with amines (imide > amide > amine) [39]. TTDD structure includes these three functional groups. Due to TTDD properties of rechargeable bactericidal action, rapid inactivation rate, and environmental safety, and high durability, TTDD which is synthesized by the halogenation of nitrogen–hydrogen (N–H) bonds-containing precursors, has a lot of potential in the medical field as an antibacterial material [40].

PVC is one of the leading polymers which are commercially important thermoplastic [41]. PVC-based materials have competed with metals, ceramics, glass, and other polymeric materials due to high mechanical strength, excellent physical and chemical durability, low-cost properties [42]. Various studies have been performed on PVC including various antibacterial agents such as zinc oxide (ZnO) [43,44], silver [45], silver zeolite (SZ) [46], and modified silver nanoparticles [46], titanium dioxide (TiO$_2$) [47]. These agents were introduced to the polymer by various methods of production. Lala et al. fabricated electrospun PVC/AgNO$_3$ fibers [49]. Zampino et al. investigated PVC-silver zeolite composite to produce antibacterial biomedical products [46]. In this study, PVC was incorporated with silver zeolite in various ratios between 2 and 20 wt %. Antibacterial tests were performed at 6 h, 24 h, and 7, 14, and 30 days. The test results indicated that PVC with 20 wt % of silver zeolite had a maximum antibacterial effect. According to the zone inhibition test, the fibers showed antibacterial protection against E.coli bacteria. Moreover, there has just one study about N-halamine containing PVC material via an extrusion and injection molding process in literature. Chylinska et al. produced PVC composites with N-chlorinated poly(3-(4'-vinyl benzyl)-7,8-benzo-1,3-diazaspiro[4.5] decane-2,4-dione) (MPS TET-Cl) [50]. The antibacterial test results showed strong antibacterial activity against S. aureus and E. coli.

Previous studies have mostly focused on PVC fibers with various antibacterial agents. However, the antibacterial agents-loaded PVC fibers have demonstrated limited antibacterial effectiveness since these antibacterial agents have no rechargable effect. In addition, TTDD has been chosen as an antibacterial agent owing to functional groups in cyclic TTDD. TTDD includes imide, amide, and amine

functionalities. When all of the above compounds were chlorinated, N-halamine compounds were formed, which worked as good biocides. [51]. To the best our knowledge, there is no study on PVC non-woven surfaces with rechargeable antibacterial properties by using electrospinning method. In the current study, we tried for the first time to introduce of TTDD into PVC nanowebs as an antibacterial compound and investigate antibacterial effect of this compound. By varying TTDD concentration, the properties of PVC nanowebs were investigated in terms of microstructure, thermal, and chemical properties. Furthermore, rechargeable chlorination capability was observed and antibacterial efficiencies were evaluated against *S. aureus* and *E. coli* bacteria.

2. MATERIAL AND METHOD

2.1 Material

The polyvinyl chloride powder (PVC, Mw=43,000 g/mol), N, N-Dimethylformamide (DMF) and potassium iodide (KI), Hydrochloric acid (HCl) with 36.5-38% purity, tetrahydrofuran (THF), sodiumthiosulfate pentahydrate (Na$_2$S$_2$O$_3$.5 H$_2$O), ethanol (99.5% purity), Triton X-100 (laboratory grade) were used. All chemicals were purchased from Sigma-Aldrich Chemical Company. ACE® brand NaOCl (P&G, Belgium) household bleach was used for chlorination. All the reagents were used without purification. Antibacterial testing was performed by Muller-Hinton II agar culture media.

2.2 Synthesis of TTDD

The TTDD was prepared according to a general procedure carried out previously [21]. TTDD was synthesized by reacting 2,2,4,4-tetramethyl-4-piperidone, potassium cyanide, and ammonium carbonate in a mole ratio of 1 : 2 : 6 in 100 mL of water/ethanol (1: 1 v/v) solution for 48 hours at room temperature. Then the reaction mixture was

filtered and TTDD was produced. Afterwards, TTDD was washed with hot water, and dried TTDD was vacuumed for 24 hours in ambient conditions. TTDD synthesis is shown in Figure 1.
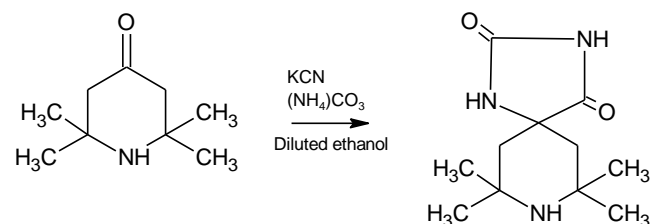
Figure 1. Synthesis of 7,7,9,9-tetramethyl-1,3,8-triazaspiro [4.5]-decane-2,4-dione (TTDD) [21].

2.3. Preparation of Antibacterial Nanowebs

The polymer solutions were electrospun using a laboratory machine called an electrospinning device (INOVENSO Nanospinner 24, Turkey). PVC was dissolved in DMF and THF binary-solvent systems (67.5:17.5, v/v) solution to obtain a 15% (w/v) PVC solution for the electrospinning process. The PVC solutions were put in a magnetic stirrer at room temperature till a homogeneous solution was obtained. Subsequently, different concentrations (1, 3 and 5 wt%) of TTDD were added to the PVC solutions concerning the total polymer solutions. After TTDD had dissolved in PVC solution, the mixture was transferred into a plastic syringe (20 mL) and attached to a stainless steel nozzle.

The electrical power supply to the nozzle of the syringe was 25 kV with a 1 mL/h flow rate (Figure 2). The distance between a collector and a needle was 15 cm. During electrospinning, the PVC nanowebs were collected on a rotating drum at 100 rpm. In the course of electrospinning, the solvent was evaporated and only nanowebs attached to the aluminum foil forming nanoweb membranes remained. Pure PVC nanowebs were prepared as a control.
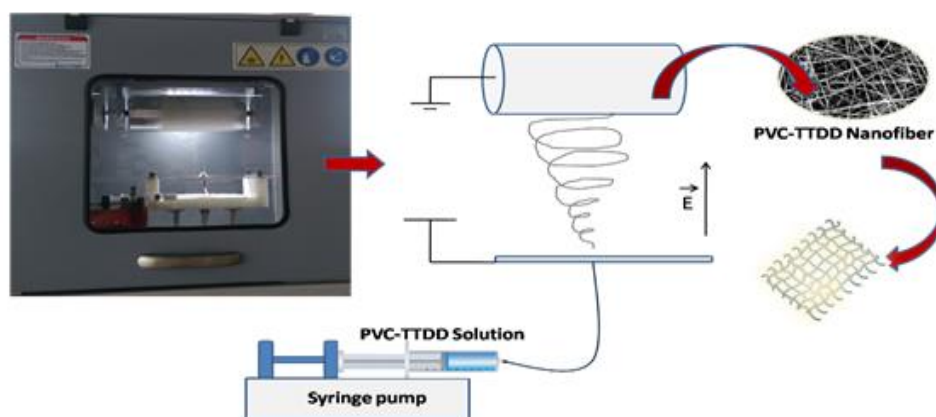
Figure 2. Schematic illustration of the electrospinning process.

2.4 Chlorination and Analytic Titration of the Nanowebs

Many prior studies on the effects of titration and chlorination have been reported [8,10,21,49]. The PVC nanowebs containing 1, 3, 5 % TTDD were chlorinated in pH 7 and pH 5 for 1, 6, and 12 h by soaking, the samples in 10, 20, and 40 % commercial aqueous sodium hypochlorite solution (NaOCl) at room temperature without stirring. Afterward, 0.15 g of the non-ionic surfactant Triton-X was added to each solution. The chlorinated nanowebs were robustly washed with distilled water, then dried in an oven at 50°C for an hour. The amount of chlorine loaded in the structure was calculated by the iodometric/thiosulfate method [52,53] according to the following formula.

$$CI^+ \% = \left(\frac{35,45 \times N \times V}{W \times 2}\right) \times 10 \tag{1}$$

In this equation, N is the normality of thiosulfate solution, V is the volume of the consumed thiosulfate solution, and W is the weight of the sample titrated. Figure 3 shows the chlorination process of the TTDD.

Figure 3. Chlorination process of the TTDD [8,21].

2.5 Rechargeable Chlorination Process
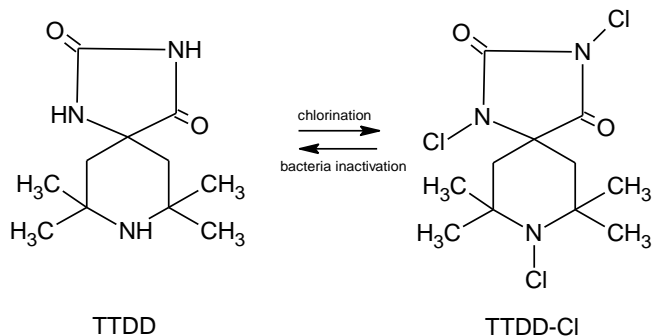
All nanowebs containing 1%, 3% and 5% TTDD was chlorinated again in 30% sodium hypochlorite solution for pH 5 for 6 h. Then, 0.15 g of non-ionic surfactant, Triton-X, was dripped into the solutions.

Afterward, the chlorinated PVC samples was washed with distilled water and dried at 50°C for 1 h to remove free chlorine from the surface of all PVC nanowebs [54].

2.6 Antibacterial Efficacy Test

The antibacterial efficacy of electrospun nanowebs was studied using ASTM 2149 method. The test method was performed with *S. aureus* (ATCC 6538) and *E. coli* (ATCC 35218). Both pure nanoweb (PVC0) and chlorinated nanoweb samples (PVC1, PVC3, and PVC5) were challenged with approximately 10 mL of known concentration of bacteria suspension. The logcfu values of the bacteria on the control samples were *9.67 for S. aureus* and 5.76 for *E. coli*. The nanowebs were divided into three pieces and then put into a sterilized glass jar. The samples were challenged to the bacteria for two different contact times (3 h and 24 h) without rinsing. After, serial dilutions were prepared with phosphate buffer solution (PBS) and placed into Muller-Hilton II agar culture media. The plates were put in an incubator at 37°C for 24 h. The bacteria colonies were counted and the logarithmic bacterial reduction was determined.

2.7 Characterization of Nanowebs

Thermogravimetric analyses of nanowebs were performed by TA Instrument DSC-Q2000 and Perkin Elmer STA 6000 TGA under 20 mL/min nitrogen flow with a heating rate of 20°C/min in room temperature to 600°C temperature range and under 20 mL oxygen flow in 600-900°C. FTIR data were obtained with a Thermo Nicolet iS50 FTIR spectrometer with a Pike ATR (Attenuated Total Reflectance) adapter, in the range of 4000-400 cm^{-1} recorded with 16 scans at 4 cm^{-1} resolution.Hitachi TM3030 plus187 Scanning Electron Microscope (SEM) (Hitachi Ltd., Tokyo, Japan) was used to characterize the surface morphology and composition of nanowebs with an accelerating voltage of 10 kV. The average fiber diameters were measured by using Image J, version 1.520 software.

3. RESULT AND DISCUSSION

3.1 Morphology of Nanofibers

The diameter of fibrous structures was measured using Image J (version 1.520 software) by randomly selecting the diameters of 100 individual fibers for each sample. According to the analysis results, the fiber diameters changed depending on the TTDD concentration. Increased TTDD concentration caused an increase in fiber diameter. As seen in SEM images, the fiber diameters are nonhomogenous [Figure 5 (A1-D1)]. Irıbarren et al. prepared relatively uniform PVC-ZnO composite fibers and they measured the average fiber diameters of obtained fibers as 720 nm. [55]. Lala et al. fabricated PVC with 5 wt% of AgNO$_3$ nanofiber. The fiber showed straighter and good fiber morphology with 509 nm [49]. The fiber diameters of electrospun PVC0, PVC1, PVC3, and PVC5 samples were measured to be 126.8 ± 42.6 nm, 157.2 ± 63 nm, 161.2 ± 65, and 169.7 ± 53 nm, respectively, and the distribution curve as shown in Figure 5 (A2-D2). Moreover, all PVC electrospun webs containing TTDD (PVC1, PVC3, and PVC5) exhibits a web of randomly oriented fiber with a broad distribution from 35 to 411 nm. PVC1 and PVC3 webs showed a bead-like web structure. Figure 5D1 indicated 3D network structure in PVC5 began to form. In a similar study, Akgül and Aykut (2019) observed PVC/Zn(NO$_3$)$_2$ nanofibers with these structures [56].

3.2 FT-IR Analysis

The FTIR analysis of the electrospun pure PVC web (PVC0), TTDD, and TTDD-loaded PVC webs is given in

Figure 4. The pure PVC webs showed their characteristic bands. The PVC0 webs exhibited peaks at 2911 cm^{-1} (-CH bond stretching), 1333 cm^{-1} (-CH$_2$ groups deformation), 1254 cm^{-1} (CH-rocking), 959 cm^{-1} (-CH wagging) which were in accordance with the literature [42,51,54,55]. Furthermore, the characteristic peaks of TTDD bands at 3400 cm^{-1} was related to -NH stretching, at 2853 cm^{-1} was due to -CH$_3$ stretching, at 1781 cm^{-1} and 1733 cm^{-1} was attributed to imide group, and also 1720 cm^{-1} was attributed to ester (-C=O) peak, at 1467 cm^{-1} was related to -CH$_3$ bending vibrations, as well [57]. The FTIR spectrum showed characteristic peaks of PVC nanoweb at 681 cm^{-1} and 604 cm^{-1} due to the C-Cl stretching mode [58,59]. The characteristic bands of both PVC0 and TTDD loaded webs were all maintained in the resulting webs. However, decreased peak intensity were detected on the spectra of TTDD loaded webs.
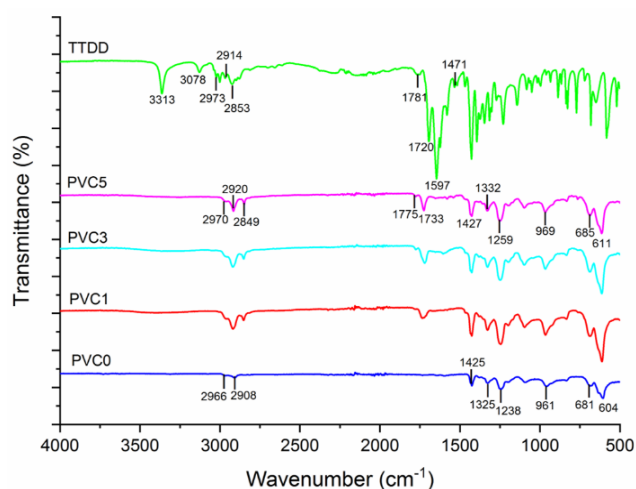
Figure 4. FTIR spectrum of PVC0, PVC1, PVC3, PVC5 nanowebs and TTDD.

3.3 Thermal Analysis

TGA thermograms of pure PVC nanowebs and TTDD-loaded PVC nanowebs in nitrogen at a rate of 20°C/min are shown in Figure 6. Moreover, all of the webs are thermally stable in nitrogen gas below 200°C and mainly displayed three-stage thermal degradation above this temperature, as well [60]. The initial stage of degradation (between 210 and 360°C) was rapid and overlapped with PVC dechlorination [61], with the formation and stoichiometric elimination of HCl and a few chlorinated hydrocarbons. The formation of aromatic compounds via cyclization of conjugated polyene [49] occurred primarily in the second stage (between 360 and 470°C). In the last stage, the degradation of PVC increased to 471°C, and the degradation was completed at 700°C, due to the degradation of complex structures induced by aromatization and pyrolysis of PVC [63,64]. The degradation starting temperature of TTDD loaded nanowebs with decreased as the concentration of TTDD increased. When N-halamine was added to the polymer, the degradation behavior of PVC changed, indeed.
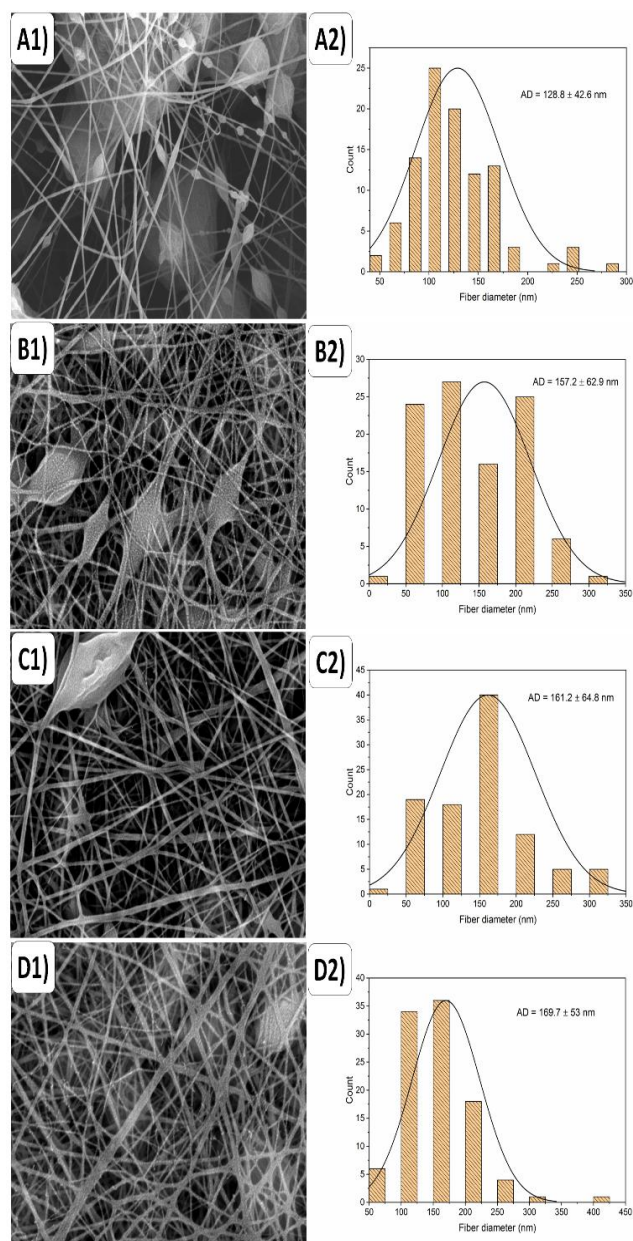
Figure 5. SEM images and fiber diameter distributions of PVC0 (A1&A2), PVC1 (B1&B2), PVC3 (C1&C2), PVC5 (D1&D2
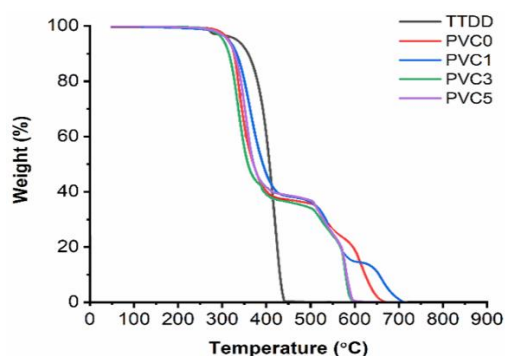
Figure 6. TGA thermograms of PVC nanowebs and TTDD.

3.4 Chlorine Loading and Rechargable Chlorination Process

The amount of chlorine uptake of all chlorinated nanowebs (PVC1, PVC3, and PVC5) increased in pH 5 due to increased NaOCl concentration. In this regard, PVC5 nanoweb samples can be chlorinated up to chlorine loading 1.54, 1.13, and 0.73 % Cl+ for 40% NaOCl solution at 1 h, 6 h, and 12 h, respectively (Table 1). All nanowebs exhibited increased chlorine uptake for the first 6 h. However, chlorine uptake reached saturation nanowebs, except PVC3. Table 2 summarized the chlorine loadings progressively increased with increasing time in pH 7. Furthermore, a high concentration of chlorine reduces interaction with bacteria, causing slower inactivation [37,63,64]. Table 2 summarized the chlorine loadings progressively increased with time in pH 7. The PVC5 nanoweb sample exhibits the highest Cl+ (1.09 percent) uptake value.

Due to amine, amide, and imide functionalities of TTDD, they were analyzed to check if they could recharge antimicrobial TTDD after interaction with NaOCl. Furthermore, even after three recharging cycles, the Cl+ concentration of PVC1 webs remained constant, whereas other TTDD-loaded PVC nanowebs showed high efficiency factors (PVC3 and PVC5). Because the active chlorine concentration of TTDD is critical for its antibacterial activities, the effects of chlorination time and pH on PVC chlorination capability were evaluated. The rechargeable chlorination process is dependent on rising N-halamine concentration, which causes an increase in rechlorination efficiency. It reduced as the procedure time increased. (See Table 3).

Table 1. Chlorination results of PVC nanowebs with N-halamine in pH 5.

Sample ID	NaOCl Concentration			Time
	10%	20%	40%	
PVC1	0.11	0.33	0.71	1h
	0.14	0.29	0.55	6h
	0.10	0.22	0.23	12h
PVC3	0.08	0.34	0.52	1h
	0.13	0.27	0.55	6h
	0.05	0.2	0.58	12h
PVC5	0.17	0.32	1.54	1h
	0.19	0.88	1.13	6h
	0.40	0.60	0.73	12h

Table 2. Chlorination results of PVC nanowebs with N-halamine in pH 7.

Sample ID	NaOCl Concentration			Time
	10%	20%	40%	
PVC1	0.07	0.24	0.42	1h
	0.13	0.26	0.47	6h
	0.21	0.27	0.54	12h
PVC3	0.13	0.34	0.64	1h
	0.19	0.38	0.83	6h
	0.26	0.47	0.87	12h
PVC5	0.26	0.61	0.82	1h
	0.23	0.48	0.98	6h
	0.25	0.47	1.09	12h

Table 3. Rechargable chlorinatonresults of PVC nanowebs with N-halamine for 6 h in pH 5.

Sample ID	Rechargable Chlorination Efficiency (%)			
	1st	2nd	3rd	4th
PVC1	0.11	0.11	0.11	0.07
PVC3	0.55	0.42	0.36	0.33
PVC5	0.95	0.90	0.83	0.75

3.5 Antibacterial Efficacy Testing

A novel antibacterial nanoweb production was aimed in this study. According to chlorination results, they were tested both S. aureus and E. coli with ASTM 2149 standard. As a result, the chlorine uptake of nanowebs in pH 5 was more than in pH 7, and as the amount of chlorine uptake increased, the antibacterial property also increased. The initial bacterial population of PVC0 9.65 and6.04 for S. aureus and E. coli bacteria, respectively, as well as the logcfu values of the control samples, are shown in Table 4. PVC0 nanoweb showed no essential antibacterial activity within 3 and 24 h, respectively. On the other hand, PVC nanowebs with TTDD compound showed complete inactivation of both S. aureus and E. coli bacteria, confirming that the nanowebs had increased antibacterial activities due to the addition of TTDD compound chlorinated nanowebs. PVC1 was challenged with *S. aureus* and *E. coli* while TTDD 88.24% and 71.76% of inactivated bacteria during the tests within the contact time of 24 h. Both PVC3 and PVC5 provided inactivation of 100% within 24 h when challenged with both *S. aureus* and *E. coli* and also the results are summarized in Table 4. The produced nanofibers have unrivaled antibacterial functionalities compared to various kinds of antimicrobial agents containing nanofibers [9].

Table 4. Antibacterial test results of PVC nanowebs.

Sample ID	Bacteria type	Contact time (h)	log CFU	Bacterial reduction (%)
PVC0 (in pH 5)	*S.aureus*	3	9.65	3.92
		24	9.63	7.84
	E.coli	3	-	-
		24	6.04	88.24
PVC1 (in pH 5)	*S.aureus*	3	9.64	4.90
		24	8.74	88.24
	E.coli	3	-	-
		24	5.21	71.76
PVC3 (in pH 5)	*S.aureus*	3	9.63	7.84
		24	0	100
	E.coli	3	-	-
		24	3.51	100
PVC5 (in pH 5)	*S.aureus*	3	0	100
		24	0	100
	E.coli	3	0	100
		24	-	100

4. CONCLUSION

In this study, organic N-halamin compound (TTDD) compound was added to PVC solution and nanoweb surfaces were successfully produced by electrospinning process. The SEM images revealed the resulting nanowebs possessed relatively non-homogenous average fiber diameters between 35-411 nm and PVC nanowebs have a beaded structure, except PVC5. The amount of TTDD dramatically affected the fiber diameter. The typical FTIR peaks of TTDD were observed in TTDD loaded-PVC and small changes in certain peaks were recorded, owing to physical interactions of TTDD with PVC matrix. According to TGA analysis, the addition of TTDD had no effect on the initial degradation temperature of the PVC. However, the thermal degradation changed after the pyrolysis temperature. The chlorinated nanowebs indicated high antibacterial activity against both *S. aureus* and *E. coli*. Antibacterial activity was found to increase with increasing TTDD amount in 3 h and 24 h. Within 24 hours, PVC5 nanowebs provided 100 % inactivation (approximately 0 logs) of E. coli and S. aureus. Moreover, rechargeable chlorination capabilities were achieved in acidic media with minimum loss during the optimum time (6 h) for all nanowebs. This procedure was carried out four times. The utilization of TTDD bactericidal groups to develop protective electrospun PVC webs with recharged antibacterial efficiency might be a potential application in medical fields.

Acknowledgement

REFERENCES

1. Boryo DEA. 2013. The effect of microbes on textile material: a review on the way-out so far. *The International Journal of Engineering and Science (IJES),* 2(8):9-13.

2. Ramachandran T, Rajendrakumar K, Rajendran R. 2004. Antimicrobial textiles-an overview. *Journal of The Institution of Engineers (India): Series E,* 84(2):42-47.

3. Tshikantwa TS, Ullah MW, He F, Yang G. 2018. Current trends and potential applications of microbial interactions for human welfare. *Frontiers in Microbiology,* 9, 1156.

4. Ducel G, Fabry J, & Nicolle L. 2002. Prevention of hospital acquired infections: a practical guide. *Prevention of hospital acquired infections: a practical guide.* (Ed. 2). Malta.

5. Şimsek EM, Grassie SS, Emre C, 2017. Relationship between environmental conditions and nosocomial infection rates in intensive care unit. *Medical Journal of Islamic World Academy Sciences,* 25, 15-18.

6. Hughes R. 2008. Patient safety and quality: An evidence-based handbook for nurses (Vol. 3). Rockville, MD: Agency for Healthcare Research and Quality.

7. Ji M, Moffett HL, Kunin CM. 1988. Guidelines for improving the use of antimicrobial agents in hospitals: a statement by the Infectious Diseases Society of America. *Journal of Infection Disease,* 157, 869-876.

8. Ren X, Kou L, Kocer HB, Zhu C, Worley SD, Broughton RM, Huang TS. 2008. Antimicrobial coating of an N-halamine biocidal monomer on cotton fibers via admicellar polymerization. *Colloids and Surfaces A: Physicochemical and Engineering Aspects,* 317(1-3):711-716.

9. Aksoy OE, Ates B, Cerkez I. 2017. Antibacterial polyacrylonitrile nanofibers produced by alkaline hydrolysis and chlorination. *Journal of Materials Science,* 52(17):10013-10022.

10. Kocer HB, Akdag A, Ren X, Broughton RM, Worley SD, Huang TS. 2008. Effect of alkyl derivatization on several properties of N-halamine antimicrobial siloxane coatings. *Industrial&Engineering Chemistry Research,* 47(20):7558-7563.

11. Kocer HB. 2012. Residual disinfection with N-halamine based antimicrobial paints. *Progress in Organic Coatings,* 74(1):100-105.

12. Worley SD, Williams DE, Crawford R. 1988. Halamine water disinfectants. *Critical Reviews in Environmental Science and Technology,* 18(2):133-175.

13. Kocer HB, Worley SD, Broughton RM, Huang TS. 2011. A novel N-halamine acrylamide monomer and its copolymers for antimicrobial coatings. *Reactive and Functional Polymers*, 71(5):561-568.

14. Ma Y, Li J, Si Y, Huang K, Nitin N, Sun G. 2019. Rechargeable antibacterial N-halamine films with antifouling function for food packaging applications. *ACS Applied Materials&İnterfaces,* 11(19): 17814-17822.

15. Demir B, Broughton RM, Qiao M, Huang TS, Worley SD. 2017. N-halamine biocidal materials with superior antimicrobial efficacies for wound dressings. *Molecules,* 22(10):1582.

16. Cerkez I, Kocer HB, Worley SD, Broughton RM, Huang TS. 2011. N-halamine biocidal coatings via a layer-by-layer assembly technique. *Langmuir,* 27(7):4091-4097.

17. Demirci F, Kocer HB. 2019. Preparation of antibacterial polyvinylidene fluoride (PVDF) ultrafiltration membranes with direct addition of N-halamine polymers. *Separation Science and Technology,* 54(5):803-814.

18. Kocer HB, Cerkez I, Worley SD, Broughton RM, Huang TS. 2011. N-halamine copolymers for use in antimicrobial paints. *ACS Applied Materials &İnterfaces,* 3(8):3189-3194.

19. Ren X, Jiang Z, Liu Y, Li L, Fan X. 2016. N-halamines as antimicrobial textile Finishes. G.S. *Antimicrobial Textiles.* USA: Elsevier: Woodhead Publishing.

20. Bhardwaj N, Kundu SC. 2010. Electrospinning: a fascinating fiber fabrication technique. *Biotechnology Advances,* 28(3):325-347.

21. Parin FN, Terzioğlu P, Sicak Y, Yildirim K, Öztürk M. 2020. Pine honey–loaded electrospun poly (vinyl alcohol)/gelatin nanofibers with antioxidant properties. *The Journal of The Textile Institute*, 112(4):628-635.

22. Parın FN, Aydemir Ç, Taner G, Yıldırım K. 2021. Co-electrospun-electrosprayed PVA/folic acid nanofibers for transdermal drug delivery: Preparation, characterization, and in vitro cytocompatibility. *Journal of Industrial Textiles,* Doi:1528083721997185.

23. Parın FN, Yıldırım K. 2021. Preparation and characterisation of vitamin-loaded electrospun nanofibres as promising transdermal patches. *Fibres & Textiles in Eastern Europe,* 1(145):17-25.

24. Ren X, Kocer HB, Worley SD, Broughton RM, Huang T. 2013. Biocidal nanofibers via electrospinning. *Journal of Applied Polymer Science,* 127(4):3192-3197.

25. Fang J, Niu H, Lin T, Wang X. 2008. Applications of electrospun nanofibers. *Chinese Science Bulletin,* 53(15):2265.

26. Goldade V, Vinidiktova N. 2017. Antimicrobial Fibers For Textile Clothing And Medicine: Current State, *ISJ Theoretical & Applied Science,* 3(47):178-194.

27. Parın FN, Yıldırım K, Kavçak Ö, Kalemtaş A, Aydın G. 2020, Eylül. Fabrication of Antibacterial Orange Essential Oil−Loaded Gelatin Fibers. In Y.U. 7. ULPAS Bildiri Kitapçığı (34-38). Bursa, Türkiye.

28. Ahmadi S, Hivechi A, Bahrami SH, Milan PB, Ashraf SS. 2021. Cinnamon extract loaded electrospun chitosan/gelatin membrane with antibacterial activity. *International Journal of Biological Macromolecules,* 173, 580-590.

29. Yina M, Wang Y, Zhang Y, Ren X, Qiu Y, Huang T. 2020. Novel quaternarized N-halamine chitosan and polyvinyl alcohol nanofibrous membranes as hemostatic materials with excellent antibacterial properties. *Carbohydrate Polymers,* 232, 115823.

30. Zhang Y, Li T, Shiu B, Sun F, Ren H, Zhang X, Lou C, Lin J. 2021. Eco-friendly versatile protective polyurethane/triclosan coated polylactic acid nonwovens for medical covers application. *Journal of Cleaner Production,* 282, 124455.

31. Chen S, Li C, Hou T, Cai Y, Liang L, Chen L, Li M. 2019. Polyhexamethylene guanidine functionalized chitosan nanofiber membrane with superior adsorption and antibacterial performances. *Reactive and Functional Polymer,* 145, 104379.

32. Ullah S, Hashmi M, Kharaghani D, Khan MQ, Saito Y, Yamamoto T, Lee J, Kim IS. 2019. Antibacterial properties of in situ and surface functionalized impregnation of silver sulfadiazine in polyacrylonitrile nanofiber mats. *International Journal of Nanomedicine,* 14, 2693-2703.

33. Zhanga T, Gua J, Liua X, Dengshuai W, Huiling Z, Haihua X, Zhuocheng Z, Huali Y, Shiguo C. 2020. Bactericidal and antifouling electrospun PVA nanofibers modified with a quaternary ammonium salt and zwitterionic sulfopropylbetaine. *Materials Science & Engineering C,* 111, 110855.

34. Lv H, Cui S, Yang Q, Song X, Wang D, Hua J, Zhou Y, Liu Y. 2021. AgNPs-incorporated nanofiber mats: Relationship between AgNPs size/ content, silver release, cytotoxicity, and antibacterial activity. *Materials Science & Engineering C,* 118, 111331.

35. Dong A, Wang Y, Gao Y, Gao T, Gao G. 2017. Chemical Insights into Antibacterial N-Halamines. *Chemical Reviews,* 117, 4806-4862.

36. Liu M, Wang F, Liang M, Si Y, Yu J, Ding B. 2020. In situ green synthesis of rechargeable antibacterial N-halamine grafted poly(vinyl alcohol) nanofibrous membranes for food packaging applications. *Composites Communications,* 17, 147-153.

37. Tian C, Wu F, Jiao W, Liu X, Yin X, Si Y, Yu J, Ding B. 2021. Antibacterial and antiviral N-halamine nanofibrous membranes with nanonet structure for bioprotective applications. *Composites Communications,* 24, 100668.

38. Ma Y, Yi J, Pan B, Nitin N, Sun G. 2020.Chlorine Rechargeable Biocidal N-Halamine Nanofibrous Membranes Incorporated with Bifunctional Zwitterionic Polymers for Efficient Water Disinfection Applications. *ACS Applied Materials Interfaces,* 12(45):51057-51068.

39. Liang M, Wang F, Liu M, Yu J, Si Y, Ding B. 2019. N-Halamine Functionalized Electrospun Poly(Vinyl Alcohol-co-Ethylene) Nanofbrous Membranes with Rechargeable Antibacterial Activity for Bioprotective Applications. *Advanced Fiber Materials*, 1, 126-136.

40. Nicholas P. 1997. *Handbook of Engineering Polymeric Materials.* USA: Marcel Dekker Inc.

41. Doble M, Kumar A. 2005. *Biotreatment of Industrial Effluents.* USA: Butterworth-Heinemann, Elsevier.

42. Li X, Xing Y, Jiang Y, Ding Y, Li W. 2009. Antimicrobial activities of ZnO powder-coated PVC film to inactivate food pathogens. *International Journal of Food Science&Technology,* 44(11):2161-2168.

43. Machovsky M, Kuritka I, Bazant P, Vesela D, Saha P. 2014. Antibacterial performance of ZnO-based fillers with mesoscale structured morphology in model medical PVC composites. *Materials Science and Engineering: C,* 41, 70-77.

44. Behboudi A, Jafarzadeh Y, Yegani R. 2018. Incorporation of silica grafted silver nanoparticles into polyvinylchloride/polycarbonate hollow fiber membranes for pharmaceutical wastewater treatment. *Chemical Engineering Research and Design,* 135, 153-165.

45. Zampino D, Ferreri T, Puglisi C, Mancuso M, Zaccone R, Scaffaro R, Bennardo D. 2011. PVC silver zeolite composites with antimicrobial properties. *Journal of Materials Science,* 46(20):6734-6743.

46. Cushen M, Kerry J, Morris M, Cruz-Romero M, Cummins E. 2013. Migration and exposure assessment of silver from a PVC nanocomposite. *Food Chemistry,* 139(1-4):389-397.

47. Lin H, Xu Z, Wang X, Long J, Su W, Fu X, Lin Q. 2008. Photocatalytic and antibacterial properties of medical‐grade PVC material coated with TiO₂ film. *Journal of Biomedical Materials Research Part B:Applied Biomaterials,* 87(2):425-431.

48. Lala NL, Ramaseshan R, Bojun L, Sundarrajan S, Barhate RS, Ying-jun L, Ramakrishna S. 2007. Fabrication of Nanofibers With Antimicrobial Functionality Used as Filters: Protection Against

Bacterial Contaminants. *Biotechnology and Bioengineering*, 97(6): 1357-1365.

49. Chylińska M, Kaczmarek H, Burkowska-But A, Walczak M. 2015. Novel biocidal N-halamine plastic based on poly (vinyl chloride): preparation and characteristics. *Journal of Industrial and Engineering Chemistry*, 28, 124-130.

50. Akdag A, Okur S, McKee ML, Worley SD. 2006. The stabilities of N−Cl bonds in biocidal materials. *Journal of Chemical Theory and Computation*, 2(3):879-884.

51. Ren X, Akdag A, Kocer HB, Worley SD, Broughton RM, Huang TS. 2009. N-Halamine-coated cotton for antimicrobial and detoxification applications. *Carbohydrate Polymers*, 78(2):220-226.

52. Liang J, Chen Y, Barnes K, Wu R, Worley SD, Huang TS. 2006. N-halamine/quat siloxane copolymers for use in biocidal coatings. *Biomaterials*, 27, 2495-2501.

53. Liang J, Wu R, Wang JW, Barnes K, Worley SD, Cho U, Lee J, Broughton RM, Huang TS. 2007. N-halamine biocidal coatings. *Journal of Industrial Microbiology and Biotechnology*, 34, 157-163.

54. Çobanoğlu B, Parın FN, Yıldırım K. 2019, Mayıs. Antibacterial Polyvinyl Chloride (PVC) Nanofibers Containing N-Halamines. In Y.U., 5. ULPAS Bildiri Kitapçığı (79-81). İstanbul, Türkiye.

55. Iribarren A, Rivero PJ, Berlanga C, Larumbe S, Miguel A, Palacio JF, Rodriguez R, 2019. Multifunctional Protective PVC-ZnO Nanocomposite Coatings Deposited on Aluminum Alloys by Electrospinning. *Coatings*, 9(216):2-13.

56. Akgül YI, Aykut Y. 2019. Partially Transformation of Zinc Nitrate to Zinc Compounds on PVC Nanofibers at Low-Temperature Heat Treatment and Investigation of the Products Optical Properties. *Tekstil ve Mühendis*, 26(114):118-124.

57. Zhong Z, Cao Q, Jing B, Wang X, Li X, Deng H. 2012. Electrospun PVDF-PVC nanofibrous polymer electrolytes for polymer lithium-ion batteries. *Materials Science and Engineering: B*, 177(1):86-91.

58. Zhong Z, Cao Q, Jing B, Li S, Wang X. 2012. Novel electrospun PAN–PVC composite fibrous membranes as polymer electrolytes for polymer lithium-ion batteries. *Ionics*, 18(9):853-859.

59. Guo JW, Lin ZY, Huang BR, Lu CH, Chen JK. 2018. Antigen detection with thermosensitive hydrophilicity of poly (N-isopropyl acrylamide)-grafted poly (vinyl chloride) fibrous mats. *Journal of Materials Chemistry B*, 6(21):3486-3496.

60. Cerkez I, Kocer HB, Worley SD, Broughton RM, Huang TS. 2012. Epoxide tethering of polymeric N-halamine moieties. *Cellulose*, 19(3):959-966.

61. Sherif EM, Es-saheb M, El-Zatahry A, Kenawyand E, Alkaraki AS. 2012. Coating electrospun polyvinyl alcohol and polyvinyl chloride fibers as corrosion passivation applications. *International Journal of Electrochemical Science*, 7, 6154-6167.

62. Hussein MA, Kumar M, Drew R, Al-Aqeeli N. 2018. Electrochemical corrosion and in vitro bioactivity of nano-grained biomedical Ti-20Nb-13Zr alloy in a simulated body fluid. *Materials*, 11(1):26.

63. Shnawa HA, Khalaf MN, Jahani Y. 2018. The effects of natural polyphenols and calcium-based thermal stabilizer on the rheological and thermal resistance behaviors of PVC. *International Journal of Plastics Technology*, 22(2):65-385.

64. Nair MR, Thomas GV, Nair MG. 2007. Thermogravimetric analysis of PVC/ELNR blends. Polymer Degradation and Stability, 92(2):189-196.

Production and Characterization of Nanoencapsulated Phase Change Materials (PCMs) and Bicomponent PCM Nanofibers

Simge ÖZKAYALAR, 0000-0002-5390-8317
Sennur ALAY AKSOY* 0000-0002-5878-6726

Süleyman Demirel University, Engineering Faculty, Textile Engineering Department, Isparta, Turkey

Corresponding Author: Sennur Alay Aksoy, sennuralay@sdu.edu.tr

ABSTRACT

The aim of this study was to fabricate the nanocapsules and nanofibers with latent heat energy storage properties. Therefore, phase change materials based on fatty alcohols were used as latent heat energy storage materials. N-Dodecanol and 1-tetradecanol fatty alcohols were nanoencapsulated by poly(methyl methacrylate-co-methacrylic acid) (p(MM-co-MA)) wall using emulsion polymerization method. Prepared nanocapsules were incorporated in polyacrylonitrile nanofibers using the co-axial electrospinning method. In this study, a two-stage (TS) emulsion polymerization process was defined and compared to the known emulsion polymerization method defined as one-stage (OS). Nanocapsules were characterized by Fourier-transform infrared (FT-IR) spectroscopy, transmission electron microscopy (TEM), differential scanning calorimeter (DSC), and thermogravimetric analyzer (TGA). According to the results, typical core-shell structured, spherical-shaped, uniform nano-sized particles having high thermal stability and energy storage capacity were fabricated successfully. Enthalpy values of the nanocapsules prepared by the TS process were higher and reached up to 171 J/g. It was concluded that the thermal degradation stability of the nanocapsules could be improved using the TS emulsion polymerization method. Moreover, the nanocapsules were incorporated in polyacrylonitrile nanofibers using the co-axial electrospinning method, and composite nanofibers having 19 J/g energy storage capacities were produced. Although the surfaces of the prepared core-sheath structured nanofibers were rough and coarse, their diameter distribution was unimodal.

1. INTRODUCTION

Phase change materials (PCMs) have attracted a great deal of attention because of their capability of storing and releasing large amounts of latent heat during their phase change from one physical state to another. They have been used as an energy storage material in many fields such as solar energy storage, energy-efficient buildings, thermoregulation clothing, and industrial textiles due to their high energy storage capacity. A large number of organic and inorganic solid-liquid PCMs are available. Organic-based PCMs such as paraffin waxes or n-alkanes, polyethylene glycol, fatty acids generally have been preferred as thermal energy storage materials in many end-use fields [1]. Their phase change temperatures and energy storage capacities have taken into account in this selection. One type of organic-based PCMs is fatty alcohols such as n-dodecanol and 1-tetradecanol. In recent years, the use of fatty alcohols as thermal energy storage material has been attracted great deal of interest because of their low cost than paraffin waxes and having high heat density and a wide range of melting temperatures. However, fatty alcohols have some disadvantages such as leakage, subcooling, low thermal conductivity, reactivity toward the outside environment, and flammability [2]. To overcome these disadvantages, encapsulation technology has been utilized. Encapsulation is to packet an oil drop or a solid particle as a

core material in a wall in order to develop micro or nano-sized capsules [3]. Encapsulated PCM is composed of a PCM as the core, and a polymer or an inorganic shell to maintain the spherical capsule shape and prevent leakage of PCM during its melting [4, 5]. The wall structure plays very important role in order to meet the requirements of the usage area of the encapsulated PCMs. According to the literature survey on usage of fatty alcohols as PCM, n-dodecanol have been encapsulated by various wall materials such as SiO_2 [2], melamine-formaldehyde resin [6-8], methanol–melamine-formaldehyde [9, 10], styrene-butyl acrylate copolymer [11], polymethyl methacrylate (PMMA) [12], acrylic-based copolymer prepared using acrylic monomers such as polyurethane acrylate and 1,4-butylene glycol diacrylate [13], graphene oxide-modified poly(melamine-formaldehyde) [14], poly(methyl methacrylate) copolymer with different type co-monomers such as acrylamide, butyl acrylate and acrylic acid [15], poly(allyl methacrylate) [16], melamine–urea-formaldehyde resins [17].

In the textile industry, phase change materials are used to improve thermal clothing comfort and produce smart thermo-regulating textiles. They have been incorporated into the fibers directly or encapsulated form, during the fiber spinning. Additionally, coating the fabrics with encapsulated PCM doped polymer has been realized. Recently, the electrospinning technique has been utilized to produce nano-sized form-stable phase change fibers containing PCMs in a supporting polymer matrix [18, 19]. Electrospinning technique has been used to fabricate the phase change-composite fibers with unique advantages such as ultrafine size, huge surface-to-volume ratio, excellent thermal performance, lightweight, and direct useage in various composites [18, 20, 21]. Electrospinning is a simple and versatile method that involves the usage of electrostatic force to draw a polymer solution into fibers whose diameters vary from a few nanometers to a submicron scale [18, 22, 23]. Phase change-composite nanofiber webs prepared by single and double nozzle (coaxial) electrospinning techniques can be applied in garments, electronic components, etc. in order to enhance the efficiency of thermal regulation [20]. Recently, the preparation of temperature-regulating composite nanofibers by coaxial electrospinning technique has attracted more and more attention. In coaxial electrospinning, concentrically aligned spinnerets have been used to fabricate core-sheath or hollow nanofibers [22, 24]. Coaxial electrospinning is a promising method to encapsulate PCM in the core of the fibers and to maintain it inside the polymer sheath layer of the fibers [25]. Coaxial electrospinning offers encapsulation of both hydrophilic and oleophilic PCMs in a variety of polymers and enhances the mechanical properties of the phase-change-composite nanofibers [21]. Oleophilic or hydrophilic solid-liquid PCMs such as long-chain hydrocarbons and polyethylene glycol have been encapsulated in core-sheath structured nanofibers by coaxial electrospinning method [21, 24-32].

The aim of this study is to produce the nanocapsules and nanofibers having latent heat storage and release properties with improved thermal properties. In literature, poly(methyl methacrylate) (PMMA) and its copolymers have been used in the encapsulation of the various solid-liquid PCMs such as n-alkanes and fatty acids [33-39]. In this study, n-dodecanol and 1-tetradecanol fatty alcohols were used as solid-liquid phase-change materials and nanoencapsulated in the wall of poly(methyl methacrylate-co-methacrylic acid) (p(MMA-co-MA)). A two-stage emulsion polymerization process was performed to investigate its performance in improving the thermal stability of the capsule shell structure. In the TS emulsion polymerization process, the methacrylic acid monomer was added to the emulsion medium during the second stage of the process. Thereby, firstly PMMA shell was synthesized to produce nanocapsules having a poly(methyl methacrylate) inner shell. In the second step of the process, MMA and MA monomers were copolymerized to produce a poly(methyl methacrylate-co-methacrylic amide) outer shell structure. Additionally, it was aimed to form the nanocapsule shell containing more numerous functional carboxylic acid groups by increasing the MA monomer in the outer surface of the nanocapsules. Thereby, the homogeneous distribution of the nanocapsules in the PEG solution, which was the core spinning solution of the bicomponent nanofibers, was aimed by increasing molecular interaction between the OH groups of PEG and carboxylic acid groups of the MA. In the study, synthesis of the single P(MMA-co-MA) shell was carried out using the conventional emulsion polymerization method which was defined as one-stage emulsion polymerization. Their properties were compared to the TS nanocapsules. The prepared TS nanocapsules were loaded in nanofibers as the core material via co-axial electrospinning technique and the placement of the nanocapsules in the fiber structure was investigated.

2. MATERIAL AND METHOD

2.1 Material

Methyl methacrylate (MMA, Merck) and methacrylic acid (MA, from Sigma Aldrich) were used as monomers to synthesize the shell of the nanocapsules. Ethylene glycol dimethacrylate (EGDM, from Merck Company) was used as a cross-linker. n-Dodecanol and (from Sigma Aldrich) 1-tetradecanol (from Merck) as PCMs, and Triton X-100 (from Sigma Aldrich) as an emulsifier were used. Ferrous sulfate heptahydrate and ammonium persulfate used as initiators were obtained from a Sigma Aldrich company. Sodium thiosulfate (from Merck) was used as a reactive material. Tert-butyl hydroperoxide (70 % in water) was obtained as an initiator from Acros Organics Company and used as received.

To produce nanofibers, polyacrylonitrile (PAN, Mw 150000 g/mole from Sigma Aldrich) and polyethylene glycol (PEG, Mw 1000 g/mol from Alfa Aesar) were used as polymers. N,N-Dimethylformamide (DMF, with a purity of > % 98.8 from Carlo Erba Reagent) was used as the solvent.

2.2 Method

2.2.1. Preparation of the nanocapsules

In this study, encapsulation of n-dodecanol and 1-tetradecanol was carried out by emulsion polymerization method. Different from the studies in literature, the emulsion polymerization process (two-stage) was carried out in two steps to manufacture nanocapsules having poly(methyl methacrylate) inner and poly(methyl methacrylate-co-methacrylic acid) outer walls.

In a two-stage (TS) polymerization procedure, a 12.5 g quantity of core material (n-dodecanol or 1-tetradecanol) was emulsified in 80 mL of distilled water at speed of 2000 rpm at 50 °C. Triton 100 (1 g) was added as an emulsifier. Then, 6.25 g MMA, 0.5 mL of ferrous sulfate heptahydrate solution (FSHS), 0.125 g of ammonium persulfate (APS), 1.25 g of ethylene glycol dimethacrylate (EGDM) were added to the emulsion. The stirring speed of the emulsion was decreased to 1000 rpm. Sodium thiosulfate (STS, 0.125 g) and 0.5 g of tert-Butyl hydroperoxide (TBHP) were added and the reaction medium was heated to 85 °C. After 2 hours of stirring at 1000 rpm, the first step of the process was completed. To start the second step of the process, 0.5 g of Triton X100, 6.25 g of MMA, 2.5 g of MA, 0.25 mL of ferrous sulfate heptahydrate solution, 0.0625 g of ammonium persulfate, and 0.625 g of ethylene glycol dimethacrylate were added to the reaction medium. After adding 0.0625 g of sodium thiosulfate and 0.25 g of tert-Butyl hydroperoxide, the reaction was continued at 85 °C for more than 2 hours. Afterward, the nanocapsules were filtered, rinsed with water at 50 °C, and dried at room temperature for analysis. Besides, the production process defined in our previous study was used to produce one walled nanocapsule and named as a one-stage process (OS) [40, 41]. The amount of the materials used in the one-stage production process was given in Table 1. In this process, the polymerization reaction was conducted at 85 °C for 4 hours by stirring at 1000 rpm. The abbreviated names and contents of the nanocapsules were given in Table 1.

2.2.2. Production of core-sheath structured nanofibers

In this study, Nanocapsule-D-TS/PAN core-sheath structured nanofibers were produced by coaxial electrospinning of polyacrylonitrile (PAN) and Nanocapsule-D-TS as the sheath polymer and core material, respectively. The coaxial electrospinning apparatus has an inner spinneret coaxially placed inside an outer one. The basic experimental setup is shown in Figure 1. In the study, 14% PEG core spinneret solution in DMF (w/v) was prepared. Nanocapsules at a specified mass ratio of 40% were mixed in PEG/DMF core solution in order to achieve their homogeneous distribution in the fiber core. To prepare sheath spinneret solution, 6% PAN (w/v) was dissolved in DMF. The outer nozzle syringe pump and the inner syringe pump were set to the flow rate of 2 mL/h and 0.4 mL/h, respectively, to be provided a continuous flow of solutions. Both nozzles were connected to the same electrical potential with the applied voltage of 19.8 kV. The distance between the needle and the collector was fixed at 11 cm.

Before the electrospinning, electrical conductivity of the core and shell solutions was measured. Measurements were performed at 25 °C using a WTW 330 model instrument. In the literature, it was stated that the conductivity of the sheath spinneret solution should be higher than the conductivity of the core spinneret solution in order to make continuous core-sheath structured nanofiber production [42,43]. In the study, electrical conductivity of the sheath spinneret solution (95.5 $\mu S\,cm^{-1}$) was measured as higher as to be contributed to electrospinning of core spinneret solution (7.4 $\mu S\,cm^{-1}$).

Table 1. The abbreviations of the capsules produced in the study and their contents with the method applied

| Production process	Capsule	Wall and core material	Added materials	
			First stage	Second stage
One-stage	Nanocapsule-D-OS	PMMA-co-MA n-dodecanol	12.5 g core 1.5 g of TritonX100 12.50 g MMA 2.5 g MA 0.75 mL FSHS 0.1875 g APS 1.875 g EGDM 0.1875 g STS 0.75 g TBHP	-
	Nanocapsule-T-OS	PMMA-co-MA 1-tetradecanol		-
Two-stage	Nanocapsule-D-TS	PMMA inner PMMA-co-MA outer n-dodecanol	12.5 g core 1 g Triton X-100 6.25 g MMA 0.5 mL FSHS 0.125 g APS 1.25 g EGDM 0.125 g STS 0.5 g TBHP	0.5 g TritonX100 6.25 g MMA 2.5 g MA 0.25 mL FSHS 0.0625 g APS 0.625 g EGDM 0.0625 g STS 0.25 g TBHP
	Nanocapsule-T-TS	PMMA inner PMMA-co-MA outer 1-tetradecanol		
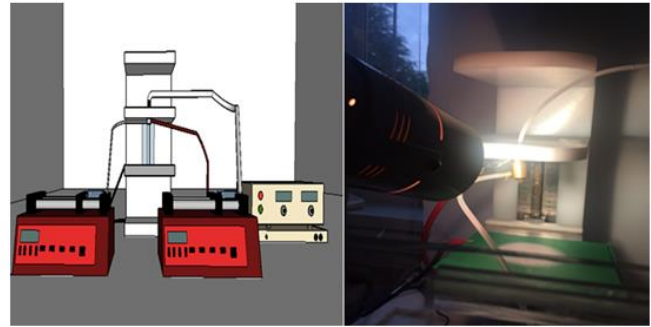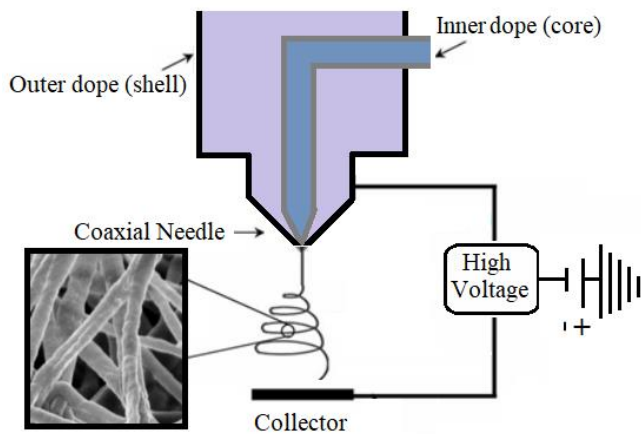
Figure 1. Co-axial electrospinning setup [40].

2.2.3. Characterization of the nanocapsules and nanofibers

The morphology and core-shell structure of the nanocapsules were analyzed using transmission electron microscopy (TEM, JEOL JEM2100). In this procedure, one drop of nanocapsule dispersion in the water was dropped onto a copper grid and allowed to dry and examined by TEM. In the study, the thickness of the nanocapsule shell on TEM images was measured using the images of about 50 nanocapsules per each nanocapsule type using an image analysis program. The Fourier transforms infrared (FTIR) transmission spectra of the nanocapsules and nanofibers were recorded between 4000 and 400 cm^{-1} at a resolution of 4 cm^{-1} and a number of scans of 16 using a Perkin Elmer Spektrum BX spectrometer. The spectroscopic analyses of the nanocapsules and nanofibers were performed on KBr disks. The particle size of nanocapsules was measured using a particle size instrument (Malvern MS2000E). Before the measurements, dried capsules were homogenized in the water by an ultrasonic homogenizer (Bandaline Sonuplus UV 2200) for 2 hours. Thermal properties of the nanocapsules and nanofibers such as latent heat storage–releasing capacities and temperatures were measured by differential scanning calorimetry (DSC, Perkin-Elmer Fronter) at a heating–cooling rate of 5 °C/min between -5 °C and + 80 °C under a constant stream of nitrogen at a flow rate of 60 mL/min. In this study, the core material permeability of the nanocapsule shell in an organic solution was investigated. In the test, nanocapsules were immersed in a 10% hexane solution for 24 hours and then washed with hot water, filtered, and dried at room temperature. Their thermal properties were also measured by a DSC instrument. Thermogravimetric analysis (TGA) of the nanoencapsulated fatty alcohols was carried out using a thermal analyzer (Perkin-Elmer TGA7) at a heating rate of 10 °C/min from 25 to 500 °C in nitrogen atmosphere. Differential Thermogravimetry (DTG) was also obtained to determine the maximum rate of weight loss. The morphologies of the nanofibers were investigated using a scanning electron microscope (SEM, LEO 440 Computer Controlled Digital). The surfaces of the nanofibers were coated with gold prior to the imaging.

3. RESULTS AND DISCUSSION

3.1. TEM analysis of the nanocapsules

The core-shell structures of the nanocapsules were examined by TEM analysis. As seen from TEM images given in Figure 2, typical core-shell structured nanocapsules were obtained and the fatty alcohols were encapsulated by a polymeric shell using the one-stage and two-stage emulsion polymerization methods. Spherical-shaped and uniform nano-sized particles were produced successfully. The particle sizes of the nanocapsules on TEM images changed between 200 and 500 nm. Nanocapsule-D-TS and Nanocapsule-D-OS had almost 63 nm and 59 nm shell thicknesses, while Nanocapsule-T-TS and Nanocapsule-T-OS had almost 49 nm and 39 nm shell thickness, respectively (Table 2). It was concluded the shell of the nanocapsules prepared by the two-stage process were thicker although the same amount of shell materials was used in the processes. This might be due to the presence of methacrylic acid comonomer used in wall structure synthesis. Methacrylic acid is a monomer that dissolves in water and swells in the polymerization environment. Addition of water-soluble monomers such acrylic and methacrylic acid into the oil-in-water emulsion medium in microencapsulation processes make the polymerization difficult and decrease the encapsulation efficiency, especially when used in high amounts (10% or more). However, in order to increase the functionality of the microcapsule wall structure, it should be used as much as possible [33]. Here, it was concluded that the addition of the MA co-monomer in the reaction medium at the second step reduced its negative effect on the polymerization process and promoted the formation of a thicker wall structure.
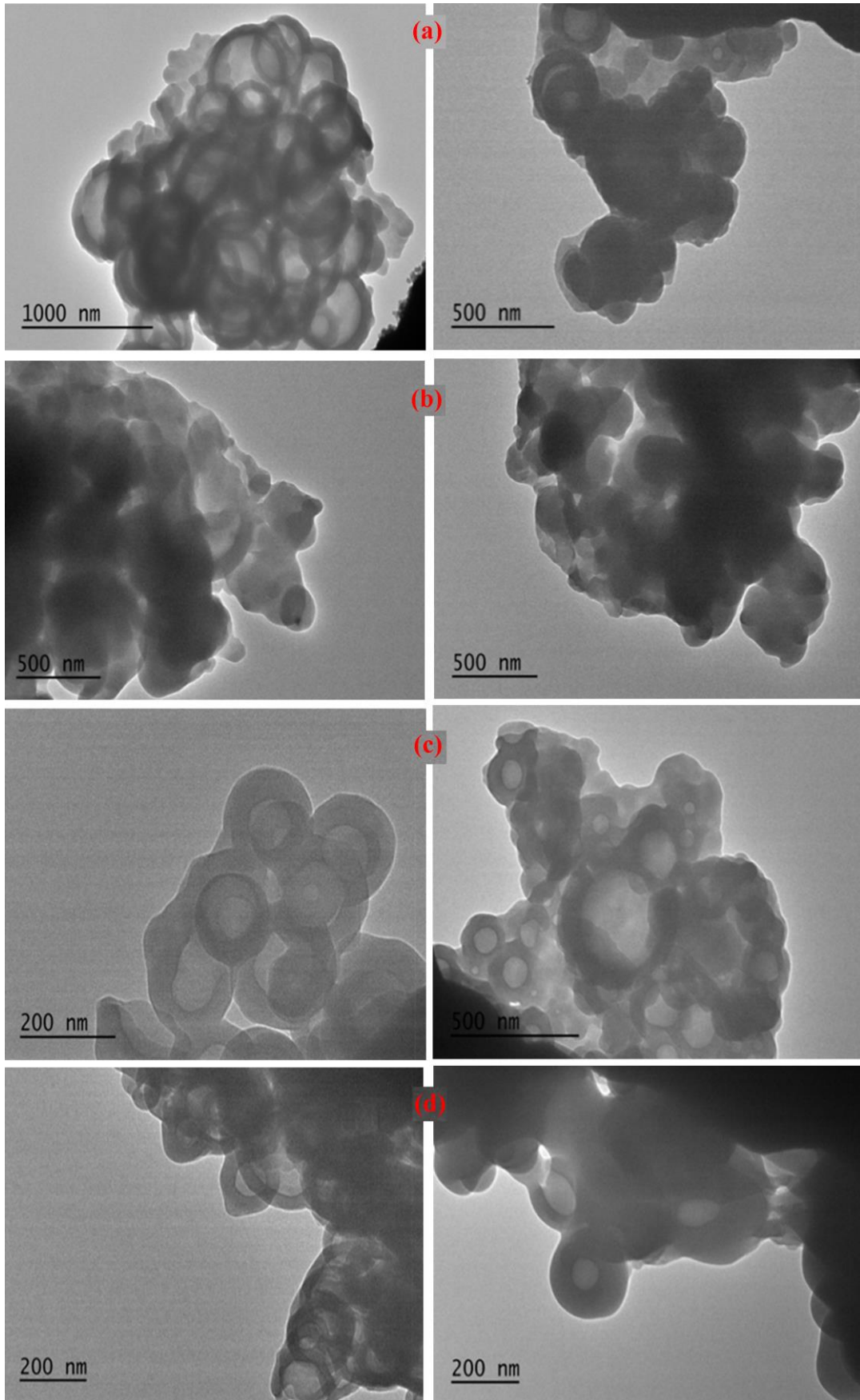
Figure 2. TEM micrographs of the nanocapsules (a: Nanocapsule-D-TS; b: Nanocapsule-D-OS; c: Nanocapsule-T-TS and d: Nanocapsule-T-OS

Table 2. Shell thickness meaurement results of the nanocapsules

Nanocapsules	Shell thickness values			
	Mean	Max.	Min.	CV%
Nanocapsule-D-OS	59	81	32	24.84
Nanocapsule-T-OS	39	44	30	15.58
Nanocapsule-D-TS	63	92	52	16.04
Nanocapsule-T-TS	49	59	37	15.61

3.1.2. FT-IR analysis of the nanocapsules

To study the chemical structures of the nanocapsules, FT-IR spectroscopy analyses were performed. The FTIR spectra of the materials and the information obtained from the FTIR spectra were given in Figure 3 and Table 3. C-H stretching peaks of the n-dodecanol were seen at 2924 cm^{-1} and 2854 cm^{-1} wavelengths in the FT-IR spectra of the Nanocapsule-D-TS and Nanocapsule-D-OS (Figure 3, Table 3). Besides, the medium-strong peaks at 1058-1059 cm^{-1} were belonging to the C-OH vibration of primary alcohol (n-dodecanol) [6,12]. The peaks at 1731 cm^{-1} in the spectra of the nanocapsules were carbonyl peaks formed by overlapping of the carbonyl peaks of the MMA and MA monomers. The peaks at 3390-3360 cm^{-1} in the spectra of nanocapsules were overlapped O-H stretching peaks both of alcohol groups of the n-dodecanol, and carboxylic acid groups of MA monomer. The peaks seen at wavelengths of 1625 cm^{-1} and 1639 cm^{-1}, respectively, in spectra of MMA and MA monomers were the vinyl group (C = C) stretch peaks and were disappeared in the spectra of the nanocapsules [41]. This finding was proof of the polymerization reaction carried out between the MMA and MA monomers. According to the FT-IR spectra of the nanocapsules containing 1-tetradecanol given in Figure 3, the peaks at 2919-2849 cm^{-1} and 2918-2849 cm^{-1} in the FT-IR spectra of the Nanocapsule-T-TS and Nanocapsule-T-OS were C-H stretching peaks of the 1-tetradecanol, which were proofs of the encapsulated 1-tetradecanol. Besides, arising of C-H stretching peaks of 1-tetradecanol at 1466 cm^{-1} in the FT-IR spectra of the nanocapsules were other proofs of its presence in nanocapsule structure [44]. The sharp peaks at a wavelength of 1733 cm^{-1} in the spectra of the nanocapsules were carbonyl (C = O) peaks, which were formed by overlapping of carbonyl peaks in the MA and MMA monomers [41]. The peaks at 3306-3311 cm^{-1} wavelengths in the nanocapsule spectra were O-H stretching peaks of the alcohol group of 1-tetradecanol and the carboxylic acid group of methacrylic acid co-monomer. The peaks at the wavelengths of 1625 cm^{-1} and 1639 cm^{-1} in FT-IR spectra of the MMA and MA monomers,

respectively, were the vinyl group (C = C) stretching peaks of the methacrylic acid and methyl methacrylate monomers [41]. These peaks were disappeared in the nanocapsules FT-IR spectra, which proved that the polymerization between methyl methacrylate and methacrylic acid monomers took place.

3.1.3. DSC analysis of the nanocapsules

To determine the thermal properties of the nanocapsules such as latent heat energy-storing/releasing capacities and temperatures, DSC analysis was performed. The DSC curves of the nanocapsules and the information obtained from the DSC curves were given in Figure 4 and Table 4. As seen from the DSC curves, two peaks were observed in the DSC spectrum during the cooling. This case resulted from liquid-solid and solid-solid phase-change processes of 1-alcohols having low temperature and high temperature crystalline forms. However, solid-solid and solid-liquid transitions during heating were overlapped [45,46]. It was seen from Table 4 that the liquid-solid and solid-solid crystallization temperatures were respectively 19 °C and 9.8 °C for Nanocapsule-D-TS, and 19 °C and 9.2 °C for Nanocapsule-D-OS. It was concluded from DSC analysis that the latent heat storage/releasing capacities of the prepared nanocapsules were very high compared to the findings in the literature [2,6,9-17]. Besides, the enthalpy values of the nanocapsules produced by the two-stage process were measured as higher. As explained before, the presence of a water-soluble MA comonomer in the emulsion medium negatively affects the microencapsulation process and decreases the microencapsulation efficiency. In the two-stage process, only the methyl methacrylate monomer dissolved in the oil phase was used in the first stage of encapsulation. However, in the one-stage process, an MMA monomer, as well as a water-soluble MA monomer, was added to the emulsion during the encapsulation period. Considering this matter, it was concluded that lower enthalpy of the OS-nanocapsules resulted from the adverse effect of the swelling of methacrylic acid monomer in water during the encapsulation process on the encapsulation of the fatty alcohol.

In this study, DSC analysis of nanocapsules was repeated after they were treated with hexane solution to determine the permeability of their shell structure in an organic solution. According to the DSC data given in Table 5, a significant change in their thermal energy storage capacity was observed after treatment with n-hexane for 24 h. They almost lost their latent heat storage capacities in the ratio of 38-40 %. This result meant that the shell structure leaks the core material in the presence of organic solvent n-hexane.

Table 3. FT-IR analysis spectrum information of the nanocapsules

Materials	FT-IR spectrum bands
n-dodecanol	3200-3600 cm^{-1} → O-H stretching peaks 2924 cm^{-1} and 2854 cm^{-1} → C-H stretching peaks 1058-1059 cm^{-1} → Medium peaks are associated with the C-OH vibration of the primary alcohol
1-tetradecanol	3200-3600 cm^{-1} → O-H stretching peaks 2919-2849 cm^{-1} and 2918-2849 cm^{-1} → C-H stretching peaks 1466 cm^{-1} → C-H stretching peak
Methyl methacrylate monomer	1731 cm^{-1} and 1733 cm^{-1} → strerching peak of the carbonyl group 1625 cm^{-1} → C = C (vinly group) peak in monomer
Methacrylic acid monomer	3390-3360 cm^{-1} and 3306-3311 cm^{-1} → Belongs to OH stretching in carboxilic acid group 1731 cm^{-1} and 1733 cm^{-1} → Peak of carbonyl group in the carboxilic acid group 1625 cm^{-1} → C = C (vinly group) peak in monomer
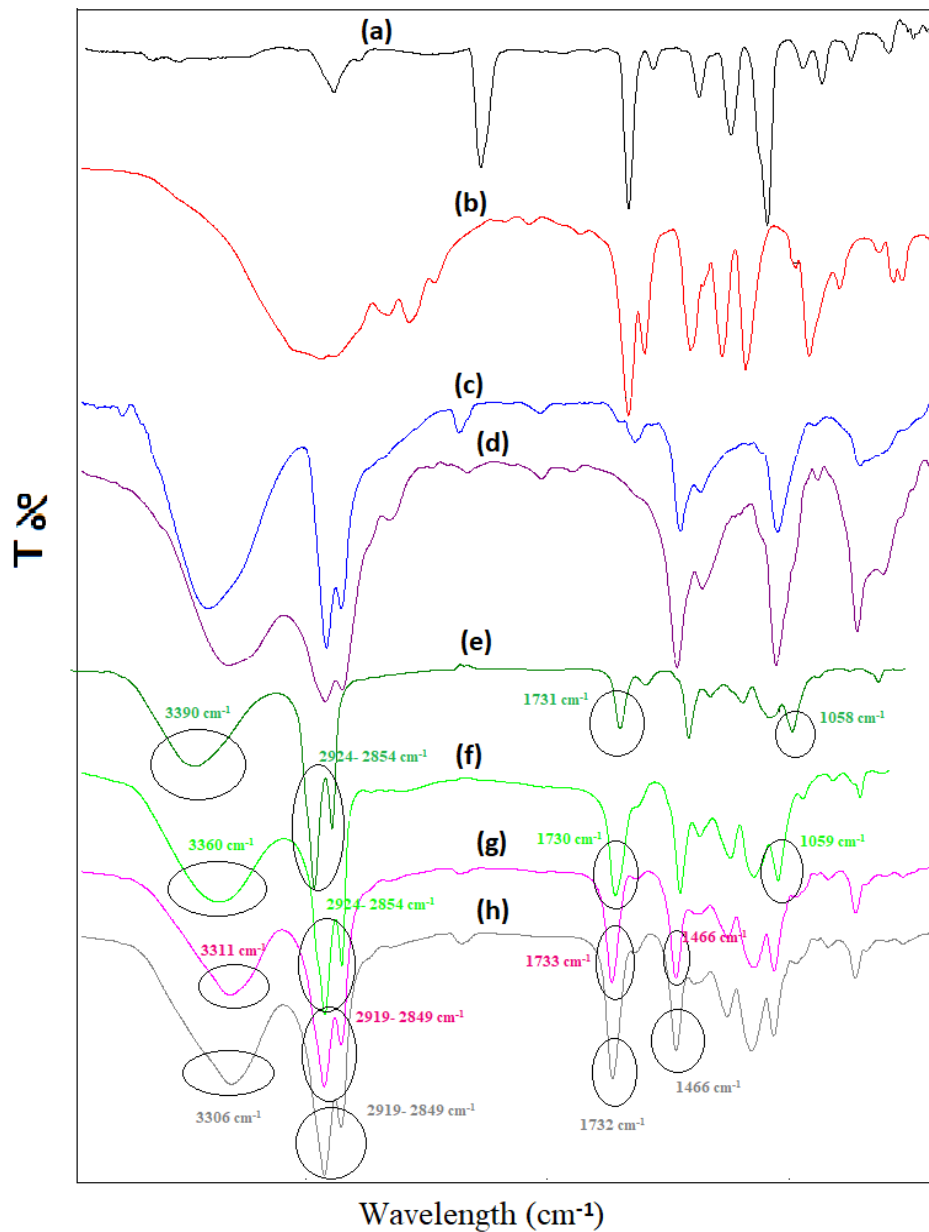
Figure 3. FT-IR spectrum of (a): methyl methacrylate monomer, (b) methacrylic acid monomer, (c) n-dodecanol, (d): 1-tetradecanol, (e):Nanocapsule-D-TS, (f): Nanocapsule-D-OS, (g): Nanocapsule-T-TS, (h): Nanocapsule-T-OS
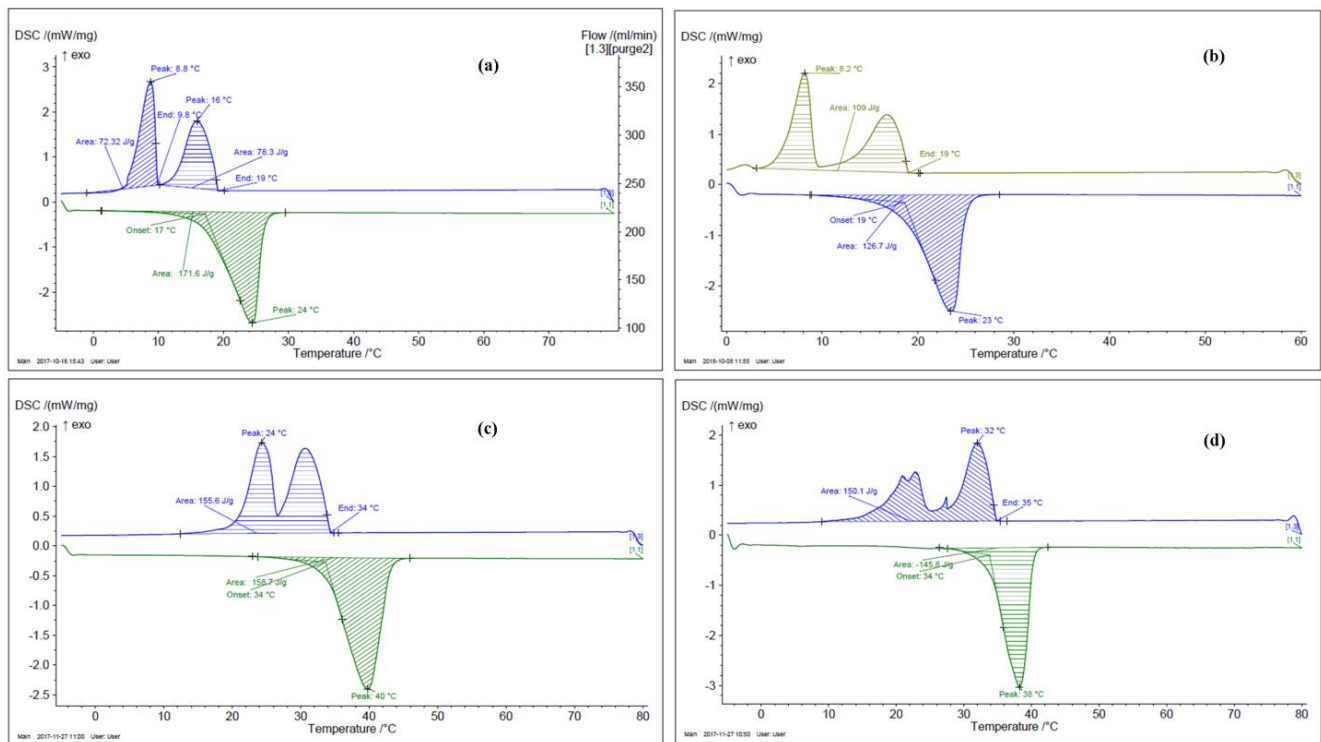
Figure 4. DSC curves of nanoencapsulated n-dodecanol (a: Nanocapsule-D-TS; b: Nanocapsule-D-OS) and 1-tetradecanol (c: Nanocapsule-T-TS; d: Nanocapsule-T-OS)

Table 4. DSC data of the nanocapsules

| Nanocapsule | Melting Temp. (°C) | Melting Enthalpy (J/g) | Crystallization Temp. (°C) | | Total Crystallization Enthalpy Measured During Crystallization (J/g) |
			Solid-Liquid	Solid-Solid	
n-dodecanol	21.58	210.13	20.13	18.23	-209.3
Nanocapsule-D-TS	17	171.6	19	9.8	-150.6
Nanocapsule-D-OS	19	126.7	19	9.2	-101.6
1-tetradecanol	35.5	192.8	35.54	28.97	- 183.4
Nanocapsule-T-TS	34	158.7	34	24	-155.6
Nanocapsule-T-OS	34	145.8	35	24	-150.1

Table 5. DSC analysis results of the nanocapsules treated with hexane

| Nanocapsule | Melting Temp. (°C) | Melting Enthalpy (J/g) | Crystallization Temp. (°C) | | Total Crystallization Enthalpy Measured During Crystallization (J/g) |
			Solid-Liquid	Solid-Solid	
Nanocapsule-T-TS	33	96.01	33	22	-90
Nanocapsule-T-OS	33	89.75	32	21	-84.77

3.1.4. TGA analysis of the nanocapsules

TGA analysis was performed to investigate the thermal stability of the prepared nanocapsules. The TGA curves of the nanocapsules and the information obtained from the TGA curves were given in Figure 5 and Table 6. As seen from the TGA curves given in Figure 5, nanocapsules exhibited two-step thermal degradation. The weight loss of the n-docecanol usually occurs between 140-245 °C as a typical one-step degradation resulting from its volatilization [2,6,9,11,13]. The first step degradation in the TGA curves of the Nanocapsule-D-TS and Nanocapsule-D-OS nanocapsules started at almost 140 °C corresponding decomposition temperature of n-dodecanol. The weight loss of 76% for the Nanocapsule-D-TS resuled between the temperatures of 148 °C and 200 °C, while the Nanocapsule-D-OS nanocapsules lost 62% of their weight between the

125 °C and 200 °C. The second step thermal degradation, which resulted from the degradation of the shell of the capsules, started at 300 °C for Nanocapsule-D-TS and 290 °C for Nanocapsule-D-OS. The second step weight loss was 21% for the Nanocapsule-D-TS and 25% for the Nanocapsule-D-OS. According to the TGA analysis of the nanocapsules containing 1-tetradecanol, the first-step degradation of the Nanocapsule-T-TS carried out between 148 °C and 290 °C and they lost 75% of their weight. Nanocapsule-T-OS capsules exposed to first step degradation between the 135 °C and 250 °C, and they lost

62% of their weight. The second-step degradation occurred between 290 °C and 480 °C for the Nanocapsule-T-TS and between 270 °C and 450 °C for the Nanocapsule-T-OS. Their weight loss values were 26% and 34%, respectively (Table 6). It was concluded from the TGA analysis results the thermal decomposition temperature of the nanocapsules produced by the two-stage process increased compared to that of the nanocapsules produced by the one-step process. It was concluded that improving the thermal stability of nanocapsules was due to increased wall thickness.
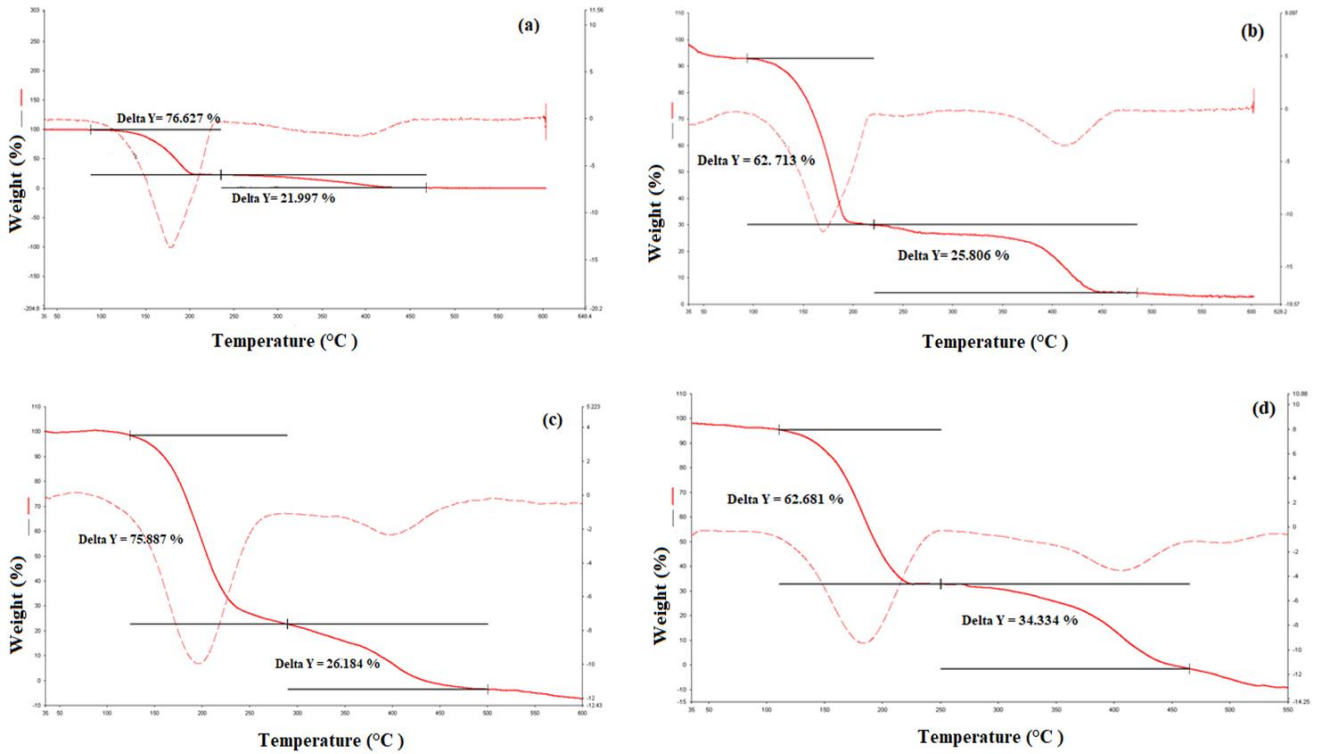
Figure 5. TGA curves of nanoencapsulated n-dodecanol (a: Nanocapsule-D-TS; b: Nanocapsule-D-OS) and nanoencapsulated 1-tetradecanol (c: Nanocapsule-T-TS; d: Nanocapsule-T-OS)

Table 6. TGA data of the nanocapsules

| Nanocapsule	Degradation temperature interval (°C)		Weight loss %
Nanocapsule-D-TS	148-200	(Stage 1)	76
	300-425	(Stage 2)	21
Nanocapsule-D-OS	125-200	(Stage 1)	62
	235-440	(Stage 2)	25
Nanocapsule-T-TS	148-290	(Stage 1)	75
	290-480	(Stage 2)	26
Nanocapsule-T-OS	135-250	(Stage 1)	62
	270-450	(Stage 2)	34
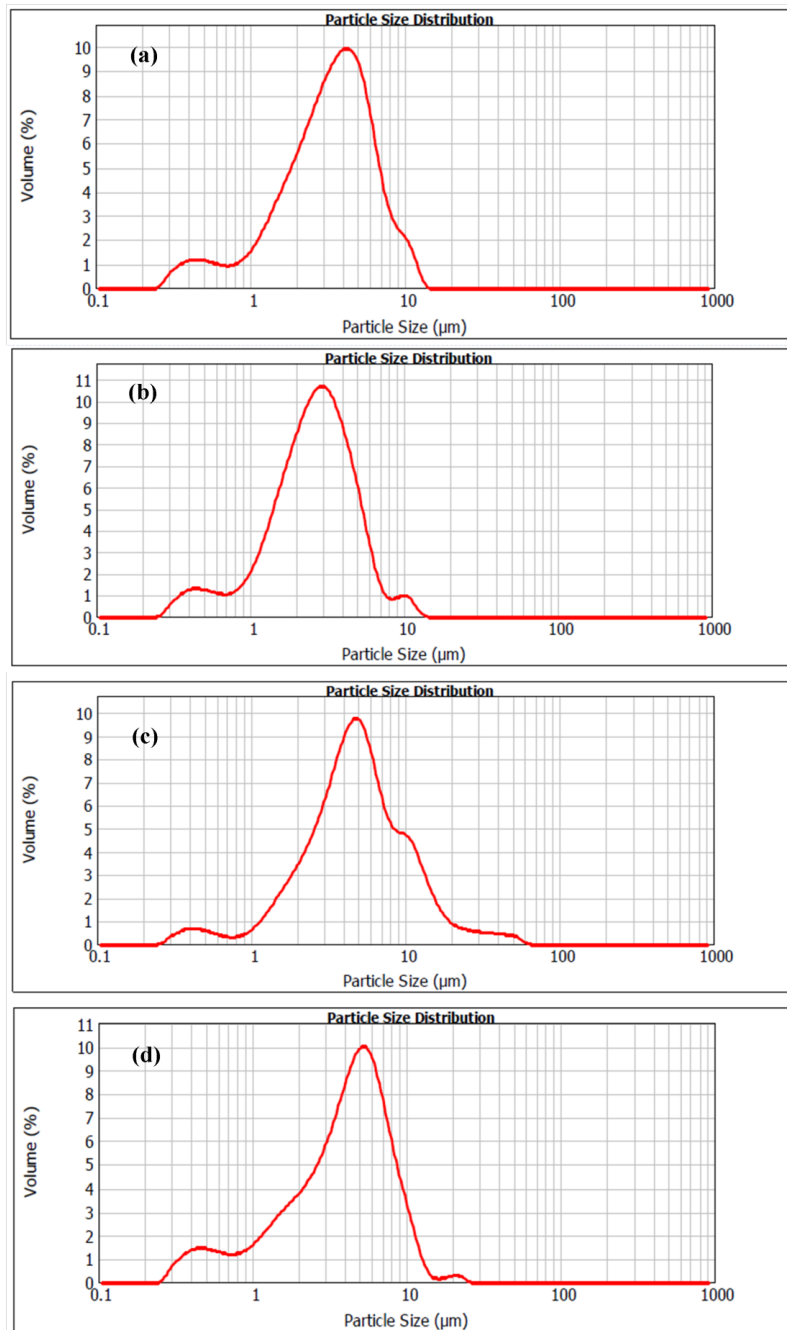
Figure 6. Particle size distribution curves of nanoencapsulated n-dodecanol (a: Nanocapsule-D-TS; b: Nanocapsule-D-OS) and 1-tetradecanol (c: Nanocapsule-T-TS; d: Nanocapsule-T-OS)

3.1.5. Particle size analysis of the nanocapsules

The particle size distribution (PSD) curves of the nanocapsules were given in Figure 6. The nanocapsules exhibited an almost homogenous particle size distribution. However, the average particle sizes measured by particle size instrument were determined bigger than the particle sizes observed as nano-size by TEM micrographics. This finding was consistent with the literature which revealed aggregation of nano-sized capsules during particle size analysis [33,41]. According to the PSD analysis, the mean particle sizes of the Nanocapsule-D-TS and nanocapsule-D-OS were measured as

3.41 μm (uniformity 0.53) and 2.65 μm (uniformity 0.51), respectively. Their particle sizes varied between 1-7 μm. Nanocapsule-T-TS and Nanocapsule-T-OS, containing 1-tetradecanol, had a mean particle size of 4.76 μm (uniformity 0.78) and 4.14 μm (uniformity 0.56), respectively. Their particle sizes varied between 1-12 μm.

3.2.1. SEM analysis of the nanofibers

In order to investigate the possibility of nanocapsule incorporation into the core of the fiber structure without clustering, core/sheath structured nanofiber production was

performed by the coaxial electrospinning method. PAN polymer solution was used as fiber sheath forming polymer and PEG/nanocapsule mixture solution was used for the production of the fiber core. Figure 7b showed the SEM images and fiber diameter distribution diagram of the core/sheath structured bicomponent nanofibers electrospun from PAN and PEG/nanocapsule solutions. Besides, SEM images of used nanocapsules (Nanocapsule-D-TS) and cross-section of the nanofiber web were given in Figure 7 a and Figure 7 c, respectively. According to the SEM images of the nanocapsules given in Figure 7a, the formation of spherical-shaped and uniform nano-sized particles was seen. The SEM images taken from the surface and cross-section of the nanofiber webs showed that nanocapsules were uniformly distributed in the whole body of bicomponent nanofibers without clustering. Both the fiber-like and nanocapsules-like morphologies were retained in the final nanofiber product similar to a rosary-like structure. PAN polymer was wrapped around the nanocapsules like a sheath. The settlement of the nanocapsules in fiber cross-section caused to become rough and coarse fiber morphological structure. However, the diameter distribution of fibers containing nanocapsules was uniform and the mean fiber diameter was almost 210 nm (210 nm, CV % 15,36). The uniformity of fiber diameters was a result of the regular distribution of nanocapsules in the fiber cross-section and was considered to be an indicator that the capsules are placed in the fiber cross-section without clustering.
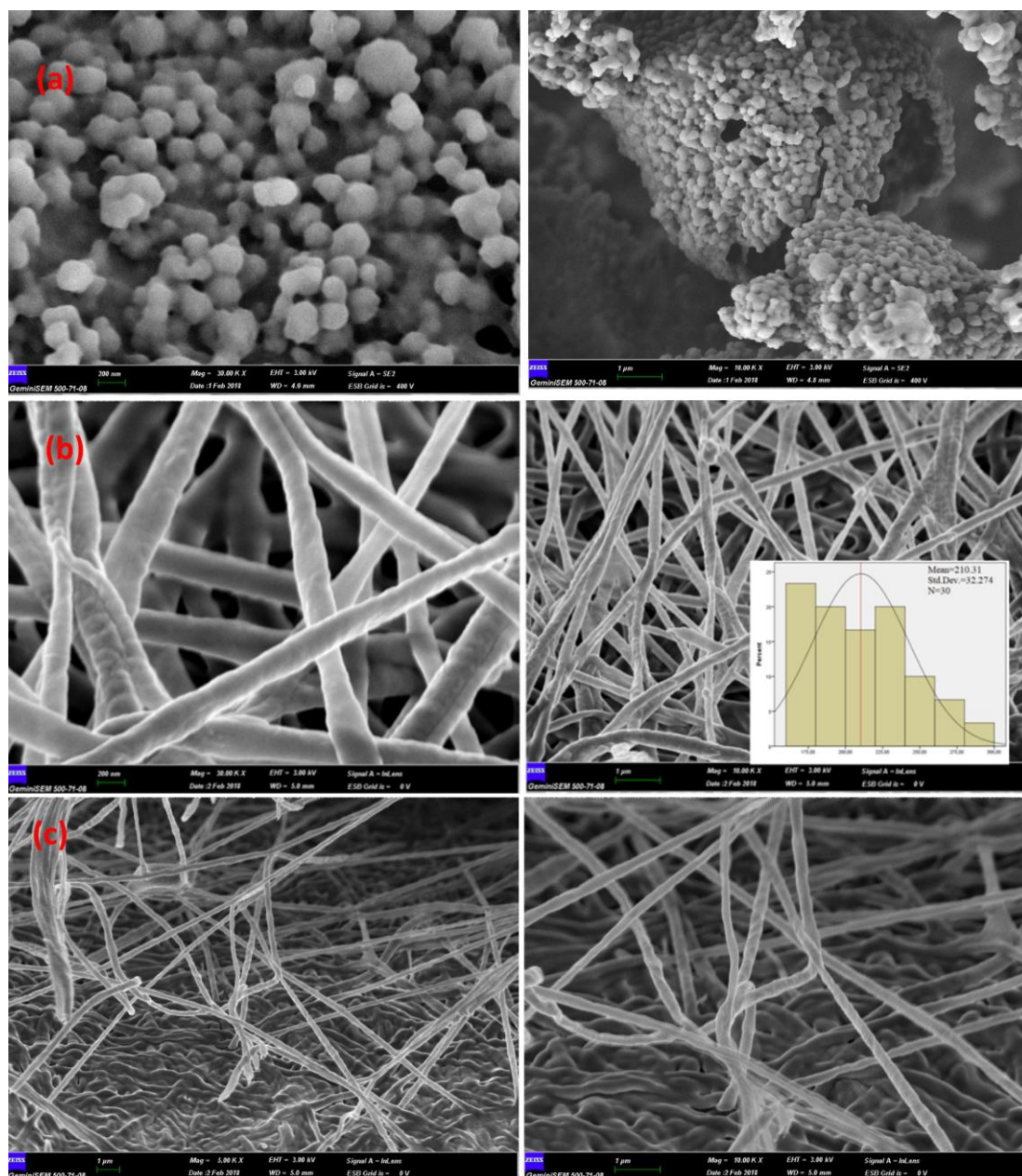

Figure 7. SEM images at different magnifications of the Nanocapsule-D-TS nanocapsules (a) and surface (b) and cross section (c) of the core/sheath structured bicomponent nanofibers

3.2.2. FT-IR analysis of the nanofibers

To investigate the chemical structure of the nanofibers containing Nanocapsule-D-TS capsules produced by the co-axial electrospinning method, FT-IR spectroscopy was used. Figure 8 showed the FTIR transmission spectra of the composite nanofibers, nanocapsules, and pure PAN nanofibers. The findings obtained from the spectra of the materials used in nanofibers production were given in the Table 7. The peak observed at 3425 cm^{-1} in the FT-IR spectrum of the nanofibers was overlapped stretching peaks of O-H groups in polyethylene glycol chains used as core polymer and O-H groups of the encapsulated n-dodecanol. Besides, –C-O stretching peaks at 1110 cm^{-1} and 1240 cm^{-1} wavelengths and C-H bending peak at 1348 cm^{-1} were characteristic peaks of the PEG polymer [21]. The peak at 2243 cm^{-1} in the FT-IR spectrum of nanofibers arose because of the stretching vibrations of the C≡N bonds of the PAN polymer. Besides, the peak at 1454 cm^{-1} was a -CH$_2$ twisting peak in the PAN chains [21,47]. The peaks at 2924 cm^{-1} and 2854 cm^{-1} were -C-H stretching vibrations of the encapsulated n-dodecanol. The peak at 1736 cm^{-1} in the FT-IR spectrum of the nanofibers belonged to the carbonyl groups of copolymer shell (P(MMA-co-MA)) of the nanocapsule.

3.2.3. DSC analysis of the nanofibers

DSC curve of the composite core-structured nanofibers containing Nanocapsule-D-TS nanocapsules was given in Figure 9. According to the DSC data, nanofibers stored 19.49 J/g of latent heat at 32.07 °C and released -24.25 J/g of energy at 27.41 °C. However, the melting and solidification temperatures of the nanofibers were found to be quite high compared to those of the capsules added to the structure.

Table 7. FT-IR analysis spectrum information of the nanofibers

| Materials	FT-IR spectrum bands
Nanocapsule-D-TS capsule	3390 cm^{-1} → O-H stretching peak of n-dodecanol 2924 cm^{-1} and 2854 cm^{-1} → C-H stretching peaks of n-dodecanol 1731 cm^{-1} → carbonyl peak of the copolymer shell
Polyethylene Glycol (PEG) polymer	3400-3450 cm^{-1} → O-H stretching peak 2890 cm^{-1} is for the C-H aliphatic stretching 1110 cm^{-1} and 1240 cm^{-1} → –C-O stretching peaks 1348 cm^{-1} → C-H bending peak
Polyacrylonitrile (PAN) polymer	2243 cm^{-1} → the stretching peak of the C≡N bonds 1454 cm^{-1} → -CH$_2$ twisting peak
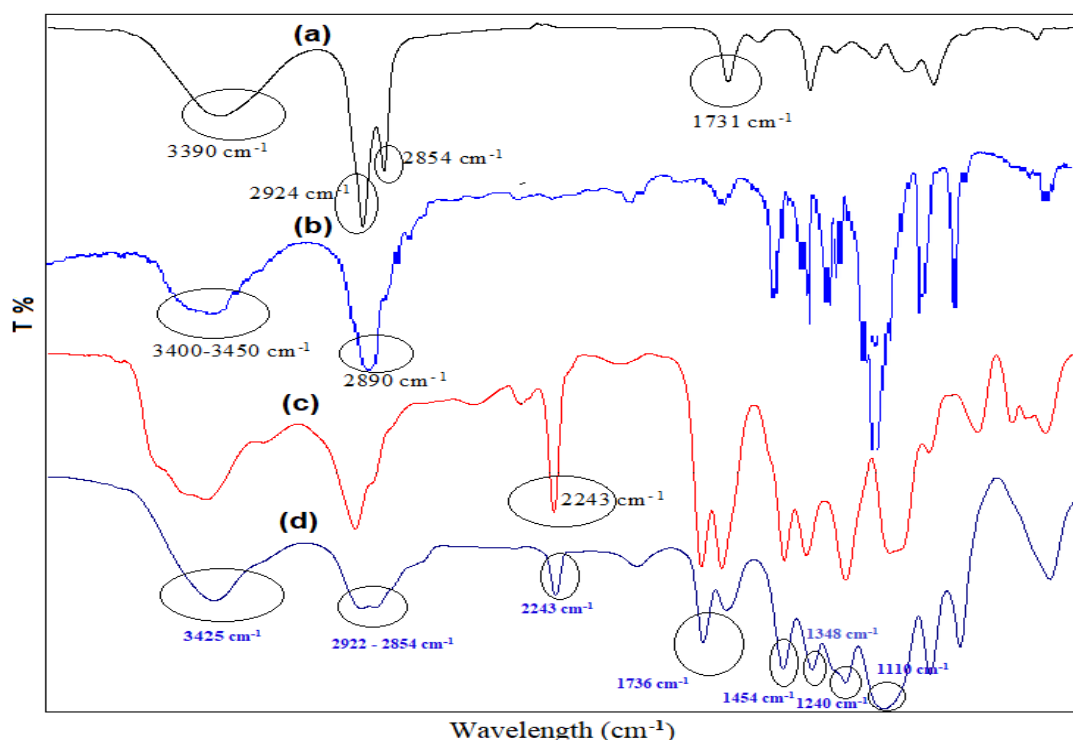
Figure 8. FT-IR spectrum of nanofibers (a: Nanocapsule-D-TS capsule; b:PEG nanofibers c:PAN nanofiber; d) the core/sheath structured bicomponent nanofibers)
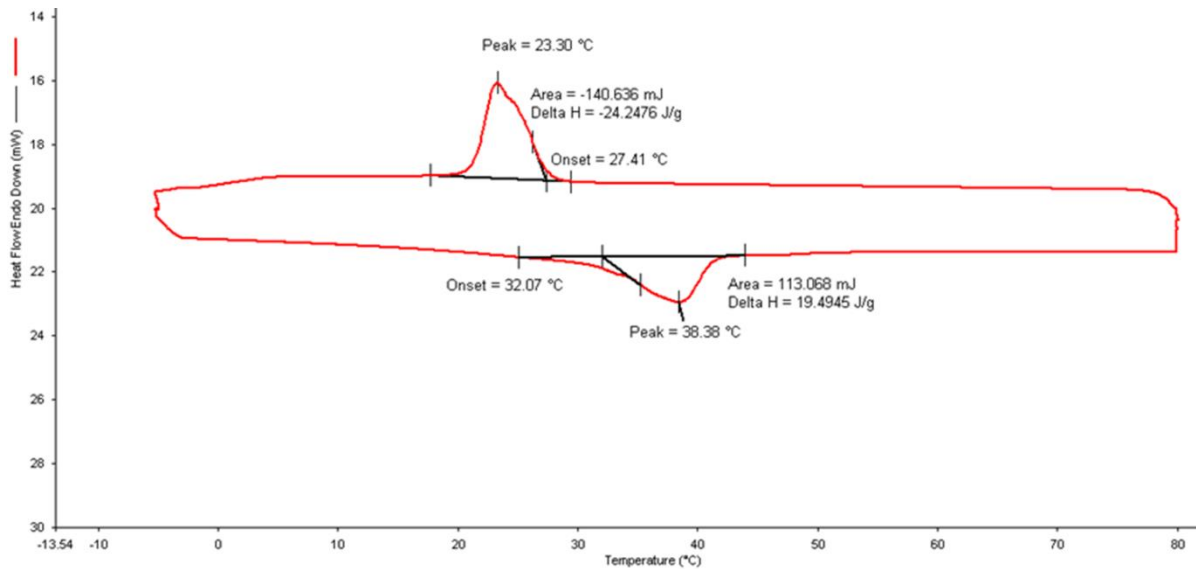
Figure 9. DSC curve of the core-structured composite nanofibers

4. CONCLUSION

In this study, n-dodecanol and 1-tetradecanol were nanoencapsulated for the usage as a thermal energy storage material. Capsule production was carried out using the oil-in-water emulsion polymerization method. Preparation of the nanocapsules with P(MM-co-MA) wall was carried out using conventional emulsion polymerization method and modified two-stage emulsion polymerization method. In the two-stage emulsion polymerization process, firstly MMA monomer was added to the emulsion, and polymerization reaction was started. After the polymerization reaction for 2 hours, both of the MMA and MA monomers were added to the reaction medium to complete the formation of the capsules' wall. According to the FT-IR analysis results, fatty alcohols were encapsulated in a poly(methyl methacrylate-co-methacrylic acid) wall successfully. Nanocapsules had typical core-shell structured, spherical-shaped, uniform nano-sized. The mean particle sizes of the nanoencapsulated n-dodecanol were measured as 3.41 μm for the TS process and 2.65 μm for the OS process. The mean particle sizes of the nanocapsules containing 1-tetradecanol were 4.76 μm for the TS process and 4.14 μm for the OS process. n-Dodecanol encapsulated by the two-stage process solidified at 19°C with the latent heat of 150.6 J/g and melted at 17 °C with the latent heat of 171.6 J/g. Nanocapsules prepared by the one-stage process solidified at 19 °C with the latent heat of 101.6 J/g and melted at 19 °C with the latent heat of 126.7 J/g. Nanoencapsulated 1-tetradecanol using the two-stage process absorbed latent heat of 158.7 J/g at 34 °C and released energy of 155.6 J/g at 34 °C. The nanocapsules prepared by the one-stage process absorbed energy of 145.8 J/g at 34 °C and released energy of 150.1 J/g at 35 °C. The enthalpy values of nanocapsules produced by the two-stage process were measured as higher and reached up to 171 J/g. TGA analysis results showed that the thermal decomposition temperature of the nanocapsules produced by the two-stage process increased compared to that of the nanocapsules produced by the one-step process. It was concluded that improvement in the thermal stability of the nanocapsules was due to increased wall thickness. According to the TEM analysis results, typical core-shell structured, spherical-shaped, uniform nano-sized particles were obtained, and the fatty alcohols were encapsulated using one-stage and two-stage emulsion polymerization processes, successfully. In the study, a nanocapsule sample prepared by the two-stage process was incorporated in polyacrylonitrile nanofibers using a co-axial electrospinning method to fabricate nanofibers with nanocapsule core and PAN sheath. Composite nanofibers having 19 J/g energy storage capacities and unimodal diameter distribution were produced. The surfaces of the nanofibers were rough and coarse but the capsules were placed in the fiber cross-section without clustering. As a result, the nanofibers produced in the study have thermal energy storage capacity, which has the potential to be integrated into technical textile structures such as protective clothing or medical textiles. Nanocapsules prepared in the study also can be evaluated as an additive to be able to apply to fabrics by conventional chemical application methods to produce textiles with thermal energy storage properties. In addition, in the future, studies on the encapsulation of the nanocapsules prepared in this study by various sheath polymers suitable for different usage areas can be conducted.

REFERENCES

1. Sarier N, Onder E. 2012. Organic phase change materials and their textile applications: an overview. *Thermochimica Acta,* 540, 7-60.

2. Geng L, Wang S, Wang R, Luo R. 2016. Facile synthesis and thermal properties of nanoencapsulated n-dodecanol with SiO2 shell as shape-formed thermal energy storage material. *Energy & Fuels,* 30(7), 6153-6160.

3. Ghosh SK. 2006. *Functional coatings by polymer microencapsulation.* Germany: Wiley-VCH Verlag GmbH&Co.KGaA.

4. Alkan C, Sarı A, Karaipekli A, Uzun O. 2009. Preparation, characterization, and thermal properties of microencapsulated phase change material for thermal energy storage. *Solar Energy Materials and Solar Cells,* 93(1), 143-147.

5. Sarı A, Alkan C, Karaipekli A, Uzun O. 2009. Microencapsulated n-octacosane as phase change material for thermal energy storage. *Solar Energy,* 83(10), 1757-1763.

6. Yu F, Chen ZH, Zeng XR. 2009. Preparation, characterization, and thermal properties of microPCMs containing n-dodecanol by using different types of styrene-maleic anhydride as emulsifier. *Colloid Polymer Science,* 287(5), 549–560.

7. Yu F, Chen ZH, Zeng XR. 2009. Preparation and characterization of thermal energy storage microcapsulated n-dodecanol by phase change. *Polymer Materials Science & Engineering,* 25(6), 135-138.

8. Huang R, Li W, Wang J, Zhang X. 2017. Effects of oil-soluble etherified melamine-formaldehyde prepolymers on in situ microencapsulation and macroencapsulation of n-dodecanol. *New Journal of Chemistry,* 41(17), 9424-9437.

9. Su JF, Wang SB, Zhou JW, Huang Z, Zhao YH, Yuan XY, Zhang YY, Kou JB. 2011. Fabrication and interfacial morphologies of methanol–melamine–formaldehyde (MMF) shell microPCMs/epoxy composites. *Colloid Polymer Science,* 289(2), 169-177.

10. Zhang H, Li W, Huang R, Wang J, Zhang X. 2017. Effects of polyvinyl alcohol modification on microstructure, thermal properties and impermeability of microencapsulated n dodecanol as phase change material. *Chemistry Select,* 2(29), 9369-9376.

11. Chen C, Chen Z. Zeng X, Fang X, Zhang Z. 2012. Fabrication and characterization of nanocapsules containing n-dodecanol by miniemulsion polymerization using interfacial redox initiation. *Colloid Polymer Science,* 290(4), 307-314.

12. Chen ZH, Yu F, Zeng XR, Zhang ZG. 2012. Preparation, characterization and thermal properties of nanocapsules containing phase change material n-dodecanol by miniemulsion polymerization with polymerizable emulsifier. *Applied Energy,* 91(1), 7-12.

13. Ma Y, Zong J, Li W, Chen L, Tang X, Han N, Wang J, Zhang X. 2015. Synthesis and characterization of thermal energy storage microencapsulated n-dodecanol with acrylic polymer shell. *Energy,* 87, 86-94.

14. Chen Z, Wang J, Yu F, Zhang Z, Gao X. 2015. Preparation and properties of graphene oxide-modified poly(melamine-formaldehyde) microcapsules containing phase change

15. Yu F, Chen ZH, Zeng XR, Gao XN, Zhang ZG. 2015. Poly(methyl methacrylate) copolymer nanocapsules containing phase change material (n-dodecanol) prepared via miniemulsion polymerization. *Journal of Applied Polymer Science,* 132(31), 1-7.

16. Li W, Zong J, Huang R, Wang J, Wang N, Han N, Zhang X. 2016. Design, controlled fabrication and characterization of narrow-disperse macrocapsules containing Micro/NanoPCMs. *Materials & Design,* 99, 225-234.

17. Wu N, Xu L, Zhang C. 2018. The influence of emulsifiers on preparation and properties of microencapsules of melamine–urea–formaldehyde resins with n-dodecanol as phase change material. *Advances in Polymer Technology,* 37(8), 3492-3498.

18. Cai Y, Ke H, Lin L, Fei X, Wei Q, Song L, Fong H. 2012. Preparation, morphology and thermal properties of electrospun fatty acid eutectics/polyethylene terephthalate form-stable phase change ultrafine composite fibers for thermal energy storage. *Energy Conversion and Management,* 64, 245- 255.

19. Cai Y, Zong X, Zhang J, Du J, Dong Z, Wei Q, Zhao Y, Chen Q, Fong H. 2014. The improvement of thermal stability and conductivity via incorporation of carbon nanofibers into electrospun ultrafine composite fibers of lauric acid/polyamide 6 phase change materials for thermal energy sorage. *International Journal of Green Energy,* 11(8), 861-875.

20. Sun SX, Xie R, Wang XX, Wen GQ, Liu Z, Wang W, Ju XJ, Chu LY. 2015. Fabrication of nanofibers with phase-change core and hydrophobic shell, via coaxial electrospinning using nontoxic solvent. *Journal of Materials Science,* 50(17), 5729-5738.

21. Noyan ECB, Onder E, Sarier N, Arat R. 2018. Development of heat storing poly(acrylonitrile) nanofibers by coaxial electrospinning. *Thermochimica Acta,* 662, 135-148.

22. Hu W, Yu X. 2014. Thermal and mechanical properties of bio-based PCMs encapsulated with nanofibrous structure. *Renewable Energy,* 62, 454- 458.

23. Zdraveva E, Fang J, Mijovic B, Lin T. 2015. Electrospun poly(vinyl alcohol)/phase change material fibers: morphology, heat properties, and stability. *Industrial & Engineering Chemistry Research,* 54(35), 8706-8712.

24. Lu Y, Xiao X, Zhan Y, Huan C, Qi S, Cheng H, Xu G. 2018. Core-sheath paraffin-wax-loaded nanofibers by electrospinning for heat storage. *ACS Applied Materials & Interfaces,* 10(15), 12759-12767.

25. Lu Y, Xiao X, Fu J, Huan C, Qi S, Zhan Y, Xu G. 2019. Novel smart textile with phase change materials encapsulated core-sheath structure fabricated by coaxial electrospinning. *Chemical Engineering Journal,* 355, 532-539.

26. McCann JT, Marquez M, Xia Y. 2006. Melt coaxial electrospinning: A versatile method for the encapsulation of solid materials and fabrication of phase change nanofibers. *Nano Letters,* 6(12), 2868- 2872.

27. Chen C, Zhao Y, Liu W. 2013. Electrospun polyethylene glycol/cellulose acetate phase change fibers with core-sheath

sctructure for thermal energy storage. *Renewable Energy, 60,* 222.-225.

28. Van Do C, Nguyen TTT, Park JS. 2013. Phase-change core/shell structured nanofibers based on eicosane/poly (vinylidene fluoride) for thermal storage applications. *Korean Journal of Chemical Engineering, 30*(7), 1403-1409.

29. Dang, TT, Nguyen TTT, Chung OH, Park JS. 2015. Fabrication of form-stable poly(ethylene glycol)-loaded poly(vinylidene fluoride) nanofibers via single and coaxial electrospinning. *Macromolecular Research, 23*(9), 819-829.

30. Sun SX, Xie R, Wang XX, Wen GQ, Liu Z, Wang W, Ju XJ, Chu LY. 2015. Fabrication of nanofibers with phase change core and hydrophobic shell, via coaxial electrospinning using nontoxic solvent. *Journal of Materials Science, 50*(17), 5729–5738.

31. Sarier N, Arat R, Menceloğlu Y, Önder E, Boz EC, Oğuz O. 2016. Production of PEG grafted PAN copolymers and their electrospun nanowebs as novel thermal energy storage materials. *Thermochimica Acta, 643,* 83- 93.

32. Babapoor A, Karimi G, Golestaneh SI, Mezjin MA. 2017. Coaxial electro-spun PEG/PA6 composite fibers: Fabrication and characterization. *Applied Thermal Engineering, 118,* 398- 407.

33 Alkan C, Alay Aksoy S, Altun Anayurt R. 2015. Synthesis of poly(methyl methacrylate-co-acrylic acid)/n-eicosane microcapsules for thermal comfort in textiles, *Textile Research Journal, 85*(19), 2051–2058.

34. Chang CC, Tsai YL, Chiu JJ, Chen H. 2009. Preparation of phase change materials microcapsules by using PMMA network-silica hybrid shell via sol-gel process. *Journal of Applied Polymer Science, 112*(3), 1850- 1857.

35. Sarı A, Alkan C, Karaipekli A. 2010. Preparation, characterization and thermal properties of PMMA/ n-heptadecane microcapsules as novel solid-liquid microPCM for thermal energy storage. *Applied Energy, 87*(5), 1529-1534.

36. Qiu X, Li W, Song G, Chu X, Tang G 2012. Microencapsulated n-octadecane with different methylmethacrylate-based copolymer shell as phase change materials for thermal energy stgorage. *Energy, 46*(1), 188-199.

37. Wang Y, Shi H, Xia TD, Zhang T, Feng HX. 2012. Fabrication and performances of microencapsulated paraffin composites with polymethylmethacrylate, *Materials Chemistry and Physics, 135*(1), 181-187.

38. Sarı A, Alkan C, Biçer A, Altuntas A. Bilgin C. 2014. Micro/nanoencapsulated n-nonadecane with poly(methyl methacrylate) shell for thermal energy storage. *Energy Conversion and Management, 86,* 614–621.

39. Al-Shannaq R, Farid M, Al-Muhtaseb S, Kurdi J. 2015. Emulsion stability and cross-linking of PMMA microcapsules containing phase change materials. *Solar Energy Materials and Solar Cells, 132,* 311-318.

40. Özkayalar S. 2019. Production and textile application of double-walled nano and microcapsules with phase change material core (Master's thesis). Available from http://tez.sdu.edu.tr/Tezler/TF04267.pdf.

41. Alay Aksoy S, Alkan C, Tözüm MS, Demirbağ S, Altun Anayurt R, Ulcay Y. 2017. Preparation and textile application of poly(methyl methacrylate-co-methacrylic acid)/n-octadecane and n-eicosane microcapsules. *The Journal of the Textile Institute*, 108(1), 30-41.

42. Moghe AK, Gupta BS. 2008. Co-axial electrospinning for nanofiber structures: preparation and applications. *Polymer Reviews, 48*(2), 353-377.

43. Onder E, Sarier N, Arat R. 2017. The manufacture of organic carbonate-poly (methyl ethylacrylate) nanowebs with thermal buffering effect. *Thermochimica Acta, 657,* 170-184.

44. Wang H, Gui P, Zhu Y, Hu S. 2020. Preparation and characterization of poly(melamine-urea-formaldehyde) tetradecanol microcapsules coated with silver particles. *Journal of Wuhan University of Technology-Material Science Edition, 35*(2), 327-334.

45. Panák O, Držková M, Svoboda R, Gunde MK. 2017. Combined colorimetric and thermal analyses of reversible thermochromic composites using crystal violet lactone as a colour former. *Journal of Thermal Analysis and Calorimetry*, 127(1), 633-640.

46. Tozum MS, Alay-Aksoy S, Alkan C. 2018. Microencapsulation of three-component thermochromic system for reversible color change and thermal energy storage. *Fiber Polymers, 19*(3), 660- 669.

47. Ribeiro RF, Pardini LC, Alves NP, Brito CAR. 2015. Thermal stabilization study of polyacrylonitrile fiber obtained by extrusion. *Polimeros, 25*(6), 523–530.

The Effect Of Recycled Polyester (rPET) Filament Fiber Properties On Various Woven Fabric Performance Properties

Gül KIRIŞ[1] 0000-0001-5209-2435
Demet YILMAZ[2] 0000-0003-4450-5935

[1] KFS Sentetik San. ve Tic. A.Ş., Sakarya, Turkey
[2] Suleyman Demirel Üniversity, Engineering Faculty, Textile Engineering Dept., West Campus, Isparta, Turkey

Corresponding Author: Demet Yılmaz, demetyilmaz@sdu.edu.tr

ABSTRACT

In order to reduce the requirement of waste eliminating and environmental pollution, recycling seems to be a suitable solution. In this study, polyester fibers with three different number of filament and two fiber cross section form (round and plus) were spun from recycled polyethylene terephthalate (rPET) polymer and texturised on an industrial scale. rPET yarns were used as a weft yarn in woven fabric production. Fabric performance properties such as breaking, tearing and seam slippage resistance, weight, breaking elongation, abrasion resistance and air permeability were analysed and compared with that of virgin PET fabrics. As a result of this study, it was determined that virgin and rPET polymers provided almost similar fabric properties. Higher number of filaments gave lower fabric breaking elongation, seam strength, abrasion resistance and air permeability values while led to higher tearing strength. Except fabric weight and tensile properties, filament cross section had a significant affect on other studied fabric properties.

1. INTRODUCTION

Today, the production and consumption of packaged products (plastics, metal, glass, paper, cardboard etc.) increase with living standards and population growth. Packaging industry constitutes the biggest part of the world polyethylene terephthalate (PET) consumption with 29% share. PET products are disposed after usage, resulting in waste. PET packaging materials make up a large amount, such as 73% of environmental waste. As well as metal, glass, paper and cardboard, PET wastes are classified as solid waste. In our country, paper/cardboard and then PET wastes constitute the biggest share of solid wastes [1]. While most of these wastes are stored in regular storage facilities, the remaining part is disposed by methods such as burning, burying in the ground, and pouring into the stream. PET wastes, which are tried to be disposed by burying in the soil or storing, can remain for a very long time (up to 3000 years) without degrading. As a result of accumulation, incineration or burial of waste, many ecological problems arise. Reduction of suitable areas for the waste disposal, increased environmental pollution and high disposal costs have led to find new methods for optimum use of resources and waste reduction or utilization. Recycling or recovery seems to be the most likely solution for waste disposal. For this reason, recycling is carried out in order to transform the wastes into secondary raw materials and thus to be included in the production process again. PET can now be recycled by mechanical and chemical methods and in modern facilities. Polyester fibers can be obtained by recycling PET wastes and the resulting fibers are called recycled polyethylene terephthalate or rPET. Therefore, in present days, PET and rPET polymers have been used for polyester spun fiber production.

In this study, polyester fibers with different number of filament (filament fineness) and fiber cross section were produced from rPET polymer in order to investigate the

possibility of different rPET polyester fibre production from PET wastes. Additionally, it was researched the effect rPET fiber properties on various performance properties of woven fabrics. On the other hand, rPET fibers have already been used for secondary textile products like as carpet bottoms, sleeping bags and insulation materials [2]. Therefore, the use of fibers in different areas needs to be explored and present study will contribute to the evaluation of plastic wastes for new usage areas.

In literature, Uyanık (2019) studied the usage of recycle polyester fiber (rPET) in different yarn count and blend ratio and so to determine which count and blend ratio is more suitable for rPET usage [3]. Qin et al. (2018) melt-spun five different poly (ethylene terephthalate) (PET) materials (two recycled and three virgin ones) into fibres using a capillary rheometer and aerodynamic stretching. In the study, surface smoothness, diameter and mechanical properties of the PET fibres were investigated [4]. Yuksekkaya et al. (2016) studied the properties of yarns and knitted fabrics produced by virgin PET, rPET, virgin and recycled cotton fibers [5]. Sanches et al. (2015) in their study compared the fabric properties knitted from two types 80/20% PET/rPET and 50/50% rPET/cotton yarns [6]. He et al. (2014) compared the surface morphology, mechanical properties, and internal fiber structure of recycled and virgin PET fibers [7]. Telli and Özdil (2015) analysed bursting strength, abrasion resistance, air permeability, surface friction, circular bending rigidity and dimensional stability properties of knitted fabrics produced from rPET and blends with PET and cotton fibers [2]. Koo et al. (2013) studied mechanical and chemical recycling processes and examined their effects on yarn properties such as tensile properties, thermal characteristics, hydrolysis and photo-degradation [8]. Kostov et al. (2013) established proper conditions for secondary polyethylene terephtalate (PET) fiber production. In the study, yarn linear density, breaking strength and elongation and thermal properties of the primary and secondary PET fibers were characterized [9]. Telli and Ozdil (2013) studied the performance of recycle polyester and virgin polyester blended yarns with cotton at different blend ratios (100%, 70/30%, 50/50%, and 30/70%) [10]. Lee et al. (2012) obtained recycled poly(ethylene terephthalate) (PET) chips from used water bottles and was extruded with virgin fiber-grade PET chips in blends of 20, 40, and 70 wt%. The mechanical properties of recycled PET/virgin PET blend fibers were analyzed using thermogravimetric analysis (TGA), differential scanning calorimetry (DSC), bi-refringence measurements, and tensile tests [11]. Abbasi et al. (2007) continuous filament yarns from virgin PET chips and used PET bottles

were produced at the two take-up speeds and compared of optical bi-refringence, crystallinity, tenacity, breaking elongation, initial modulus, and shrinkage of yarns [12].

As given above, majority of the studies conducted in the literature focused on the analysis of rPET fiber spinning parameters and also yarn production from rPET staple fibers. However, there is not enough research on the effect of different rPET fiber properties on various fabric properties. The main objective of this research is to present a comparative analysis of breaking, tearing and seam slippage resistance, breaking elongation, abrasion resistance and air permeability properties of multifilament rPET fabrics having different number of filaments and cross-section shapes of a filament. In scope of the study, woven fabrics obtained from virgin and recycled PET polymers were also compared. Therefore, with this study, it will be presented many findings about the effect of polymer type, number of filament (filament fineness) and fiber cross section on woven fabric performance properties.

2. MATERIAL AND METHOD

2.1 Material

In the study, firstly, virgin polyester (PES) yarn with 125 denier filament fineness, 36 number of filament and round section form was produced from semi-matt polyethylene terephthalate (PET) polymer. And then, 125 denier filament fineness and 36-48-72 number of filaments recycled polyester (rPET) yarns were spun with round and plus cross section forms from the recycled polyethylene terephthalate (rPET) polymer. Physical properties of virgin polyethylene terephthalate (PET) and recycled polyethylene terephthalate (rPET) polymers are given in Table 1.

2.2 Method

Fibre production was realized under three stages as following:

- In the first part of the study, partially oriented polyester yarns (POY) were produced from virgin polyethylene terephthalate (PET) and recycled polyethylene terephthalate (rPET) polymers with the usage of the same fineness (125 denier), number of filament (36F) and fiber cross-section form (round), and the obtained yarns were texturized. The effect of polymer type on woven fabric properties was investigated. Virgin polyester yarns were named as PET-36R while recycled yarns were shown by rPET-36R.

Table 1. Physical properties of virgin (PET) and recycled polyethylene terephthalate (rPET) polymers

PET	Colour	Ash (%)	Polymer Size (Chips/g)	Melting temperature (°C)	Viscosite (dL/g)
PET	Semi-dull	0.3	30	255	0.62
rPET	Semi- dull	0.3	35	253	0.65

- In the second part of the study, partially oriented polyester yarns (POY) having three different number of filaments (36F, 48F and 72F) were produced from rPET polymer with the usage of the same fineness (125 denier) and fiber cross-section form (round), and the obtained yarns were texturized. The effect of different filament fineness on woven fabric properties was examined. rPET-36R, rPET-48R and rPET-72R naming was used for 36, 48 and 72 number of filaments.

- In the third part of the study, round and plus form fiber cross sectional polyester yarns (POY) were produced from rPET polymer with the usage of the same fineness (125 denier) and number of filaments (48F), and the obtained yarns were texturized. In this section, the effect of different fiber cross-section form on woven fabric properties was researched. rPET-48R and rPET-48P naming was used for round and plus fiber cross section forms [13].

Partially oriented (POY) polyester filament yarn production

This study was realized at the polyester yarn production mill, and virgin and recycled polyester fibres were spun based on melt spinning method on an industrial scale. Polyethylene terephthalate (PET) and recycled polyethylene terephthalate (rPET) polymers with chips form were conveyed to silos and subjected to crystallization process. The crystallized polymers were delivered to the drying unit and then to the extruder. The extruder line used in the study has a 4-stage heating system by increasing the amount of heat at each stage. Since the pollution rate of the rPET polymer is higher than that of the original PET polymer, heater temperature in the extruder were increased by 2 degrees for rPET polymer in comparison to that of the PET polymer. Melt polymer was filtered and filter pore size was set as 20 micron. The filtered solution was translated to nozzle having 36, 48 and 72 number of holes, and circular and plus hole cross sections (Figure 1). Each spun polyester fiber was cooled with cold air flow at the exit of the nozzle holes and air flow rate for all yarns was 0.40 m/sec. The spin-finish oil (oil rate 0.4%) was applied to the yarn in order to remove the static load and to decrease the friction coefficient. In partially oriented yarn (POY) production, the draft ratio was close to 1. Virgin and recycled polyester (POY) spun yarn production parameters were given in Table 2. Cross-sectional images of some yarn samples were taken by Projectina DMM2000 model microscope (Figure 2).

| (a) | (b) |

Figure 1. Circular (a) and plus cross section form (b)

Table 2. Production parameters of the virgin (PET) and recycled polyethylene terephthalate (rPET) yarns

Parameters	Sample type				
	PET-36R	rPET-36R	rPET-48R	rPET-72R	rPET-48P
1st zone temperature of extruder (°C)	274	275	275	275	275
2nd zone temperature of extruder (°C)	279	280	280	280	280
3rd zone temperature of extruder (°C)	284	286	286	286	286
4th zone temperature of extruder (°C)	285	287	287	287	287
Winding speed (m/min)	3200	3200	2900	2900	2900
Godet 1 speed (m/min)	3239	3239	2937	2937	2937
Godet 2 speed (m/min)	3251	3251	2947	2947	2947
Pomp speed (rpm)	14.3	14.3	13	13	13

| PET-36R | rPET-36R | rPET-48P |
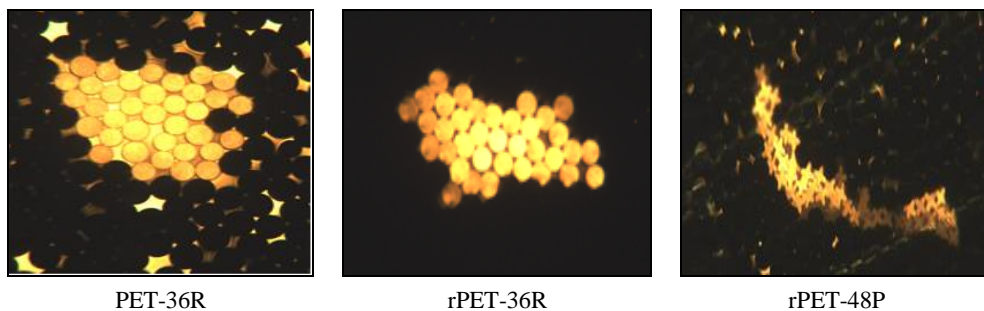
Figure 2. The optical microscope images of yarn samples

Texturing

Partially oriented (POY) yarns were textured by friction-disc texturing method and friction-disc texturing machine (Barmag). Before texturing, filament yarns were heated, cooled and then drafted between the Godet cylinders and heater. In the texturing process, polyurethane (PU) discs were used and the disc layout consisted of 1-5-1 combination. After the texturing, fixing was realized by second heating process and then cone oil was applied to the yarn. Textured yarn samples were produced on the same line and production parameters are given in Table 3.

Woven fabric production

Fabric samples were woven from all spun and texturized polyester yarn samples. Yarn samples were used as a weft yarn. Jacquard loom woven machine (Itema firm) and sateen weave type was used. During the weaving process, fully drawn polyester yarn (FDY) was used as a warp yarn for all woven samples. Warp yarns were kept constant to analyse the fabric properties. The parameters of woven fabric production are given in Table 4.

2.3. Test and analysis

Fabric weight of all woven fabrics was tested according to TS 251. Tensile and tearing strength, breaking elongation as well as the seam slippage are one of the properties determining the usage area of textile fabrics. Tensile strength and breaking elongation properties of woven fabrics obtained from all texturized polyester yarns were tested according to the strip method by Titan-Universal Strength Tester based on the EN ISO 13934-1 test standard. Tearing strength of woven fabrics was analysed on the Titan-Universal Strength Tester test device using the single-tonque method according to EN ISO 13937-2 test standard. Three samples were tested for each fabric type in the weft and warp direction for tensile properties of the fabrics. Seam slippage resistance is common test for the textile mill and therefore seam slippage resistance properties of woven fabrics were determined by Titan-Universal Strength Tester according to EN ISO 13936-2 (60 N) standard. In order to determine the abrasion resistance of woven fabrics, fabric samples were tested by Martindale abrasion tester according to EN ISO 12947-2 standard and number of abrasion cycles was determined when the first three yarn breaks occurred. Air permeability properties of the fabric samples were tested to evaluate the comfort-related properties of the fabrics according to TS 391 EN ISO 9237 standard by FX 3300 model air permeability.

All the tests were carried out on the same testers and test results were analysed statistically by SPSS 16.0 statistical software to determine any significant differences. ANOVA tests were used for two-way analysis of variance for the analysis of the production parameters, multiple-range test LSD method for the comparison of filament fineness and t-test for the comparison of polymer type and fiber cross section form and ANOVA analyses were performed for $\alpha=0.05$ significance level [13].

3. RESULTS AND DISCUSSION

Within the scope of the study, woven fabrics produced from virgin and recycle polyester filament yarns and their performance properties were examined. Sample codes are summarized in Table 5 and the results for warp and weft directions of woven fabrics were shown by WRP and WFT, respectively.

Table 3. Production parameters for texturing process

Parameters	Sample				
	PET-36R	rPET-36R	rPET-48R	rPET-72R	rPET-48P
Production speed (m/min)	650	600	600	600	600
Draft ratio	1.73	1.71	1.67	1.71	1.67
Disk speed (m/min)	1170	1100	1070	1100	1070
First heater temperature (°C)	180	140	175	140	175
Second heater temperature (°C)	160	130	150	130	150

Table 4. Woven fabric production parameters

Parameters	Value
Machine speed (rpm)	278
Weft density (yarn/cm)	50
Warp density (yarn/cm)	60
Weave type	Sateen (5:1)
Weft yarn	PET-36R, rPET-36R, rPET-48R, rPET-72R, rPET-48P
Warp yarn	30 denier, 12F, FDY circular fiber cross section, 1000 tpm (Z)

Table 5. Explanation for sample codes

Sample code	Polymer	Filamant fineness	Number of filament	Fiber cross-section
PET-36R	PET		36	Round (R)
rPET-36R	rPET		36	Round (R)
rPET-48R	rPET	125 denye	48	Round (R)
rPET-72R	rPET		72	Round (R)
rPET-72P	rPET		48	Plus (P)

3.1 Fabric weight

Fabric weight results of woven fabrics were given in Figure 3. When the results were examined, it was observed that different polymer (PET-36R and rPET-36R) and filament cross section types (rPET-48R and rPET-48P) had no significant effect on fabric weight. As to the effect of filament fineness (number of filament), all the fabrics (rPET-36R, rPET-48R and rPET-72R) had almost similar fabric weight values. However, fabric weight slightly decreased with the increase in the number of filaments and the lowest weight value was obtained in the highest filament number. In any case, as seen in Figure 3, all the fabrics had almost similar fabric weight values and there were not considerably differences in the fabric weight values. On the other hand, this study was realized in a mill and the firm planned to use the yarns for sport textiles. Finer warp yarns were used during the woven fabric production and produced yarn samples were used as a weft yarn. Due to finer warp yarns, the weight of fabric samples varied about 67-69 g/m^2.
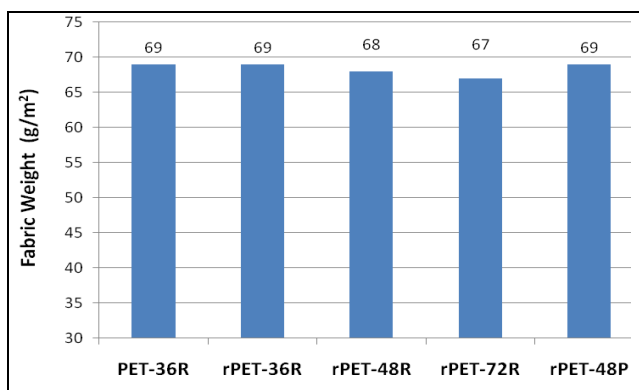

Figure 3. Fabric weight results

3.2. Breaking strength

In order to determine the effect of different polymer type, number of filament and fiber cross section on the mechanical properties of the fabrics, the breaking strength of woven fabrics was tested in the warp and weft directions. Particularly, in the weft direction, it was determined that all the fabrics have tensile strength values above 600 N and they exhibit similar behaviour. As to warp direction, it was observed different trends depending on fiber properties. The results are given in Figure 4 while ANOVA statistical analysis results were shown in Table 6-7.

When the effect of different polymer type on breaking strength of fabrics was examined, similar tensile strength values were determined for the fabrics (PET-36R and rPET-36R) obtained from virgin and recycled PET polymers. Additionally, the polymer type did not have statistically significant effect on the fabric tensile strength values (Table 6). Similar case was also observed for the effect of the number of filaments and filament cross section shape. There were not statistically significant differences in

the rPET-36R, rPET-48R and rPET-72R fabrics (Table 7). Also, the differences between circular (rPET-48R) and plus (rPET-48P) fiber cross sections were found statistically insignificant at 5% level (Table 6).
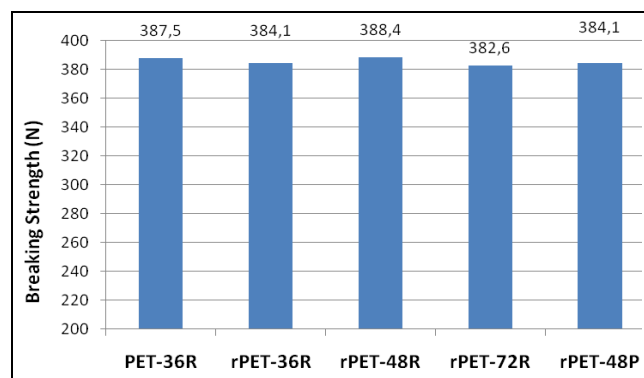
Figure 4. Breaking strength results of woven fabrics for warp direction

Actually, this result is not surprising and it was determined that texturized yarns produced from different polymer type (PET-36R and rPET-36R) and fiber cross section (rPET-48R and rPET-48P) had statistically similar yarn strength values [13]. Therefore, there was not statistically significant difference in breaking strength values of the fabrics woven from PET-36R and rPET-36R, or rPET-48R and rPET-48P yarns.

In literature, Koo et al. (2013) determined that tensile strains of mechanical and chemical recycled PET yarns are lower than that of virgin PET yarn [8]. However, He et al. (2014) indicated that recycled polyester fibers have a better tensile strength and breaking elongation than virgin ones and this result was explained by a bigger intermolecular force and thus, higher degree of crystallinity [7]. Therefore, the findings of virgin and recycled polyester fibers on yarn strength and breaking elongation do not show a single trend. Regarding the effect of filament cross section, Babaarslan and Haciogullari (2013) determined high tenacity and breaking elongation values in round cross sectional shaped POY yarns and reported that tensile properties of the yarns with multi-channelled cross-sectional shapes such as hexsa were low. This case was interpreted that multi-channelled structure makes the yarn less resistant to breaking due to the change in individual fiber tenacity [14]. In this study, it was also determined that the fabric obtained from circular cross section form had insignificantly higher fabric breaking strength values compared to plus cross-sectional shape. On the other hand, Behera and Singh (2014) determined that cross sectional shapes have minor influence on tensile behaviour of polyester fabric [15].

On the other hand, Özkan and Babaarslan (2010) determined that yarn strength values increase up to a certain number of filaments and then tend to decrease with the increase in the number of filaments [16]. This result was similar to the breaking strength of woven fabrics. In fact,

they expected an increase in yarn strength and breaking elongation values as the number of filaments in the yarn section increased. However, an unexpected trend was observed and a reduction was determined in yarn strength and elongation values beyond certain number of filaments. The explanation for unexpected case was reported that the yarns with higher number of filaments are exposed to more friction effects during the false-twisted texturing process, and thus some weakening occurs in their structure. As a result, texturing process based on friction method realized in this study might be more effective on breaking strength of the fabrics rather than the effect of number of filaments and filament cross section form. As seen in Table 8, virgin PET polymer gave higher yarn strength values than recycled PET polymer. Additionally, 48F regarding number of filaments and round cross-section regarding filament cross-section form led to produce stronger yarns after texturing process [13]. As to woven fabric, the highest breaking strength values were obtained the woven fabrics having 48F and round cross section, and the lowest values were determined at 72F and plus cross-section.

Table 6. t-test results of fabric tensile strength values for warp direction

Parameter	Sig.
Polymer type	0.105
Cross section form	0.237

Table 7. ANOVA LSD test results of fabric tensile strength values for warp direction

Fabric type		Sig.
rPET-36R	rPET-48R	0.176
	rPET-72R	0.631
rPET-48R	rPET-72R	0.088

Table 8. Yarn strength results after texturing process

Yarn type	Strength (g/denier)
PET-36R	4.63
rPET-36R	4.48
rPET-48R	4.11
rPET-72R	4.00
rPET-48P	3.84

3.3. Breaking elongation

Breaking elongation results of woven fabrics are shown in Figure 5 and ANOVA statistical analysis results are given in Table 9-10.
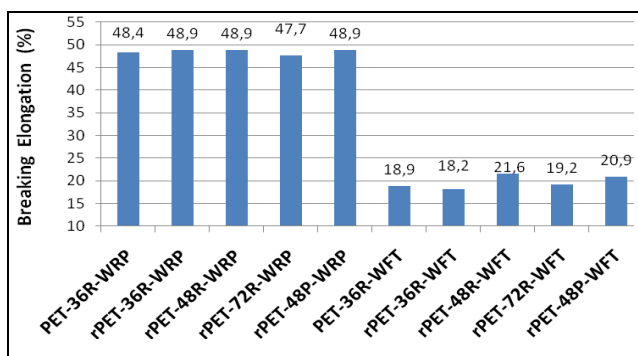

Figure 5. Breaking elongation results of woven fabrics for warp and weft directions

When the effect of the polymer type was examined, it was determined that the woven fabrics obtained from the virgin and recycled PET polymers had statistically similar breaking elongation values in the warp and weft directions (PET-36R and rPET-36R) (Table 9).

Regarding the effect of number of filaments (rPET-36R, rPET-48R and rPET-72R), it was observed different trends in the warp and weft directions. As the number of filament increased, breaking elongation of woven fabrics decreased in warp direction while the values of weft direction changed depending on number of filaments. In weft direction, breaking elongation increased up to a certain number of filaments (from 36 filaments to 48) and then decreased with the higher number of filaments (from 48 filaments to 72). When the results are evaluated statistically, it was determined that there were not statistically significant differences in breaking elongation values of warp direction (Table 10). Therefore, all filaments gave similar fabric breaking elongation values in warp direction. However, the differences in the weft direction was determined to be significant (Table 10) and number of filaments led to significantly different fabric breaking elongation values. As in yarn breaking elongation results after texturing process (Table 11), the highest elongation values were obtained in 48 filaments and the lowest in 36 filaments. In literature, Özkan and Babaarslan (2010) determined similar trend and reported that breaking elongation of texturized polyester yarns slightly increased when the number of filaments increased from 24 to 34. Then the elongation value decreased with the increase in the number of filaments [16]. This case was explained by the fact that POY yarns with high number of filaments exposed to more friction during texturing and the resulting lower breaking elongation due to less resistant structure. The effect of texturing process based on friction-disc method might be the reason for breaking elongation results of woven fabrics.

As to the effect of the filament cross sectional form, fabrics with round (rPET-48R) and plus cross-sections (rPET-48P) forms in the warp direction had statistically similar values (Table 9). In the weft direction, it has been determined that the round form (rPET-48R) gave insignificantly higher breaking elongation values compared to the plus cross section form (rPET-48P). In literature, Babaarslan and Haciogullari (2013) detected high tenacity and breaking elongation values in round cross sectional shaped yarns and tensile properties of multi-channelled cross-sectional shapes were low [14]. Varshney et al. (2011) and Babaarslan and Haciogullari (2013) explained the polyester yarn tenacity having different cross section shapes with the change in individual fiber tenacity [14, 17]. This case might be reason for lower breaking elongation values of woven fabrics obtained from plus cross section form. On the other hand, breaking elongation of the fabrics woven from plus cross sectional shape might be decreased as a result of subjecting more friction during texturing process due to higher surface area of the rPET-48P filament (Figure 2).

3.4. Tearing strength

Tearing strength results of woven fabrics are indicated in Figure 6 and ANOVA statistical analysis results for mean values are given in Table 12-13.

When the effect of polymer type on the tearing strength of fabrics (PET-36R and rPET-36R) was examined, different trends were observed in the weft and warp directions. Higher strength values were determined in the fabrics obtained from rPET (rPET-36R) polymer in the warp direction while PET polymer (PET-36R) gave better values in the weft direction. However, the differences in tearing strength values of warp direction were found statistically insignificant (Table 12). However, in weft direction, the differences in tearing strength of PET-36R and rPET-36R fabrics were statistically significant.

On the other hand, tearing strength values decreased slightly in warp direction while increased in weft direction with higher number of filaments (rPET-36R, rPET-48R and rPET-72R). In particular, the differences in tearing strength values of the warp direction were found statistically insignificant level for three different number of filament values. As to weft direction, all fabrics had almost statistically similar tearing strength values. However, difference in the fabrics between rPET-36R and rPET-48R was found statistically significant level (Table 13). rPET-48R and rPET-72R fabrics having higher number of filaments had similar fabric tearing strength values. In literature, tearing strength is defined as a function of the strength of the yarns in a fabric and the force required to make them slip over the crossing threads [18]. When the friction between the yarns in a fabric structure is increased, freedom of movement of the yarns decreases. Thus, the yarns do not slide over each other and this case lead to a reduction in tearing strength values. Hu and Chan (1998) reported that slack and exposed structures allow the yarns to transfer and group together, and thus the result in a great tearing strength in comparison to tight structures [19]. Thanikai Vimal et al. (2020) reported that fabrics with longer floats have higher tearing strength in comparison of the fabric having no floats like plain weave [20]. From these findings, it was thought that the increased surface area with higher number of filaments in the yarn cross section prevent the filament slippage during tearing and thus the fabrics having higher number of filaments give lower tearing strength values.

As the filament cross section form was circularized, it was determined that fabrics with round (rPET-48R) and plus cross section (rPET-48P) form in warp direction had statistically similar values. In the weft direction, as in breaking strength results, it was found that the round form gave higher tearing strength values and the difference was found statistically significant level (Table 12). In literature, Behera and Singh (2014) worked on the characterization of the effect of fibre cross-sectional shape on various structure–property relationship of fabric. In the study, mean frictional coefficient calculated twelve different cross-sectional shape filament yarns such as circular, octagonal, plus, square, dumble, trilobal etc. mean frictional coefficient was 0.127 for circular cross-section while it was 0.138 for plus one [21]. Therefore, as seen in Figure 2, higher surface area and friction characteristic of plus cross-section might be a reason for lower tearing strength of the fabrics produced with this cross-section.

Table 9. t-test results for fabric breakage elongation values

Parameter	Sig.	
	Warp direction	Weft direction
Polymer type	0.159	0.288
Cross section form	0.989	0.288

Table 10. ANOVA LSD test results for fabric breaking elongation values for warp and weft directions

Fabric type		Sig.	Fabric type		Sig.
rPET-36R-WRP	rPET-48R-WRP	10.000	rPET-36R-WFT	rPET-48R-WFT	0.000*
	rPET-72R-WRP	0.283		rPET-72R-WFT	0.017*
rPET-48R-WRP	rPET-72R-WRP	0.283	rPET-48R-WFT	rPET-72R-WFT	0.000*

*: The mean difference is significant at the 0.05 level.

Table 11. Yarn breaking elongation results after texturing process

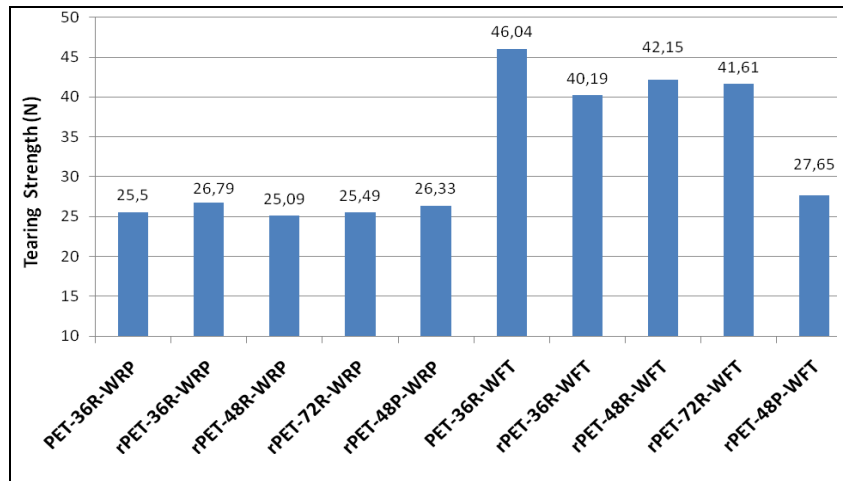| Yarn type	Breaking elongation (%)
PET-36R	26.04
rPET-36R	23.93
rPET-48R	25.52
rPET-72R	25.00
rPET-48P	18.68

Figure 6. Tearing strength results of woven fabrics

3.5. Seam slippage resistance

Seam slippage resistance results of woven fabrics are shown in Table 14. The seam slippage resistance was given as the shear length and seam resistance to slippage and hence seam strength decreases as the shear length increases.

When the shear length results were examined, it was determined that the values of warp direction are similar in general, the polymer type, the number of filaments and the cross-sectional form have no significant effect on shear length values. As to weft direction, the results indicated that shear length values of the fabrics obtained from the rPET (rPET-36R) polymer was somewhat higher and therefore rPET-36R fabric had slightly lower seam slippage resistance than PET-36R. On the other hand, a clear trend was not observed in shear length values of rPET-36R, rPET-48R and rPET-72R fabrics, as the number of filaments increased. However, the highest shear length and hence the lowest seam slippage resistance was determined in rPET-72R having the highest number of filaments (72 filament). On the other hand, the highest seam slippage resistance values were obtained in rPET-48R fabric with 48 filaments. Actually, an improvement in seam slippage resistance values were expected from higher number of

filaments due to increased surface area. However, in the study, rPET-72R woven fabric having higher number of filaments gave lower seam slippage resistance values. The decrease in filament strength given in Table 8 was thought to be more effective on lower seam slippage resistance rather than the increase in surface area against slip resistance. As a consequence, strength of the filament and hence resistance to seam slippage decreased as the number of filaments increased. Coarser filaments having lower number of filaments might give higher seam slippage resistance and seam strength values.

Regarding the effect of the filament cross section form, it was found that the slip length and therefore seam slippage resistance values in the weft direction (rPET-48R and rPET-48P) were the same. In warp direction, the fabrics with a circular (rPET-48R) section form had a higher shear length and hence a lower seam slippage resistance. This result meant that higher seam slippage resistance is obtained as the fiber cross section move away from circularity. Increased surface area with plus cross section form (mentioned in tearing strength results) might be a reason for better seam slippage resistance of plus cross section shape.

Table 12. t-test results of mean fabric tearing strength values of woven fabrics

Parameter	Sig.	
	Warp direction	**Weft direction**
Polymer type	0.604	0.039*
Cross section form	0.401	0.006*

*: The mean difference is significant at the 0.05 level.

Table 13. ANOVA LSD test results for mean fabric tearing strength values

Fabric type		Sig.	Fabric type		Sig.
rPET-36R-WRP	rPET-48R-WRP	0.064	rPET-36R-WFT	rPET-48R-WFT	0.027*
	rPET-72R-WRP	0.135		rPET-72R-WFT	0.148
rPET-48R-WRP	rPET-72R-WRP	0.611	rPET-48R-WFT	rPET-72R-WFT	0.254

*: The mean difference is significant at the 0.05 level.

Table 14. Seam length results of woven fabrics

Shear length (mm)	PET-36R	rPET-36R	rPET-48R	rPET-72R	rPET-48P
Warp direction	2	2	3	2	2
Weft direction	4.5	5	4	6	4

3.6. Abrasion resistance

Abrasion resistances of the textile materials are important features to determine using life of the fabrics. In addition, abrasion resistance is one of the most important mechanical properties that affect fabric appearance during and after use. In order to evaluate the abrasion resistance properties of woven fabrics, two samples of each fabric type were abraded between 8.000-50.000 rubbing cycles. Abrasion resistance of the fabrics were assessed according to the rubbing cycles which led to first three yarn breakages. As is known, the abrasion resistance of the woven fabrics increases with the increase in abrasion cycles where the yarn break is observed. According to the results given in Table 15, 1, 2 and 3 symbolizes the first, second and third yarn breakages, respectively. As seen, yarn breakages were observed at 40.000 and above rubbing cycles for the rPET-36R coded fabrics obtained from rPET polymer, while yarn breakages occurred between 25.000-32.000 rubbing cycles in PET-36R fabric obtained from PET polymer. Therefore, the fabrics woven from recycled polyester yarns represented a bit slight more resistance to abrasion than the fabrics with virgin polyester weft yarns.

Regarding the effect of number of filaments, yarn breakages were determined at lower rubbing cycles as the number of filaments increased. This case indicated that resistance to abrasion decreases with finer filaments. Yarn breakages were observed at 40.000 rubbing cycles for rPET-36R having the lowest number of filaments (36F) while it was 12.000-15.000 for rPET-72R having the highest number of filaments (72F). As similar to this result, Akgun (2014) reported that high number of filaments in yarn structure led to higher structural abrasion of the textured polyester woven fabric surfaces [22]. This case was explained that yarns with high number of filaments were more affected by abrasion and number of the pulled filaments from yarn surfaces increased as abrasion cycles increased. Lower abrasion resistance of the polyester yarns having higher number of filaments might be resulted from lower individual fiber tenacity of these yarns. As seen in Table 8, yarn tenacity decreased with higher number of filaments and this case led to lower resistance to abrasion for rPET-72R than that of the rPET-36R and rPET-48R.

On the other hand, effect of cross section form on abrasion resistance, the first three yarn breakages were observed in 22.000-28.000 rubbing cycles in rPET-48R fabric with round section form and in 8.000-10.000 cycles in rPET-48P fabric with plus cross section form. Abrasion resistance results indicated that rPET polyester filament yarns having lower number of filaments and round cross section form enhance the resistance to abrasion. Shape of filament cross section directly effects abrasion resistance. In literature, it was stated that woven fabrics with high surface roughness were affected more by abrasion. Plus filament cross section had higher surface areas than round cross section and therefore this case led to more abrasion. As stated in breaking strength results of woven fabrics, another reason might be higher fiber tenacity of round cross section form. In literature, it was stated that tenacity values of the two fibers with the same length and linear density values in the circular and trilobal cross-sectional shapes were different [14, 23]. On the other hand, Behera and Singh (2014) determined that yarn tenacity values of multifilament yarns are 2.52 g/denier for circular and 2.41 g/denier plus cross-sections [21]. In present study, it was also determined that yarn tenacity is 4.48 g/denier for round and 3.84 g/denier for plus cross-section (Table 8). As similar to this case, the higher fiber tenacity resulted from round cross section shape caused more resistance to yarn breakages.

3.7. Air permeability

Air permeability results of woven fabrics are shown in Figure 7 and ANOVA statistical analysis results are given in Table 16-17.
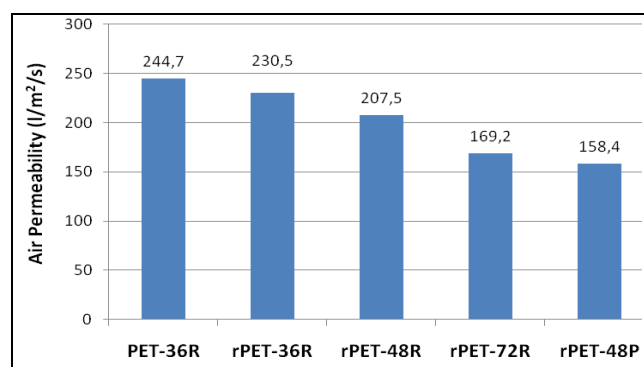
Figure 7. Air permeability results

When the effect of polymer properties on the air permeability of the fabrics was examined, it was determined that the PET-36R fabrics obtained from the PET polymer had significantly more air permeability values than the rPET-36R fabrics woven from rPET yarns (Table 16).

Table 15. Abrasion cycle results occurred the first three yarn breakages

Sample	Rubbing cycles (rpm)												
	8000	10000	12000	14000	15000	22000	25000	28000	30000	32000	40000	45000	50000
PET-36R (sample 1)	-	-	-	-	-	-	1	2	-	3	-	-	-
PET-36R (sample 2)	-	-	-	-	-	-	-	-	1	2	-	-	-
rPET-36R (sample 1)	-	-	-	-	-	-	-	-	-	-	1	2	3
rPET-36R (sample 2)	-	-	-	-	-	-	-	-	-	-	-	1	3
rPET-48R (sample 1)	-	-	-	-	-	1	2	3	-	-	-	-	-
rPET-48R (sample 2)	-	-	-	-	-	-	1	3	-	-	-	-	-
rPET-72R (sample 1)	-	-	1	2	3	-	-	-	-	-	-	-	-
rPET-72R (sample 2)	-	-	-	2	3	-	-	-	-	-	-	-	-
rPET-48P (sample 1)	2	3	-	-	-	-	-	-	-	-	-	-	-
rPET-48P (sample 2)	1	3	-	-	-	-	-	-	-	-	-	-	-

Regarding the effect of filament fineness, the air permeability values tended to decrease as the number of filaments increased in yarns with the same yarn fineness. It was determined that rPET-36R fabric with the lowest number of filaments (36 filament) had the highest air permeability while rPET-72R fabric having the highest number of filaments (72 filament) led to the lowest air permeability value. Additionally, the difference between the air permeability values of all three fabrics was found to be statistically significant (Table 17) and therefore it was concluded that number of filaments affected the air permeability of the fabrics significantly. As known, air permeability depends on porosity of textile materials and permeability improves with the increase in porosity. Behera and Singh (2014) stated that air permeability of the fabrics decreases with the increase of filament fineness as a consequence of higher specific surface area of the filament [15]. As seen in Figure 2, lower porosity resulted from higher number of filaments in yarn structure led to lower air passage from the fabric. Lower air permeability of the woven fabrics obtained from higher number of rPET filaments was agreed with this finding.

As to the effect of the filament cross section form, air permeability results of the woven fabrics indicated that round filament cross section (rPET-48R) gave significantly higher air permeability than plus cross section form (rPET-48P) (Table 16). In literature, a geometrical parameter of Shape Factor (SF) was defined that relates a closed curve path to its equivalent circle perimeter to express the irregularity of the cross-section. Various researchers have expressed this relationship in different ways. Neckar (1998) defined SF≈0 for circular cross-section [24]. SF and hence surface area of the fiber/filament increase with the irregularity of fibre cross-sectional shapes [15]. In consequence of higher specific surface area of each fiber/filament, space between the fibres in the fabric decrease and this case will increase higher drag resistance to air and result in low air and water vapour permeability for these fabrics. For plus cross section, it was stated that actual SF was 0.361 while theoretical SF was 0.52 [25]. Higher surface area of plus cross-section form might be a reason for lower air permeability of rPET woven fabrics comparing with that of the circular cross section

Table 16. t-test results of air permeability values of woven fabrics

Parameter	Sig.
Polymer type	0.805
Cross section form	0.000*

*: The mean difference is significant at the 0.05 level.

Table 17. ANOVA LSD test results for fabric air permeability values

Fabric type		Sig.
rPET-36R	rPET-48R	0.000*
	rPET-72R	0.000*
rPET-48R	rPET-72R	0.000*

*: The mean difference is significant at the 0.05 level.

4. CONCLUSION

In this study, it was studied the effect of virgin and recycled PET polymer, number of rPET filament and rPET filament cross section form on breaking, tearing and seam strength, breaking elongation, abrasion resistance and air permeability properties of woven fabrics. The results are as following:

- Regarding the effect of polymer type, it was not determined any significant differences in fabric weight, breaking strength and breaking elongation results. However, the fabrics obtained from virgin PET polymer gave better tearing strength, seam slippage resistance and air permeability while fabrics woven from recycled polyester yarns represented a bit slight more resistance to abrasion than the fabrics with virgin polyester yarns.

- Except fabric tearing strength results of weft direction, the differences in all analysed performance properties of the woven fabrics obtained from virgin and recycled PET polymer were not statistically significant and therefore both polymer types gave similar fabric properties.

- The results of warp direction were found statistically insignificant level due to the usage of FDY polyester yarn (30 denier and 12F) in warp direction of all woven fabrics.

- As to the effect of number of filaments, it was determined that woven fabrics having 36, 48 and 72 filaments had statistically similar fabric weight and breaking strength values. On the other hand, the results indicated that higher number of filaments gave lower fabric breaking elongation, seam slippage resistance, abrasion resistance and air permeability values while led to higher tearing strength.

- The effect of increased surface are with higher number of filaments might be the main reason for fabric breaking elongation, tearing strength and air permeability results. On the other hand, increased fiber fineness and hence lower fiber tenacity resulted from higher number of filaments in the same yarn cross section was thought to have affected on seam slippage resistance and abrasion resistance results.

- Except fabric weight and tensile properties, filament cross section shapes had a significant affect on other studied fabric properties. It was determined that circular cross section form gave higher fabric breaking strength and elongation, tearing strength, abrasion resistance and air permeability values while higher seam slippage resistance values were obtained with plus cross section form.

- Higher individual fiber tenacity of circular cross section form might be a reason for better tensile strength, breaking elongation, tearing strength and abrasion resistance values while increased surface area of plus cross section shape might be effective higher seam slippage resistance and lower air permeability results.

In recent years, recycled fibre usage has been attracting attention due to concerns about environment protection and increased raw material costs. This research makes several noteworthy contributions to production possibility of polyester yarns from polyethylene terephthalate (PET) wastes exhibiting comparable woven fabric properties with that of the virgin polyester yarns such as fabric strength and comfort. Additionally, this study showed that polyester yarns with different filament fineness and cross-sectional shapes can be produced from recycled PET polymer. Recycled polyester yarn could be used as an alternative to the virgin polyester yarns and this case enhances to benefit the low price and enviromentally friendly of the recycled material.

As reported, this study was realized at the polyester yarn production mill, and virgin and recycled polyester fibres were spun based on melt spinning method on an industrial scale. Due to limited yarn length, the current study has only examined the recycled polyester yarns as a weft yarn. The scope of this study was limited in terms of the analysis of usage of the recycled polyester yarns as a warp yarn and also fabric production parameters such as different weave types, warp/weft yarn densities (fabric weight), etc. and limited fabric properties. A future study investigating various woven fabric properties produced with different fabric production parameters would be very interesting. Considerably detailed work will need to be done to determine the tensile properties of the fabrics produced from recycled yarns and to compare with that of the virgin one. It is recommended that further research would be undertaken about knitted fabric properties.

ACKNOWLEDGEMENTS

REFERENCES

1. TUİK. 2011, April 18. Atık Bertaraf ve Geri Kazanım Tesisleri İstatistikleri (2011). Retrieved from https://data.tuik.gov.tr/Bulten/Index?p=Atik-Bertaraf-ve-Geri-Kazanim-Tesisleri-Istatistikleri

2. Telli A, Özdil N. 2015. Effect of recycled PET fibers on the performance properties of knitted fabrics. *Journal of Engineered Fibers and Fabrics*, 10(2), 47-60.

3. Uyanık S. 2019. A study on the suitability of which yarn number to use for recycle polyester fiber. *The Journal of the Textile Institute*, 110(7), 1012-1031.

4. Qin Y, Qu M, Kaschta J, Schubert DW. 2018. Comparing recycled and virgin poly (ethylene terephthalate) melt-spun fibres. *Polymer Testing*, 72, 364-371.

5. Yuksekkaya ME, Celep G, Dogan G, Tercan M, Urhan B. 2016. A comparative study of physical properties of yarns and fabrics produced from virgin and recycled fibers. *Journal of Engineered Fibers & Fabrics*, 11(2), 68–76.

6. Sanches RA, Takamune KM, Guimaraes BM, Alonso RS, Jr DK, Marcicano JPP, Duarte AYS, Dedini FG. 2015. Comparative study of characteristics of knitted fabrics produced from recycled fibres

employing the Chauvenet criterion, factorial design and statistical analysis. *Fibres & Textiles in Eastern Europe,* 23(4), 19–24.

7. He SS, Wei MY, Liu MH, Xue WL. 2014. Characterization of virgin and recycled poly(ethylene terephthalate) (PET) fibers. *The Journal of The Textile Institute,* 106(8), 800– 806.

8. Koo HJ, Chang GS, Kim SH, Hahm WG, Park SY. 2013. Effects of recycling processes on physical, mechanical and degradation properties of PET yarns. *Fibers and Polymers,* 14(12), 2083-2087.

9. Kostov G, Atanassov A, Kiryakova D. 2013. Preparation and characterization of fibers of waste and fresh polyethylene terephtalate and mixtures of them. *Fibers and Polymers,* 14(2), 216-222.

10. Telli A, Özdil N. 2013. Properties of the yarns produced from r-pet and their blends. *Tekstil ve Konfeksiyon,* 23(1), 3-10.

11. Lee JH, Lim KS, Hahm WG, Kim SH. 2013. Properties of recycled and virgin poly (ethylene terephthalate) blend fibers. *Journal of Applied Polymer Science,* 128(2), 1250-1256.

12. Abbasi M, Mojtahedi MRM, Khosroshahi A. 2007. Effect of spinning speed on the structure and physical properties of filament yarns produced from used PET bottles. *Journal of Applied Polymer Science,* 103(6), 3972-3975.

13. Kırış G. 2020. Farklı filament inceliği ve filament kesit formu kullanılarak geri dönüşüm pet polimerinden (rPET) POY ve tekstüre (DTY) polyester ipliklerin eldesi ve örme ve dokuma kumaşların çeşitli performans özelliklerinin incelenmesi (Master dissertation). Available from Ulusal Tez Merkezi (Accesion https://tez.yok.gov.tr/UlusalTezMerkezi/tezSorguSonucYeni).

14. Babaarslan O, Hacıoğulları S. 2013. Effect of fibre cross-sectional shape on the properties of POY continuous filaments yarns. *Fibers and Polymers,* 14(1), 146-151.

15. Behera BK, Singh MK. 2014. Role of filament cross-section in properties of PET multifilament yarn and fabric. Part I: Effect of fibre cross-sectional shape on transmission behaviour of fabrics. *The Journal of the Textile Institute,* 105(9), 895-904.

16. Özkan S, Babaarslan O. 2010. İplik kesitindeki filament sayısının filament ve tekstüre ipliklerin özellikleri üzerindeki etkisi. *Journal of Textile & Apparel/Tekstil ve Konfeksiyon,* 20(1), 17-22.

17. Varshney RK, Kothari VK, Dhamija S. 2011. Influence of polyester fibre fineness and cross-sectional shape on low-stress characteristics of fabrics. *The Journal of the Textile Institute,* 102(1), 31-40.

18. Taylor HM. 1999. Tensile and tearing strength of cotton cloths. *Journal of the Textile Institute*, 50, 161–188.

19. Hu J, Chan YF. 1998. Effect of fabric mechanical properties on drape. *Textile Research Journal*, 68(1), 57–64.

20. Thanikai Vimal J, Prakash C, Jebastin Rajwin A. 2020. Effect of weave parameters on the tear strength of woven fabrics. *Journal of Natural Fibers,* 17(9), 1239-1248.

21. Behera BK, Singh MK. 2014. Role of filament cross-section in properties of PET multifilament yarn and fabric. Part II: effect of fibre crosssectional shapes on fabric hand. *The Journal of The Textile Institute*, 105(4), 365-376.

22. Akgun M. 2014. Surface roughness properties of polyester woven fabrics after abrasion. *The Journal of the Textile Institute,* 105(4), 383-391.

23. Dhamija S, Kothari VK, Varshney RK. 2011. Effect of polyester fibre fineness and cross-sectional shape on physical characteristics of yarns. *The Journal of the Textile Institute,* 102(4), 293-307.

24. Neckar B. 1998. *Morphology and structural mechanics of fibrious assemblies*. Liberec, Czech Republic: TU Liberec.

An Investigation on Some Mechanical Properties of the Tuft Carpets Produced by Homopolymer, Copolymer and Thermoplastic Polyolefin Mixed Polypropylene Bulked Continuous Filament Yarns

Cemile Emel YAZ[1] 0000-0003-4463-7815
Cem GÜNEŞOĞLU[2] 0000-0002-8796-9679
Mehmet TOPALBEKİROĞLU[2] 0000-0003-4345-8815

[1]Gaziantep University / Naci Topçuoğlu Vocational School / Gaziantep, Turkey
[2]Gaziantep University / Department of Textile Engineering / Gaziantep, Turkey

Corresponding Author: Cemile Emel YAZ, ekirlangic@gantep.edu.tr

ABSTRACT

There are several parameters that affect the mechanical properties of carpets such as yarn characteristic and carpet construction. Yarn material is one of the most important factors which determine the usage performance of carpets by consumers. This study investigated the mechanical behaviours of carpets produced from polypropylene (PP) bulked continuous filament (BCF) yarns with not only polypropylene homopolymer but also mixing with copolymer (coPP) or thermoplastic polyolefins (TPO). In this respect, nine carpet samples produced by different types of BCF yarns used as pile were examined. Experimental results indicated that mixing polypropylene homopolymer with copolymer or thermoplastic polyolefin resulted with improvement in thickness loss and resilience properties. In addition, thermoplastic polyolefin mixed samples exhibited higher performance compared to those of copolymer, in both dynamic and static loading. PP BCF yarn composition had considerable influences on compressibility behaviours of carpets, whereas there was no significant effect on tuft withdrawal force.

1. INTRODUCTION

The carpet industry utilises both filament and spun yarns as pile materials. In tufted sector, filament yarns are more popular. All of the filament yarns are bulked continuous filament (BCF) and there is a widespread use of BCF polypropylene (PP) in face-to-face carpets [1]. PP has a handle like wool and also has low specific gravity that provides better cover in the carpet than other pile fibres, thus it is one of the most important pile fibres used in tufted carpets. It also does not absorb water so it resists to water-borne stain, although oily stains may be a problem. In addition, the resilience (elastic recovery) of PP is not as good as that of some other textile fibres, but this can be compensated by increasing the pile density of carpet. The low cost of its monomer is one of the main advantages of PP [1, 2]. PP yarn used in the machine carpet industry is in generally homopolymer structure which is more rigid than PP copolymer and has better thermal resistance, but impact resistance is low at low temperatures. In addition, ethylene-propylene copolymer structure gives higher elongation and impact resistance in injection molding applications with PP material although it is more expensive than homopolymer [3,

4]. In addition, thermoplastic polyolefins (TPO) are physical blends of rubbers and crystalline thermoplastics. The rubber component is usually an ethylene-propylene rubber (either EPM or EPDM) and the thermoplastics material is polypropylene. The material is characterized by high-impact strength, low density and good chemical resistance [5, 6].

In literature, there are several studies focused on mechanical performances of carpets produced from different types of pile yarns. By many researchers the effects of various parameters, such as pile material, yarn and carpet structure, on the carpet performances were investigated. Most of the studies indicated that due to their characteristic features, different raw materials such as polypropylene, acrylic, nylon or wool have varied effects on carpet deformation behaviours. In addition to this, since the constructional properties, such as pile density and pile height, directly affect the energy of pile yarns, these are defined as decisive parameters on resilience properties of carpets [7-17]. It was also emphasized that, increase pile density and decrease in pile height are the main factors that decrease the deformation [14]. Besides these constructional parameters, the effects of production parameters of BCF yarn on yarn properties and carpet behaviours were focused on by some researchers. It was noted that yarn characteristics are not only based on structural properties such as cross-section and yarn linear density, but also depend on production parameters like heat-setting temperature, twisting, drawing ratio, etc. [18-21].

As seen from the literature survey, most of the studies investigated the influences of specific raw material characteristics and yarn production parameters on yarn and carpet behaviours. There is an only study which researched polymer mixing in PP BCF. Tavanai et all searched the properties of BCF yarns produced by mixing at different ratios with polyamide 6 to improve the low stretchability properties of PP [22]. However, the effects of BCF yarns on carpet performances were not investigated. Additionally, in literature, there are some studies that had examined the toughening effect of coPP or TPO in blends on samples prepared by injection-molded [23-25]. To the best of our knowledge, there is no research on coPP and TPO usage in BCF yarn production as pile yarns at carpets. With the aim of determine the effects of polymer mixing on pile yarn deformation behaviours, BCF yarns were produced by at different mixing ratios of PP homopolymer with coPP or TPO and carpets were manufactured keeping the all other pile and carpet parameters constant. In order to determine experimental results, carpet samples were applied dynamic and short-term static loadings, compression and recovery, hexapod appearance retention and tuft withdrawal force tests.

2. MATERIAL AND METHOD

2.1 Material

In this study, nine different types of PP BCF yarns, four types of TPO mixed, four types of coPP mixed and a pure PP as a reference, were used as pile with linear density 2100/144 dtex. The compositions of BCF yarns consisted of commercially available polypropylene homopolymer (NATPET H25FBA), polypropylene impact copolymer (coPP) (LyondellBasell Moplen EP548Q) and thermoplastic polyolefin (TPO) (LyondellBasell Adflex Z101H). Mechanical properties of polymers are given in Table 1. BCF yarns were produced by laboratory scale BCF machine in Kartal Halı Tekstil San. Tic. A.Ş.. The production parameters and the composition percentages of BCF yarns are shown in Table 2 and Table 3, respectively. The heat-setting process parameters of BCF yarn samples were applied as 135 °C setting temperature, 450 rpm winding speed, 17.5 m/min band speed, 0.75 bar tunnel pressure and 1 minute tunnel waiting time. Carpet samples were produced by Booria Robotuft tufting machine in Royal Halı İplik Tekstil Mobilya San. Tic. A.Ş.. Production parameters were kept constant for all samples, with 210 (pile/cm) pile density and 12 mm pile height. Tufted samples were dried after applying SBS latex and bonding the second ground fabric (%100 PET plain weave).

Table 1. Mechanical properties of polymers

Property	Melt Flow Rate (g/10min)	Flexural Modulus (MPa)	Impact Strength (kJ/m²)
PP Homopolymer	25	1700	2.2
PP Copolymer	19	1450	9
TPO	27	80	No break

Table 2. Production parameters of BCF yarns

Extruder Unit		
Cabin	**Temperature (°C)**	**Pressure (bar)**
1	241	
2	243	
3	245	105
4	247	
5	245	
6	247	

Cooling Unit
Cooling temperature is 25 °C, lubrication tank pressure 255 bar

Drawing Unit		
Godet	**Temperature (°C)**	**Cycle Speed (rpm)**
1	25	1020
2	90	1050
3	138	2470
4	37	2490
5	145	2490
Cabin	-	1100
Barrel	145	800

Table 3. Composition percentages of BCF yarns

Sample Code	Pile Yarn (content)
100PP	100% PP
5TPO	5% TPO – 95% PP
15TPO	15% TPO – 85% PP
20TPO	20% TPO – 80% PP
25TPO	25% TPO – 75% PP
5coPP	5% coPP – 95% PP
15coPP	15% coPP – 85% PP
20coPP	20% coPP – 80% PP
25coPP	25% coPP – 75% PP

2.2 Method

In order to investigate the effect of coPP and TPO mixed PP BCF yarns on the mechanical performances of carpets hexapod tumbler, short-term static loading, dynamic loading and compression/recovery tests were performed. All carpet specimens were conditioned with 65±4 % relative humidity and 20±2 °C temperature according to ISO 139:2005 before the tests were conducted.

Thickness loss after dynamic loading was performed to investigate the thickness loss of carpet pile due to the prolonged foot traffic. WIRA dynamic loading machine was used to carry out the test in accordance with the standard of TS 3375 ISO 2094. For this study 50, 100, 200 and 1000 impacts were applied to samples in order to determine the percentage of thickness loss by calculating with Equation (1), where, h_0 is the initial thickness and h_c is the thickness after impacts.

$$Thickness\ Loss\ (\%) = \frac{h_0 - h_c}{h_0} \times 100 \quad (1)$$

With the aim of determine the resilience performance of carpets, short-term static loading test was performed with WIRA Carpet Static Loading Tester. The specimen was applied 220 kPa pressure for 2h and then the load was removed at the end of the duration. The thickness of the samples measured under 2 ± 0.2 kPa after 15 min, 30 min and 60 min recovery periods, according to the standard of TS 3378. The percentage of resilience was calculated with Equation (2), where, h_0 is the initial thickness and h_c is the thickness after 2 h compression and h_r is the thickness after 60 min recovery time.

$$Resilience\ (\%) = \frac{h_r - h_c}{h_0 - h_c} \times 100 \quad (2)$$

Compression and recovery behaviours of carpets were interpreted at different loading and unloading levels according to the standard of BS 4098 by using WIRA Digital Thickness Gauge. Specimens were applied from 2 kPa to 200 kPa gradually, and then the weights were removed sequentially from 200 kPa to 2 kPa at 30 s intervals. The percentage compression recovery of each carpet sample after

loading-unloading procedure was measured with Equation (3), where, t_2 is the thickness under 2 kPa pressure at the beginning of the loading process (Figure 1, point A), t_r is the thickness at 2 kPa pressure after unloading all weights (Figure 1, point C) and t_{200} is the thickness at 200 kPa pressure (Figure 1, point B).

$$Percentage\ Compression\ Recovery\ (\%) = \frac{t_r - t_{200}}{t_2 - t_{200}} \times 100 \quad (3)$$

Compression work was determined by estimating the area under the loading curve (Figure 1, area ADB). Similarly, recovery work was measured by the area under the unloading curve (Figure 1, area BEC). The percentage work recovery was calculated by the ratio of recovery work to the compression work as shown in Equation (4).

$$Percentage\ Work\ Recovery\ (\%) = \frac{Area_{BEC}}{Area_{ADB}} \times 100 \quad (4)$$
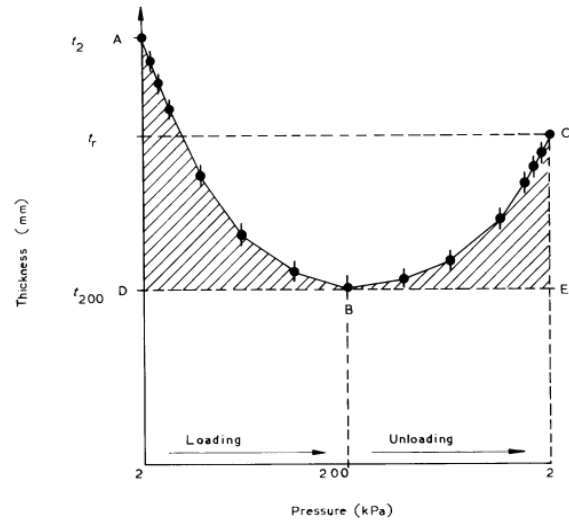
Figure 1. Typical thickness versus pressure curve

Besides thickness loss and resilience determinations, hexapod tumbler test was carried out in order to evaluate the changes in appearance of carpets. Specimens were tested for 4000 revolutions using WIRA Hexapod Tumbler Carpet Tester in accordance with the standard of TS ISO 10361. Assessments of appearance changes were interpreted subjectively depending on the appropriate set of ISO reference scales.

Determination of tuft withdrawal force test was also performed to investigate whether BCF yarn composition has an effect on the tuft retention. Test was done according to the BS ISO 4919:2012 standard, using WIRA Tuft Withdrawal Tensometer device.

In order to determine the statistical importance of content type and % percentage on carpet performances, two-way ANOVA was performed for TPO or coPP mixed samples. The statistical software package SPSS 25.0 was used to interpret the experimental data. All test results were assessed at 95% confidence interval.

3. RESULTS AND DISCUSSION

3.1. Thickness loss after dynamic loading

Dynamic loading test, which is a simulation of walking on carpet, was performed in the study in order to determine thickness loss after different number of impacts. Percentage thickness loss of carpet samples after 50, 100, 200 and 1000 impacts were calculated by Equation (1) and shown in Figure 2. The results showed that; 5TPO and 20coPP had lowest and highest thickness loss, respectively. It was also observed that, when the TPO and coPP materials were considered, TPO mixed samples had lower thickness loss than those of coPP and neat PP. It can be said that, TPO's elastic structure provided better impact resistance due to the its higher toughness, as seen from the Table 1, compared to coPP and PP homopolymer. Depending on the results, it was also deduced that, thickness loss increased as the % percentage increased until 20%, after which it decreased. This situation probably occurred because of the deformed internal structure as % percentage increased until 20%. However, when the % percentage reached up to 25%, coPP and TPO contributed more effectively to the impact resistance. Finally, it can be concluded that since the thickness changes of the carpets under impact are related to increase in load carrying capacity; with the addition of coPP and TPO, the load carrying capacity of BCF yarns increased and the thickness loss of carpets produced from these yarns also improved. As the impact level increased thickness loss also increased for all samples.

Table 4 and Table 5 shows mean, standard deviation and %CV of the results for all impacts levels and two-way ANOVA results of the TPO or coPP mixed samples for thickness loss under dynamic loading after 1000 impacts, respectively. According to Table 5, it can be said that both content type (p=0.000<0.05) and % percentage (p=0.035<0.05) had statistically significant effect on thickness loss in 95% confidence interval. In addition, content type (F=20.672) was more effective on thickness loss than % percentage (F=3.358). No statistically significant interaction was observed between the content type and % percentage (p=0.433>0.05).
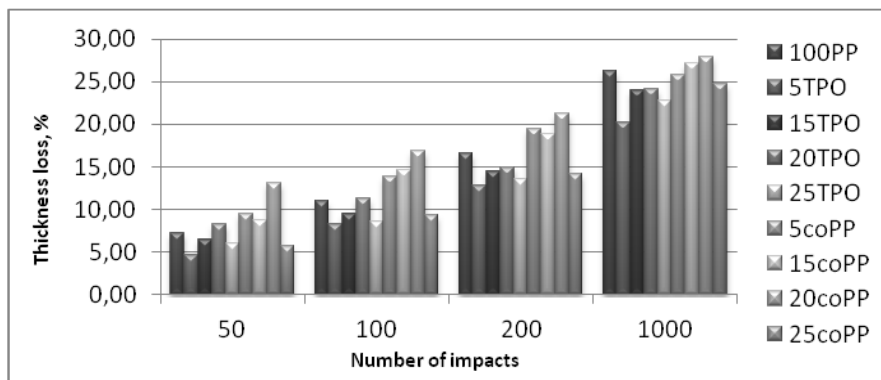
Figure 2. Thickness loss of samples after number of impacts

Table 4. Mean, standard deviation and %CV of dynamic loading test results

Sample code		100PP	5TPO	15TPO	20TPO	25TPO	5coPP	15coPP	20coPP	25coPP
50 impacts	Mean	7.28	4.71	6.42	8.27	6.07	9.52	8.65	13.06	5.65
	SD	2.75	2.16	1.78	1.82	3.09	1.06	1.97	0.76	1.81
	%CV	37.76	46.09	27.83	22.10	50.89	11.16	22.88	5.84	32.05
100 impacts	Mean	10.99	8.20	9.47	11.32	8.51	13.92	14.69	16.82	9.28
	SD	1.24	1.67	1.91	2.49	2.90	2.01	0.64	0.86	2.35
	%CV	11.37	20.45	20.21	22.06	34.12	14.45	4.35	5.15	25.33
200 impacts	Mean	16.56	12.74	14.40	14.94	13.56	19.41	18.83	21.23	14.22
	SD	1.82	2.61	2.33	3.37	3.06	0.88	1.23	0.75	1.72
	%CV	11.03	20.51	16.20	22.61	22.56	4.55	6.53	3.55	12.10
1000 impacts	Mean	26.24	20.15	24.04	24.15	22.74	25.81	27.19	27.84	24.69
	SD	1.34	1.77	2.06	4.39	2.31	1.49	0.72	1.44	1.84
	%CV	5.11	8.82	8.60	18.22	10.16	5.80	2.66	5.20	7.45

Table 5. Two-way ANOVA for thickness loss under dynamic loading after 1000 impact of TPO or coPP mixed samples

Source	Type IV Sum of Squares	df	Mean Square	F	Sig.	Partial Eta Squared
Corrected Model	169.605a	7	24.229	4.799	0.002	0.583
Intercept	19327.255	1	19327.255	3828.194	0.000	0.994
content_type	104.365	1	104.365	20.672	0.000	0.463
%_percentage	50.866	3	16.955	3.358	0.035	0.296
content_type * %_percentage	14.374	3	4.791	0.949	0.433	0.106
Error	121.168	24	5.049	-	-	-
Total	19618.028	32	-	-	-	-
Corrected Total	290.773	31	-	-	-	-

3.2. Thickness loss and resilience after short-term static loading

Thickness loss of samples immediately after removing load and after 15, 30 and 60 min (%) recovery periods were determined by short-term static loading. Percentage thickness loss and resilience values were calculated by Equation (1) and Equation (2), shown in Figure 3 and Figure 4, respectively. According to the results which are similar to dynamic loading test, TPO mixed samples exhibited lower thickness loss than those of coPP. Since the toughness of TPO is higher compared to coPP, it was an expected result that to perform lower thickness loss. It was also determined that, mixing coPP with homopolymer did not contribute an improvement on thickness loss. On the other hand, 100PP, with the lowest thickness loss immediately after removing the load, underperformed recovery behavior after 60 min period when compared to other all samples. This situation means that coPP and TPO addition to homopolymer ensured pile yarn better recovery after a given period of time. 5TPO not only had the proximate value to 100PP as the thickness loss immediately after removing load, but also showed the lowest thickness loss after 15, 30 and 60 min recovery periods. Contrary, 15coPP exhibited the highest thickness loss after all recovery periods. For all samples, it was observed that thickness loss decreased by recovery time increases for static loading test.

Resilience can be defined as the ability of pile yarn to return its initial form after loading. Depending on the Figure 4, it was determined that 5TPO had the highest resilience.

Furthermore, TPO mixed samples had generally higher resilience percentages than those of coPP and 100PP. This was attributed to the higher toughness of TPO material compared to coPP and homopolymer. On the other hand, at low % percentages, carpets had better thickness loss and resilience performance as seen from the figures. So, it can be concluded that, as the content percentage increased, the mixed samples had become softer due to the lower flexural modulus of coPP and TPO, and resulted in to perform low resistance to static loading by having higher thickness loss, therefore lower resilience.

Mean, standard deviation and %CV of static loading test results are shown in Table 6. Tables 7 and Table 8 exhibit two-way ANOVA results of TPO or coPP mixed samples for thickness loss after static loading and resilience after 60 min recovery period, respectively. As seen from Table 7, it can be said that content type (p=0.011<0.05) had a significant effect, whereas % percentage (p=0.055>0.05) was insignificant on thickness loss. Table 8 shows that, both parameters; content type (p=0.002<0.05) and % percentage (p=0.009<0.05) was found to be statistically significant, and also it was seen that the effect of content type (F=11.929) was more than % percentage (F=4.535), on resilience property. Besides, it was determined from the tables that, the interaction between the parameters was statistically significant (p=0.027<0.05 and p=0.005<0.05) for thickness loss and resilience properties, respectively.
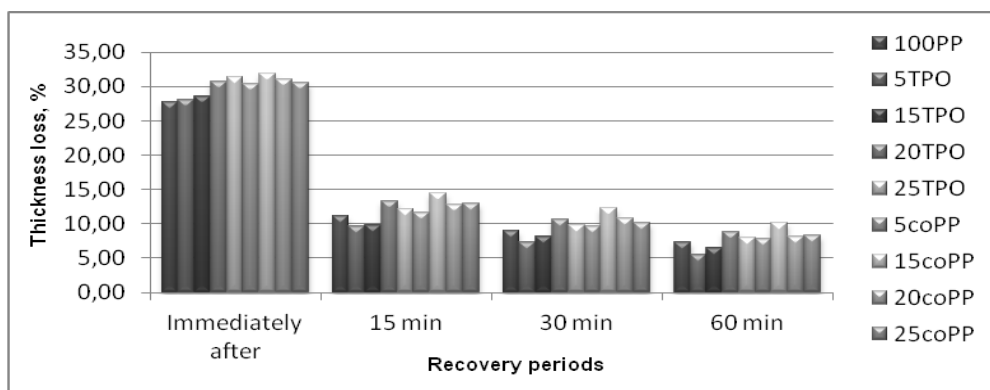

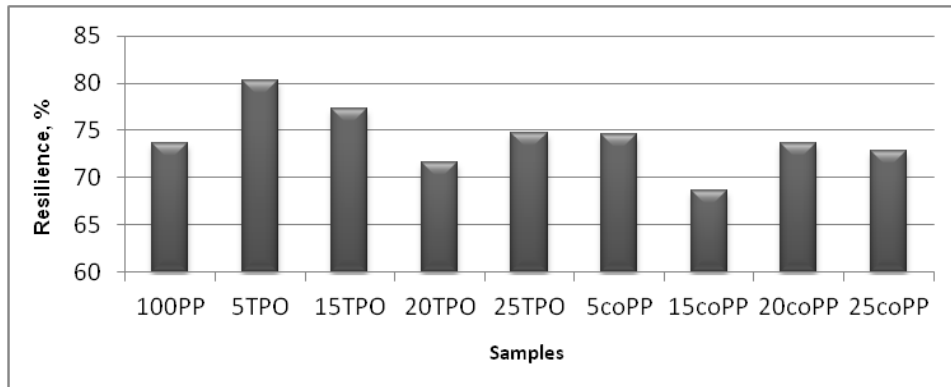**Figure 3.** Thickness loss of samples after 2-h loading

Figure 4. Resilience of samples after 60 min recovery period

Table 6. Mean, standard deviation and %CV of short-term static loading test results and resilience

Sample code			100PP	5TPO	15TPO	20TPO	25TPO	5coPP	15coPP	20coPP	25coPP
	Immediately after	**Mean**	27.81	28.06	28.50	30.64	31.44	30.39	31.82	31.06	30.53
		SD	1.27	2.39	3.06	4.27	0.63	4.87	4.32	2.12	1.65
		%CV	4.56	8.53	10,74	13,95	2,00	16,02	13,57	6,83	5,41
Short-term static loading	**15 min**	**Mean**	11.07	9.66	9.77	13.32	12.12	11.67	14.49	12.85	12.88
		SD	0.83	1.13	1.35	3.90	0.37	2.24	1.47	1.70	1.48
		%CV	7.54	11.71	13.86	29.29	3.01	19.20	10.17	13.21	11.52
	30 min	**Mean**	8.99	7.31	8.12	10.62	9.81	9.61	12.34	10.82	10.14
		SD	0.91	1.27	1.12	3.61	0.67	1.97	2.75	1.12	1.90
		%CV	10.14	17.33	13.82	33.97	6.81	20.51	22.30	10.37	18.69
	60 min	**Mean**	7.32	5.52	6.48	8.87	7.94	7.73	10.08	8.17	8.31
		SD	0.93	0.50	1.12	2.85	0.47	1.72	2.30	0.91	1.39
		%CV	12.76	8.99	17.23	32.14	5.90	22.28	22.78	11.17	16.69
Resilience		**Mean**	73.62	80.26	77.32	71.59	74.74	74.54	68.65	73.69	72.88
		SD	3.70	1.42	2.57	5.94	1.32	3.45	3.51	2.05	3.13
		%CV	5.02	1.78	3.33	8.30	1.77	4.63	5.12	2.78	4.30

Table 7. Two-way ANOVA for thickness loss after static loading of TPO or coPP mixed samples

Source	Type IV Sum of Squares	df	Mean Square	F	Sig.	Partial Eta Squared
Corrected Model	68.090a	7	9.727	3.736	0.005	0.450
Intercept	2488.506	1	2488.506	955.677	0.000	0.968
content_type	18.824	1	18.824	7.229	0.011	0.184
%_percentage	21.989	3	7.330	2.815	0.055	0.209
content_type * %_percentage	27.277	3	9.092	3.492	0.027	0.247
Error	83.325	32	2.604	-	-	-
Total	2639.921	40	-	-	-	-
Corrected Total	151.415	39	-	-	-	-

Table 8. Two-way ANOVA for resilience after 60 min recovery period of static loading of TPO or coPP mixed samples

Source	Type IV Sum of Squares	df	Mean Square	F	Sig.	Partial Eta Squared
Corrected Model	432.872a	7	61.839	5.878	0.000	0.563
Intercept	220277.543	1	220277.543	20938.975	0.000	0.998
content_type	125.493	1	125.493	11.929	0.002	0.272
%_percentage	143.121	3	47.707	4.535	0.009	0.298
content_type * %_percentage	164.258	3	54.753	5.205	0.005	0.328
Error	336.639	32	10.520	-	-	-
Total	221047.055	40	-	-	-	-
Corrected Total	769.512	39	-	-	-	-

3.3. Compression and recovery

Percentage compression recovery and percentage work recovery of carpets were calculated by Eq. (3) and Eq. (4) and given in Figure 5 and Figure 6, respectively. Compression recovery can be defined as the pile yarn tends to return to its initial shape after loading-unloading As seen from the Figure 5, percentage compression recovery decreased as the content percentage increased, for the mixed samples. This was an expected result that, at lower mixing percentages the mixed samples had comparable compression recovery with 100PP, but as far as at higher mixing ratios the samples performed lower recovery, as a result of reduced rigidity of pile yarns. In consideration with TPO and coPP materials, it was deduced that, the higher flexural modulus of coPP provided higher stiffness and because of that, coPP mixed samples had generally higher compression recovery than those of TPO, after continuing loading-unloading. On the other hand, since the TPO is a softer material due to its significantly lower bending rigidity, TPO mixed samples had lower compression recovery, in other word they deformed easier than 100PP. Additionally, since the flexural modulus of coPP material is closer to that of PP homopolymer, coPP blends did not become softer as much as TPO blends, so the deformation was observed more limited under continuing loading. Finally, it can also be said that, since the flexural modulus of PP homopolymer is higher compared to other polymer, mixed samples generally performed lower compression recovery.

Percentage work recovery generally determines the resistance of carpets to compression. As shown in Figure 6, TPO mixed samples had higher resistance to compression than those of coPP. This situation was attributed TPO's high-impact strength characteristic or in other word higher

toughness, due to the rubber component in its structure. Both coPP and TPO polymers have ethylene units in their structure, Furthermore, TPO has elastomer properties due to the rubber components. So its toughness is much more than that of coPP. Consequently, it can be said that, the higher toughness resulted in higher resistance to compression. In addition, it was also observed from the figure that, the increased mixing ratio enhanced more effectively the work recovery.

Compression work is a measure of compressibility of carpets, in other word; it can be defined as the amount of work done for compression of pile yarns. Figure 7, which represents the compression work of samples, showed that, coPP mixed samples had higher values than those of TPO which is softer than coPP. The flexural modulus of coPP material was significantly higher than that of TPO and slightly lower than that of homopolymer. In practical, it is known that, the higher the flexural modulus of a material, the harder it is to bend. For this reason, the lower stiffness of TPO caused the mixed samples to absorb lower energy compared to coPP mixed samples, during compression period. Besides, it was determined that, mixing coPP with homopolymer did not contribute the compression work significantly.

Recovery work, a measure of released energy after the load is removed, can be defined as the amount of work done for recovery of the piles to their initial position. The recovery work of samples are given in Figure 8. As seen from the figure, similar to compression work results, coPP mixed samples had higher values than those of TPO. This means that, TPO mixed samples absorbed and released lower energy compared to coPP samples because of its lower rigidity, during compression and recovery periods.
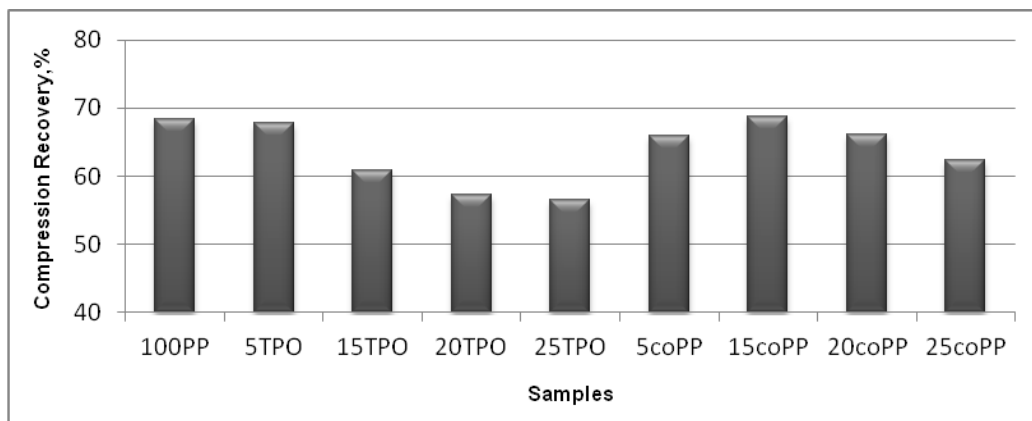

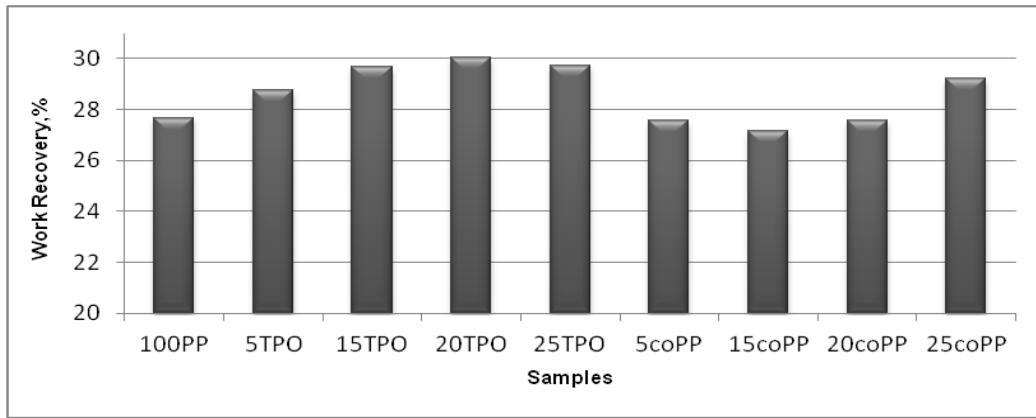**Figure 5.** Percentage compression recovery of samples

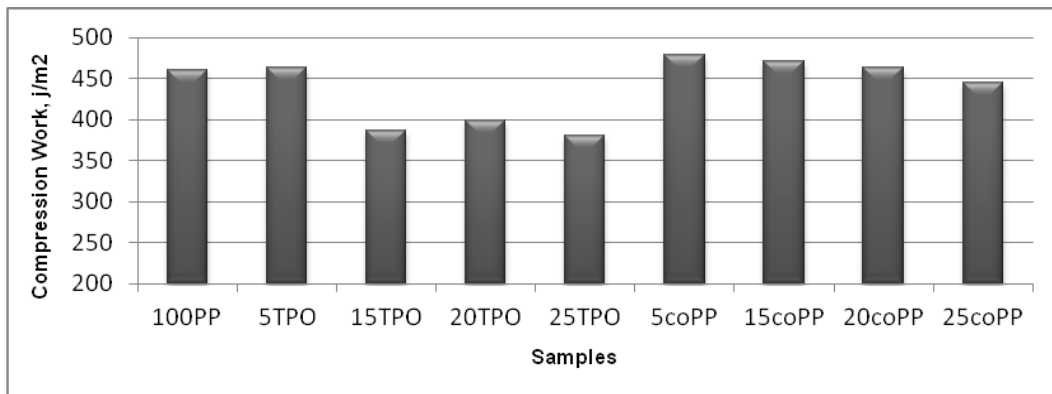**Figure 6.** Percentage work recovery of samples

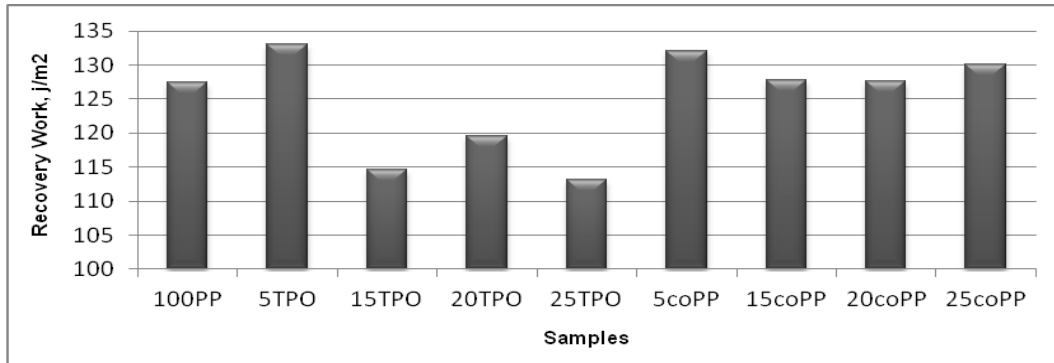

Figure 7. Compression work of samples

Figure 8. Recovery work of samples

Table 9 exhibits mean, standard deviation and %CV of the compression and recovery test results. Two-way ANOVA results of TPO or coPP mixed samples for percentage compression recovery, percentage work recovery, compression work and recovery work are shown in Table 10-Table 13, respectively. According to the Table 10 and Table 11, both parameters; content type (p=0.002<0.05 and p=0.000<0.05) and % percentage (p=0.012<0.05 and p=0.040<0.05) had statistically significant effect; besides, content type was more effective than % percentage, (F=10.800>F=4.286 and F=26.460>F=3.108), on percentage compression recovery and percentage work recovery, respectively. No statistically significant interaction was observed between the parameters (p=0.088>0.05 and p=0.066>0.05) from Table 10 and Table 11. As seen from the Table 12 and Table 13, both content type (p=0.000<0.05 and p=0.000<0.05) and % percentage (p=0.000<0.05 and p=0.004<0.05) factors were statistically significant on compression work and recovery work. It was also seen from the tables that; the effect of content type was higher than of % percentage (F=65.873>F=12.116 and F=16.884>F=5.408) on compression work and recovery work. Besides, it was determined that the interaction between content type and % percentage was statistically significant (p=0.013<0.05 and p=0.049<0.05) for work of compression and recovery, respectively.

Table 9. Mean, standard deviation and % CV compression and recovery test results

Sample code		100PP	5TPO	15TPO	20TPO	25TPO	5coPP	15coPP	20coPP	25coPP
Percentage compression recovery	Mean	68.44	67.81	60.88	57.19	56.52	65.95	68.75	66.04	62.45
	SD	3.93	3.29	6.59	4.04	2.39	4.02	4.26	6.55	6.80
	%CV	5.74	4.85	10.83	7.06	4.24	6.10	6.19	9.92	10.89
Percentage work recovery	Mean	27.68	28.72	29.69	30.04	29.70	27.63	27.12	27.55	29.24
	SD	0.55	0.38	0.57	1.12	0.68	1.48	0.92	1.48	0.96
	%CV	1.97	1.29	1.91	3.68	2.28	5.37	3.40	5.35	3.29
Compression work	Mean	460.90	462.75	386.17	398.07	380.91	479.06	470.96	463.09	445.16
	SD	23.51	26.24	28.56	10.78	23.66	32.11	20.69	8.65	17.67
	%CV	5.10	5.67	7.39	2.70	6.21	6.70	4.39	1.86	3.96
Recovery work	Mean	127.52	132.98	114.62	119.53	113.20	132.01	127.82	127.67	130.11
	SD	5.96	8.91	7.59	3.54	8.63	3.30	8.43	9.07	4.74
	%CV	4.67	6.70	6.62	2.96	7.62	2.50	6.59	7.11	3.64

Table 10. Two-way ANOVA for percentage compression recovery of TPO or coPP mixed samples

Source	Type IV Sum of Squares	df	Mean Square	F	Sig.	Partial Eta Squared
Corrected Model	770.272a	7	110.039	4.399	0.002	0.490
Intercept	159788.561	1	159788.561	6388.153	0.000	0.995
content_type	270.140	1	270.140	10.800	0.002	0.252
%_percentage	321.608	3	107.203	4.286	0.012	0.287
content_type * %_percentage	178.524	3	59.508	2.379	0.088	0.182
Error	800.424	32	25.013	-	-	-
Total	161359.258	40	-	-	-	-
Corrected Total	1570.697	39	-	-	-	-

Table 11. Two-way ANOVA for percentage work recovery of TPO or coPP mixed samples

Source	Type IV Sum of Squares	df	Mean Square	F	Sig.	Partial Eta Squared
Corrected Model	45.308a	7	6.473	6.245	0.000	0.577
Intercept	32979.752	1	32979.752	31821.758	0.000	0.999
content_type	27.423	1	27.423	26.460	0.000	0.453
%_percentage	9.662	3	3.221	3.108	0.040	0.226
content_type * %_percentage	8.223	3	2.741	2.645	0.066	0.199
Error	33.164	32	1.036	-	-	-
Total	33058.225	40	-	-	-	-
Corrected Total	78.473	39	-	-	-	-

Table 12. Two-way ANOVA for compression work of TPO or coPP mixed samples

Source	Type IV Sum of Squares	df	Mean Square	F	Sig.	Partial Eta Squared
Corrected Model	57830.356a	7	8261.479	16.407	0.000	0.782
Intercept	7595963.521	1	7595963.521	15085.493	0.000	0.998
content_type	33168.673	1	33168.673	65.873	0.000	0.673
%_percentage	18302.461	3	6100.820	12.116	0.000	0.532
content_type * %_percentage	6359.222	3	2119.741	4.210	0.013	0.283
Error	16112.887	32	503.528	-	-	-
Total	7669906.763	40	-	-	-	-
Corrected Total	73943.243	39	-	-	-	-

Table 13. Two-way ANOVA for recovery work of TPO or coPP mixed samples

Source	Type IV Sum of Squares	df	Mean Square	F	Sig.	Partial Eta Squared
Corrected Model	2152.328a	7	307.475	5.981	0.000	0.567
Intercept	622470.065	1	622470.065	12108.495	0.000	0.997
content_type	867.972	1	867.972	16.884	0.000	0.345
%_percentage	834.078	3	278.026	5.408	0.004	0.336
content_type * %_percentage	450.278	3	150.093	2.920	0.049	0.215
Error	1645.047	32	51.408	-	-	-
Total	626267.440	40	-	-	-	-
Corrected Total	3797.375	39	-	-	-	-

3.4. Hexapod appearance retention assessment

Texture appearance retention levels of samples after 4000 revolutions were assessed subjectively depending on the appropriate reference scale and shown in Figure 9. According to the results, the highest and lowest appearance retention grades were obtained by 15coPP and the 15TPO, respectively. Contrary to the results of dynamic and static loading tests, it was determined that TPO mixed samples exhibited lower performance in terms of appearance retention than those of coPP. As mentioned before, TPO is a softer material compared to coPP. So this structural property caused TPO mixed samples to have lower ability of appearance retention than those of coPP. On the other hand, it was observed that % percentage has no regular tendency on appearance retention of samples.

Table 14 and Table 15 exhibits mean, standard deviation, %CV and two-way ANOVA results of TPO or coPP mixed samples for hexapod appearance retention levels, respectively. Depending on the Table 15, it can be seen that; content type had a statistically significant effect ($p=0.001<0.05$), whereas % percentage was found to be statistically insignificant ($p=0.705>0.05$), on hexapod appearance retention. Additionally, no statistically significant interaction was observed between the parameters ($p=0.172>0.05$) from the table.
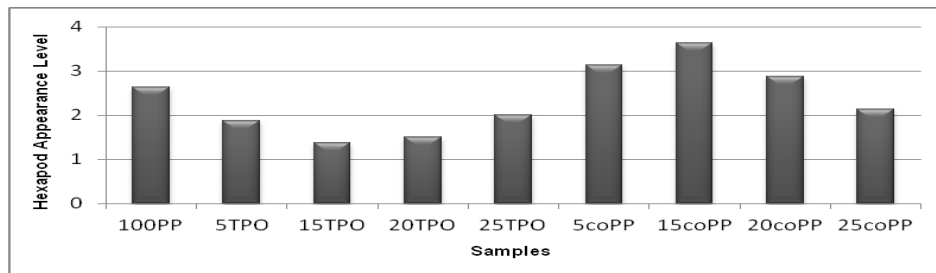
Figure 9. Appearance retention levels of samples

Table 14. Mean, standard deviation and %CV of hexapod appearance retention results

Sample code		100PP	5TPO	15TPO	20TPO	25TPO	5coPP	15coPP	20coPP	25coPP
	Mean	2.625	1.875	1.375	1.500	2.000	3.125	3.625	2.875	2.125
Hexapod	SD	1.03	0.85	0.75	1.00	1.00	0.94	0.75	0.85	1.10
	%CV	39.26	45.54	54.54	66.66	50.00	30.28	20.68	29.70	52.17

Table 15. Two-way ANOVA for hexapod appearance retention of TPO or coPP mixed samples

Source	Type IV Sum of Squares	df	Mean Square	F	Sig.	Partial Eta Squared
Corrected Model	18.250a	7	2.607	3.109	0.018	0.476
Intercept	171.125	1	171.125	204.075	0.000	0.895
content_type	12.500	1	12.500	14.907	0.001	0.383
%_percentage	1.188	3	0.396	0.472	0.705	0.056
content_type * %_percentage	4.563	3	1.521	1.814	0.172	0.185
Error	20.125	24	0.839	-	-	-
Total	209.500	32	-	-	-	-
Corrected Total	38.375	31	-	-	-	-

3.5. Tuft withdrawal force

Results of tuft withdrawal force of carpet samples is given Figure 10. It was determined that the tuft withdrawal forces of the samples did not show a significant difference with respect to the mixing of materials with different types and quantities. Depending on the results, it was evaluated that, measurements had high variation due to the unevenness of latex applied to carpet samples. In addition, no linear relationship was observed between content type and percentage of mixes.

Mean, standard deviation, % CV of and two-way ANOVA results of TPO or coPP mixed samples for tuft withdrawal force are shown in Table 16 and Table 17, respectively. As it is seen from the table, both content type (p=0.339>0.05) and % percentage (p=0.230>0.05) were detected statistically insignificant on tuft withdrawal force.

4. CONCLUSION

Depending on the dynamic and static loading test results, it was concluded that TPO mixed samples had generally lower thickness loss than those of coPP and neat PP. Furthermore, for both loading tests it was revealed that, mixing 5% TPO to homopolymer performed the best result in terms of thickness loss and resilience. As the % percentage increased for both mix type, thickness loss also increased, whereas resilience decreased. This is a desirable situation with regard to cost of production, because coPP and TPO are more expensive than PP homopolymer.

According to the compression and recovery test results, TPO mixed samples had lower values than those of coPP, for work of compression and recovery. This was attributed TPO's softer structure due to the its lower flexural modulus (bending rigidity) compared to coPP affected the work done, therefore TPO absorbed lower energy when it was compressed, and so released lower energy after the load was removed. Additionally, coPP mixed samples had generally higher compression recovery than those of TPO, since the higher flexural modulus of coPP ensured higher stiffness. In addition, TPO mixed samples had higher resistance to compression than those of coPP. This situation was attributed TPO's high-impact strength characteristic or
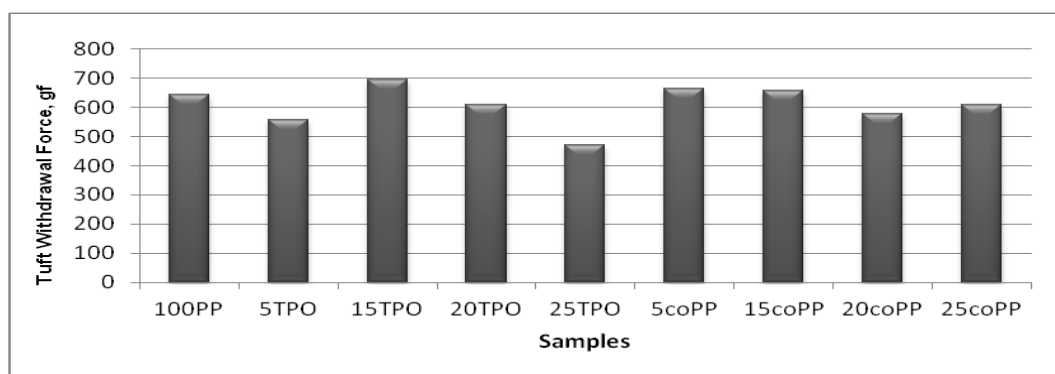

Figure 10. Tuft withdrawal forces of samples

Table 16. Mean, standard deviation and %CV of tuft withdrawal force test results

Sample code		100PP	5TPO	15TPO	20TPO	25TPO	5coPP	15coPP	20coPP	25coPP
Tuft withdrawal force	**Mean**	644	556	696	610	470	665	657	579	610
	SD	186.22	211.81	335.07	293.54	243.69	346.46	347.45	238.28	309.32
	%CV	28.91	38.09	48.14	48.12	51.85	52.09	52.88	41.15	50.70

Table 17. Two-way ANOVA for tuft withdrawal force of TPO or coPP mixed samples.

Source	Type IV Sum of Squares	df	Mean Square	F	Sig.	Partial Eta Squared
Corrected Model	718717.500a	7	102673.929	1.180	0.317	0.052
Intercept	58636622.500	1	58636622.500	674.052	0.000	0.816
content_type	80102.500	1	80102.500	0.921	0.339	0.006
%_percentage	379087.500	3	126362.500	1.453	0.230	0.028
content_type * %_percentage	259527.500	3	86509.167	0.994	0.397	0.019
Error	13222660.000	152	86991.184	-	-	-
Total	72578000.000	160	-	-	-	-
Corrected Total	13941377.500	159	-	-	-	-

in other word higher toughness. It was also determined that, as the % percentage increased, percentage compression recovery, work of compression and recovery decreased, while percentage work recovery increased. This result confirmed that, coPP and TPO enhanced the toughness property of mixed samples, as stated in some studies in the literature [23-25]. In addition, the amount of coPP or TPO in PP homopolymer changed internal structure, therefore pile yarns showed different load carrying performances.

Hexapod test assessments exhibited that coPP mixed samples had better texture retention than those of TPO. This can be interpreted as coPP had better appearance retention than TPO. On the other hand, no linear relationship was observed between % percentages of mixes.

Tuft withdrawal force results of samples showed that, content type and % percentage had no significant effect. High variation was observed on withdrawal forces, and this was a probable result of unevenness of applied latex on the back of carpets.

REFERENCES

1. Crawshaw GH. 2002. *Carpet Manufacture*. New Zealand: Wronz Developments.

2. Gong RH. 2011. *Specialist Yarn and Fabric Structures Developments and Applications*. United Kingdom: Woodhead Publishing Limited.

3. Hannay F. 2002. *Rigid Plastics Packaging - Materials, Processes and Applications*. United Kingdom: Rapra Technology Limited.

4. Tripathi D. 2002. *Practical Guide to Polypropylene*. United Kingdom: Rapra Technology Limited.

5. Brydson JA. 1995. *Thermoplastic Elastomers – Properties and Applications*. United Kingdom: Rapra Technology Limited.

6. Massey LK. 2004. *Film Properties of Plastics and Elastomers, A Guide to Nonwovens in Packaging Applications*, *Second Edition*. United Kingdom: William Andrew Applied Science Publishers.

7. Grover G, Zhu S, Twilley IC. 1993. Dynamic Mechanical Properties of Carpet Yarns and Carpet Performance. *Textile Research Journal,* 63(5), 257-266.

8. Vangheluwe L, Kiekens P. 1997. Resilience Properties of Polypropylene Carpets. *Textile Research Journal,* 67(9), 671-676.

9. Laughlin KC, Cusick GE. 1968. Carpet Performance Evaluation. *Textile Research Journal,* 38(1), 78-80.

10. Önder E, Berkalp ÖB. 2001. Effects of Different Structural Parameters on Carpet Physical Properties. *Textile Research Journal,* 71(6), 549-555.

11. Koç E, Çelik N, Tekin M. 2005. An Experimental Study on Thickness Loss of Wilton-Type Carpets Produced with Different Pile Material after Prolonged Heavy Static Loading. Part-I: Characteristics Parameters and Carpet Behaviour. *FIBRES & TEXTILES in Eastern Europe*, 13(4), 56-62.

12. Koç E, Çelik N. 2007. An Experimental Study on Thickness Loss of Wilton-Type Carpets Produced with Different Pile Material after Prolonged Heavy Static Loading. Part-II: Characteristics Parameters and Carpet Behaviour. *FIBRES & TEXTILES in Eastern Europe*, 15(4), 87-92.

13. Çelik N, Koç E. 2010. Study on the Thickness Loss of Wilton-Type Carpets under Dynamic Loading. *FIBRES & TEXTILES in Eastern Europe,* 18(1), 54-58.

14. Korkmaz Y, Koçer SD. 2010. Polipropilen Makine Halısı Üretim Parametrelerinin Halı Performansına Olan Etkileri. *Tekstil Teknolojileri Elektronik Dergisi,* 4(1), 48-58.

15. Özdil N, Bozdoğan F, Özçelik Kayseri G, Süpüren Mengüç G. 2012. Compressibility and Thickness Recovery Characteristic of Carpet. *Tekstil ve Konfeksiyon,* 3, 203-211.

16. Dayiary M, Shaikhzadeh Najar S, Shamsi M. 2009. A New Theoretical Approach tu Cut-Pile Carpet Compression Based on Elastic-Stored Bending Energy. *The Journal of the Textile Institute,* 100(8), 688-694.

17. Dayiary, M, Shaikhzadeh Najar, S, Shamsi, M. 2010. An Experimental Verification of Cut-Pile Carpet Compression Behavior. *The Journal of the Textile Institute,* 101(6), 488-494.

18. Sarkeshick S, Tavanai H, Zarrebini M, Morshed M. 2009. An Investigation on the Effects of Heat-Setting Process on the Properties of Polypropylene Bulked Continuous Filament Yarns. *The Journal of the Textile Institute,* 100(2), 128-134.

19. Dadgar M, Merati AA, Varkiyani MH. 2015. Evaluation of Heat Setting Parameters in Carpet Comfort. *Fibers and Polymers,* 16(5), 1169-1176.

20. Kebabcı M, Babaarslan O, Özkan Hacıoğulları S, Telli A. 2015. The Effect of Drawing Ratio and Cross-Sectional Shapes on the Properties of Polypropylene CF and BCF Yarns. *Tekstil ve Mühendis Dergisi,* 22(100), 46-53.

21. Erdoğan ÜH. 2012. Effect of Pile Fiber Cross Section Shape on Compression Properties of Polypropylene Carpets. *The Journal of the Textile Institute,* 103(12), 1369-1375.

22. Tavanai H, Morshed M, Hosseini SM. 2003. Effect of On-Line Melt Blending of Polypropylene with Polyamide 6 on the Bulk and Strength of the Resulting BCF Yarn. *Iranian Polymer Journal,* 12(5), 421-430.

23. Lotti C, Correa CA, Canevarolo SV. 1999. Mechanical and Morphological Characterization of Polypropylene Toughened with Olefinic Elastomer. *Materials Research,* 3(2), 37-44.

24. Fasihi M, Mansouri H. 2016. Effect of Rubber Interparticle Distance Distribution on Toughening Behavior of Thermoplastic Polyolefin Elastomer Toughened Polypropylene. *Journal of Applied Polymer Science,* 133, 44068.

25. Rungswang W, Saendee P, Thitisuk B, Pathaweeisariyakul T, Cheevasrirungruang W. 2013. Role of Crystalline Ethylene-Propylene Copolymer on Mechanical Properties of Impact Polypropylene Copolymer. *Journal of Applied Polymer Science,* 128, 3131-3140.

Investigation of the Effect of the Use of Bamboo and Silver Yarn on Antibacterial Activity in Towel Fabric

Navruz PAKSOY[1] 0000-0002-0741-1174
Seval KONUKOĞLU[2] 0000-0001-6171-1883
Levent Güven AYAR[2] 0000-0001-8917-6157
Cansu BATCIK[2] 0000-0002-1400-5852
Hüseyin AYDIN[1] 0000-0003-3593-8712

[1]Sanko Textile Enterprises Industry and Trade Corporation (Towel) R&D Center, Gaziantep/Türkiye
[2]Sanko Textile Enterprises Industry and Trade Corporation (Yarn) R&D Center, Gaziantep/Türkiye

Corresponding Author: Navruz Paksoy, nevruzpaksoy_@hotmail.com

ABSTRACT

Towel fabrics provide a suitable environment for bacterial growth due to the moisture on them. For this reason, studies are carried out on the antibacterial properties of the towel. In this study, it is aimed to conduct research activities within the scope of developing antibacterial terry fabric. For this purpose, different terry fabric productions were made using silver yarn, bamboo and antibacterial chemicals, and their antibacterial properties were examined. In this context, the antibacterial chemical finishing process, known as the classical method, was applied to the towels, which were first woven from 100% cotton yarn. In addition, towel fabrics were produced by using 70% bamboo-30% cotton yarn and 92% cotton-8% silver yarn. Antibacterial activities of the obtained fabric samples against *S. aureus* and *K. pneumonie* bacteria according to AATCC 100 standard were examined.

1. INTRODUCTION

Microorganisms are too small to be seen with the naked eye. This structure includes bacteria, fungi, algae and viruses. Textile materials carry microorganisms as bacteria and fungi due to the adhesion of these organisms to their surfaces. These microorganisms are found almost everywhere in the environment and multiply rapidly when they encounter moisture and temperature. The proliferation of microorganisms on the textile during use and storage both negatively affects the textile product and causes health problems for the user [1-4].

Natural fibers such as cotton are more susceptible to microorganism related problems than synthetic fibers due to their porous and hydrophilic structure. Cellulosic fibers, which are widely used in the textile industry due to these properties, provide a suitable environment for microorganisms. Textiles tend to harbor micro-organisms

responsible for proliferation of diseases, unpleasant odors, discoloration and deterioration of fabrics. The most common active ingredients used in antimicrobial applications are triclosan, quaternary ammonium salts and metals (silver, copper, zinc, etc.). Human and environmental health, process-related concerns have especially increased interest in silver-doped antimicrobial materials. Although many metals are known to have antimicrobial effects, silver is more preferred than other metals. The main reasons for this are that it is the most resistant metal against bacteria, it has been known for a long time that it does not have harmful effects on the body in its controlled use, it is cheaper to make it into a final product compared to most materials, and the easy production process [2, 5-9, 10, 11].

Silver compounds with a pronounced antibacterial effect against most pathogenic microorganisms are widely used

[12]. Silver, on the other hand, is a relatively non-toxic disinfectant that can significantly reduce many types of bacteria and fungi. At the same time, the powerful antimicrobial activity of silver is known to be effective against nearly 650 types of bacteria. Silver is generally applied to textiles in colloidal form and nano metallic form or in insoluble silver salt dispersion. In the case of synthetic fibers, silver can be incorporated into a spinning solution in the form of a zeolite complex or nanoparticles. Silver nanoparticles show good antibacterial properties due to their large surface area [9, 11]. Silver is used safely in many areas of textile [13].

Towel fabric is one of the main consumer products used by people around the world. Bathroom, sports, swimming pool, kitchen, beach, etc. towels with different water absorption properties are used in various places [14]. Terry fabrics consist of ground warp, pile warp and weft yarns [14, 15]. Cotton fiber has been used in towel production for many years. Today, however; It is observed that bamboo fiber, which is claimed to have soft, anti-bacterial, high level of absorbency and high level of washing fastness, is preferred as much as cotton fiber in towel production [16]. Because bamboo contains bamboo extract, a substance called Bamboo Kun, it is difficult for disease-causing organisms or insects to affect this plant. This is why bamboo is grown naturally without pesticides. Bamboo fiber is an environmentally friendly fiber. Bamboo fiber is a type of regenerated cellulose fiber produced from the raw materials of bamboo pulp. The fineness and whiteness of bamboo fiber is similar to classic viscose [17-20]. Tusief et al. [21] reported that the use of bamboo fiber has a significant effect on its antibacterial activity feature.

Many studies have shown that textile materials made of antimicrobial fibers show longer durability against microorganisms. However, the applications made with the finishing chemical on the finished product also have various advantages such as ease of application [5, 22]. Perelshtein et al. conducted an antibacterial activity study by coating silver nanoparticles on different fabric types in their study. The Ag-fabric composite has been shown to show excellent antibacterial activity against Escherichia coli (gram-negative) and Staphylococcus aureus (gram-positive) cultures [23].

Antibacterial towel feature is provided with finishing chemicals as a classical method. Antibacterial feature can also be achieved with fiber. The natural structure of bamboo fiber shows antibacterial properties. Silver fiber is also known as the fiber that provides another antibacterial property. While bamboo fiber from these fibers is used in the production of terry cloth, silver fiber was not used in the production of terry cloth in the literature screenings. Within the scope of the study, it was aimed to investigate the antibacterial properties of terry fabric by using bamboo and silver fiber, which are antibacterial fibers, in addition to the antibacterial chemical finishing process. In this direction, as

an alternative to the classical method, chemical antibacterial finishing process, towels with bamboo and silver yarn were obtained. The antibacterial properties of the yarns obtained with bamboo fiber are provided by the substance called Bamboo Kun in the structure of the fiber. An alternative has been created by using yarns obtained with bamboo fiber to provide antibacterial properties from the raw material. In the study conducted by Yüksek, it was observed that 60% bamboo-40% cotton experiments did not show antibacterial activity, and they obtained antibacterial activity in the experiments with 70% bamboo-30% cotton. Based on this result, experiments were made from 70% bamboo-30% cotton yarns in this study [24]. Another alternative work is towels woven with yarn obtained using silver fiber. The main purpose of the study within the scope of antibacterial towel studies is to obtain antibacterial towels with antibacterial finishing chemicals, bamboo and silver thread. The antibacterial properties of the obtained towels were investigated.

2. MATERIAL AND METHOD

2.1 Material

Yarns made of 100% cotton, 70% bamboo - 30% cotton and 92% cotton - 8% silver fiber were used as materials in the study. Organofunctional silane-based antibacterial finish with a solid substance ratio of 4.12% was used to obtain antibacterial properties by chemical finishing method. In the study, the experiments were evaluated on the optical process without painting. Wetting agent, combined bleaching chemical, caustic (48 Beo), hydrogen peroxide (50%), optical brightener, acetic acid (80%), antiperoxide enzyme and softening chemicals were used for the optical treatment of the towels obtained. The companies from which the chemicals used are supplied are given in Table 1.

Table 1. Chemical supply companies

	Suppliers
Wetting Agent	Denge Chemistry
Combined Bleaching Chemical	Rudolf
Caustic	Alde
Hydrogen Peroxide	Alde
Optical Brightener	NF Chemistry
Acetic Acid	Alde
Antiper Enzyme	Dystar
Softener	Rudolf

2.2 Method

2.2.1 Yarn Production

The properties of pile warp, ground warp and weft yarns used in the study are given in Table 2. The part that touches the human skin in the towel fabric is mainly the pile yarn. Therefore, the raw material to be used in the pile yarn should provide the performance expected from the towel and be suitable in terms of production. For this reason, cotton and bamboo raw materials are used in pile yarn. Yarns containing cotton, bamboo and silver fibers were used in the weft and ground warp threads. In the study, the

effect of the fiber content in the yarn on antibacterial properties was investigated. In this context, vortex air-jet spinning system has been used as the spinning method for the production advantages of bamboo fiber, which is a regenerated cellulosic fiber.

2.2.2 Towel Weaving Process

In the study, the towels weaved by weft, ground warp and pile warp threads. The weaving process was carried out with a 3-weft method with two loops on both sides. Weaving processes were carried out on jacquard weaving machine (Dornier). The weaving processes were given in Table 3. The weft density in weaving operations was 19 pieces / cm and the comb number was 11 teeth / cm.

2.2.3 Wet Processes

Optical whitening process was applied to the towel fabrics obtained within the scope of the study according to the exhaustion method in the MCS Model HT dyeing machine under the conditions given in Table 4. In this direction, optical treatment was applied to all experiments in the exhaustion method under the same process conditions. For the 4th experiment, antibacterial finishing process was applied as wet in the same process vessel in exhaustion method after standard optical treatment. As an antibacterial treatment, antibacterial treatment was performed with a solution containing 3% organofunctional silane-based antibacterial finish at 40 ºC at a ratio of 1/7 liquor for 30 minutes. Process parameters of the experiments performed are given in Figure 1 and Figure 2.

Table 2. Yarn information

	Type Code	Yarn Count	Yarn Production Technique	Fiber Content
Pile Warp Yarn	A	Ne 14/1	Open End	100 % Cotton
	B	Ne 14/1	Vortex	70 %Bamboo -30 %Cotton
Ground Warp Yarn	C	Ne 20/2	Open End	%100 Cotton
	D	Ne 20/2	Vortex	70% Bamboo – 30% Cotton
Weft Thread	A	Ne 14/1	Open End	100 %Cotton
	E	Ne 16/1	Ring/Comped	92 %Cotton -8% Silver Fiber
	F	Ne 16/1	Vortex	70 %Bamboo -30 %Cotton
	G	Ne 16/1	Ring/Carded	100 %Cotton

Table 3. Experimental parameters

Experimental No	Pile Warp Yarn	Ground Warp Yarn	Weft Thread	Fiber Content
1	A	C	A + E	98,4 %Cotton -1,6 %Silver
2	A	C	A + E	99,2 %Cotton -0,8 %Silver
3	B	D	F	70 %Bamboo-30 %Cotton
4	A	C	G	100 %Cotton

Table 4. Optical prescription

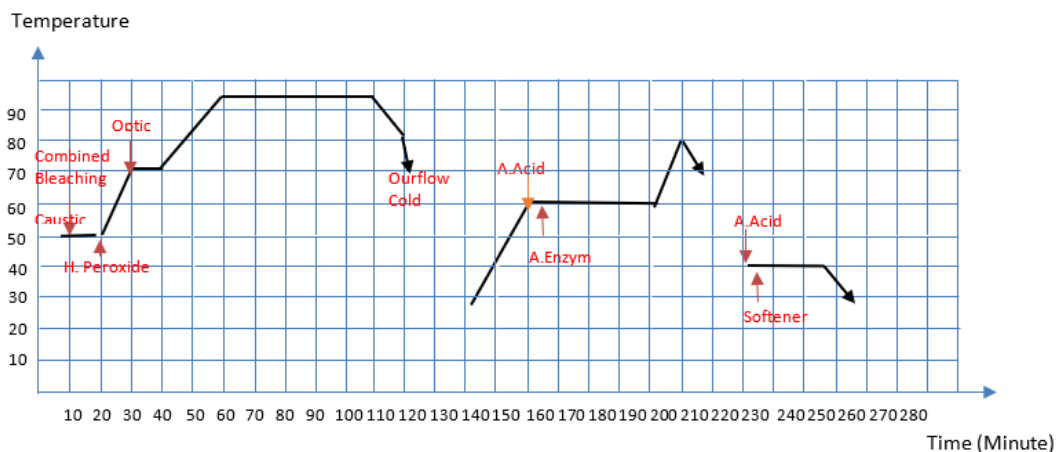| Chemical	Prescription
Wetting Agent	0,7 g/L
Combined Bleaching Chemical	2 g/L
Caustic	4,5% (by the ratio of fabric weight)
Hydrogen Peroxide	11% (by the ratio of fabric weight)
Optical Brightener	0,7% (by the ratio of fabric weight)
Acetic Acid	1,2 g/L
Antiper Enzyme	0,6 g/L
Softener	1%(by the ratio of fabric weight)
Flotte Ratio	1/7

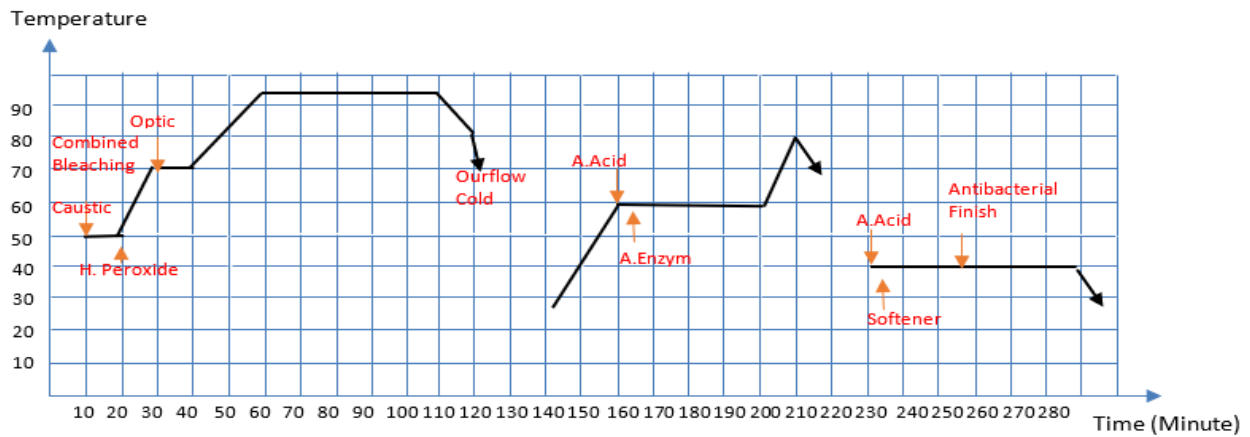
Figure 1. Standard optical connection

Figure 2. Optical and antibacterial treatment parameters for experiment 4

2.3 Research Methods

AATCC 100 antibacterial test method was applied to the samples to determine the antibacterial activity of the towel fabrics obtained. The tests were made with ATCC 6538 coded gram positive *S. aureus* bacteria and ATCC 4352 coded gram negative *K. pneumoniae* bacteria.

The hydrophilicity properties of the samples in the study were made in the TS 866 standard. In this study, the experiments were made with 7 repetitions and the average was taken. Images of the yarns used in terry fabrics were taken with the JVC C1380 color video CCD camera.

CIELab values of the samples in the study were measured using a spectrophotometer. Measurements were carried out using Color i7 brand spectrophotometer and x-rite software. All measurements were made under D65 daylight and using a 10º observer angle. Through the software used, Berger, L

*, a *, b * values and color difference values were calculated with the CIELab 1976 formula.

3. RESULTS AND DISCUSSION

Different experiments were conducted within the scope of the study. Antibacterial efficacy performance and hydrophilicity results of the samples obtained were examined. Color differences were also detected. The microscope images of the yarns used in the study are given in Figure 3. Images of terry fabrics obtained from these yarns are given in Figure 4.

When Figure 3 is examined, the silver thread appears darker in the E-coded thread. Silver fiber is produced in ring spinning system together with cotton fiber. In the yarn, which has 8% silver fiber content, the silver fiber appears in the yarn structure as darker than cotton.
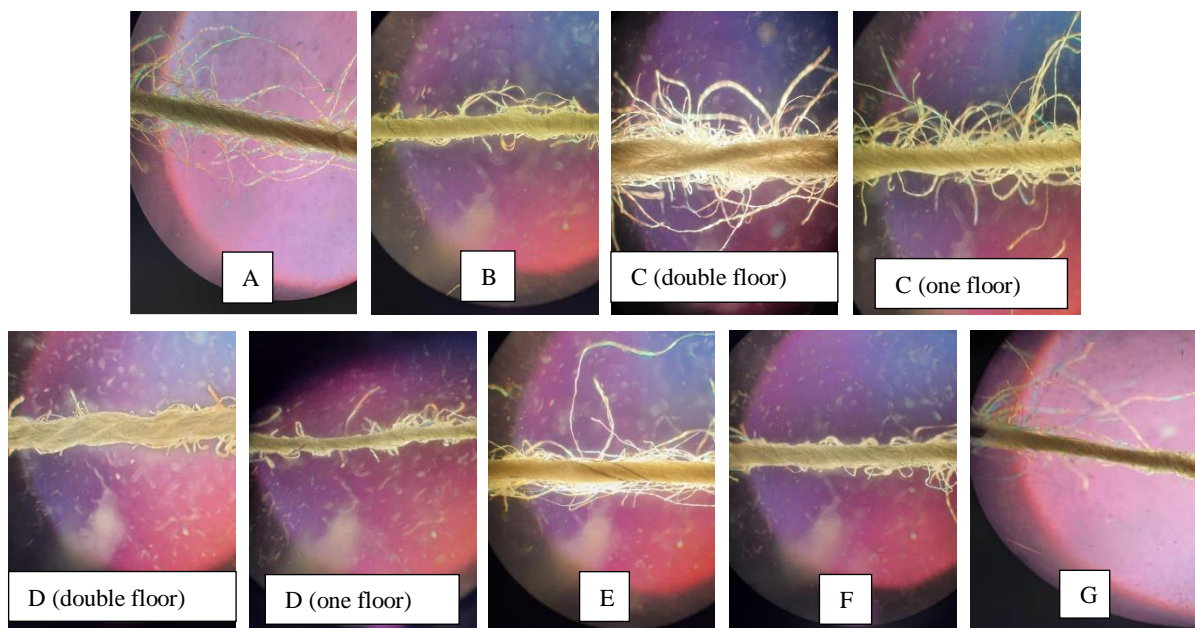

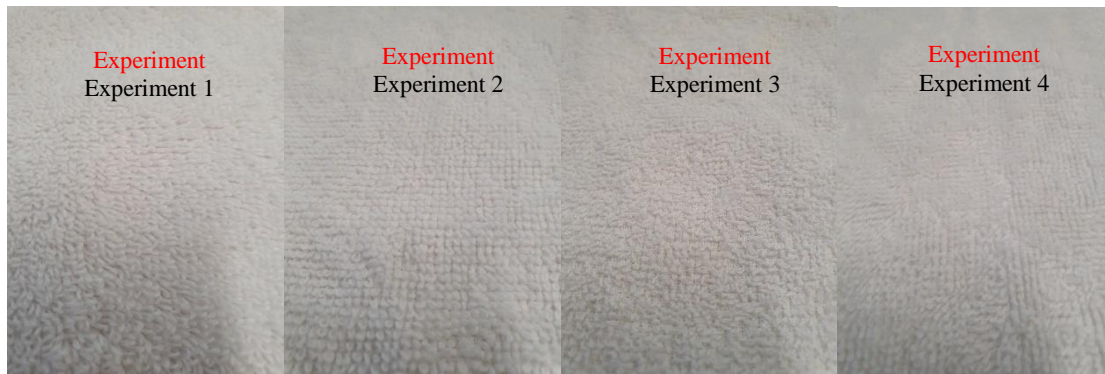
Figure 3. Images of experiment samples

Figure 4. Images of experiment samples

3.1 Antibacterial Test Results

Two different types of bacteria were selected for the antibacterial activity test. Antibacterial test results of towel fabrics obtained as a result of the study are given in Figure 5.

When the antibacterial efficacy results of the study are examined, it is seen that all experiments show antibacterial efficacy close to each other. There are still new studies on silver-containing fibers and the subject remains up-to-date. In their study, Smiechowicz et al. (2020) conducted studies on obtaining antibacterial fibers containing nanosilica with immobilized silver nanoparticles. Antibacterial activity against S. Aureus and E. Coli bacteria was studied. As a result, fibers with antibacterial activity were obtained [25]. In their study, Xu et al (2017) coated the cotton fiber surface with silver and gained antibacterial properties. After 50 consecutive wash cycles in the study, bacterial reduction rates (BR) against both S. aureus and E. coli remained above 95% [26]. The antibacterial activities obtained in the study gave similar results to the literature.

Sabir and Ünal (2017) examined the antibacterial activity of 100% cotton raw terry fabric within the experimental parameters by testing it in the AATCC 100 standard. When the results obtained from this study were examined, it was determined that the untreated (raw) 100% cotton fabric did not show antibacterial activity [27]. When this study is taken as reference, it is seen that raw 100% cotton terry fabric has no antibacterial activity. However, high rates of antibacterial activity were obtained in the experiments conducted in the present study. Within the scope of the study, the antibacterial activity was investigated by evaluating the microorganism decrease in different periods (30 minutes, 2 hours, 4 hours, 6 hours, 12 hours and 24 hours) for the experiment using 0.8% silver yarn and the antibacterial chemical finishing experiment. Thus, the change of antibacterial activity depending on the time was determined. The data obtained are given in Figure 6 and Figure 7.

When Figure 5 and 6 are examined in the study, it is seen that the antibacterial activity increases with time. In the antibacterial efficacy test, it is expected that the microorganisms will decrease as the contact time of the samples that come into contact with microorganisms increases. The results confirm this. Bacteria increases between 30 minutes and 24 hours were 0.16% in *S. aureus* ATCC 6538 bacteria, 0.22% in *K. pneumonie* ATCC 4352 bacteria for Experimentl 2. Bacteria increases between 30 minutes and 24 hours were 0.15% in *S. aureus* ATCC 6538 bacteria, 0.19% in *K. pneumonie* ATCC 4352 bacteria for Experiment 4.
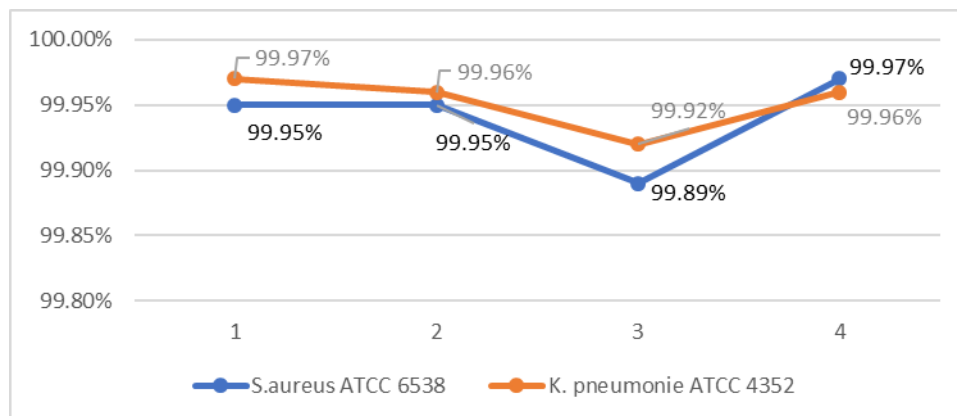

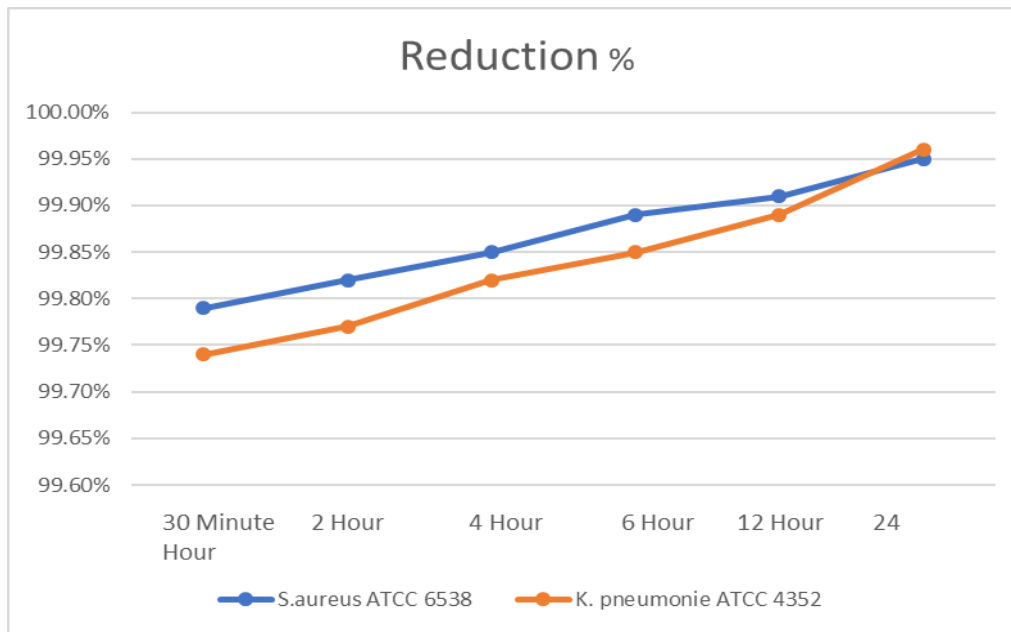**Figure 5.** Antibacterial efficacy results (Reduction %)

Figure 6. Antibacterial efficacy results for the experiment 2 sample (Reduction %)
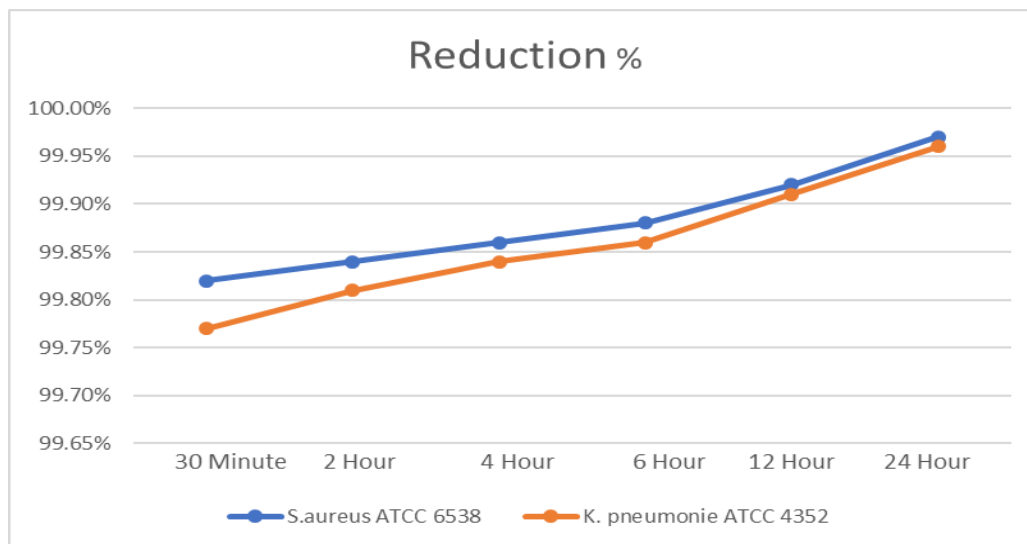

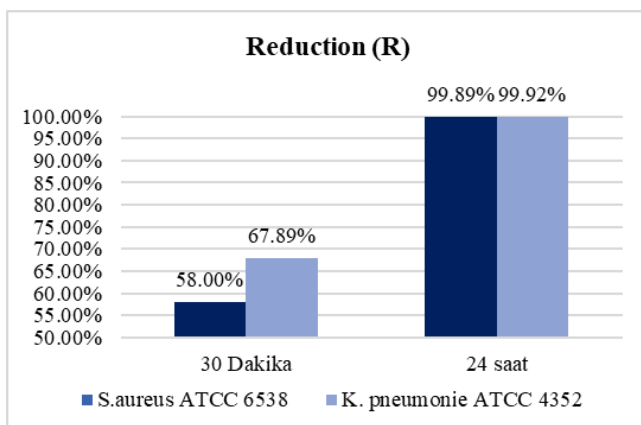**Figure 7.** Antibacterial efficacy results for experiment 4 samples (Reduction %)

Figure 8. Antibacterial efficacy results for experiment 3 samples (Reduction %)
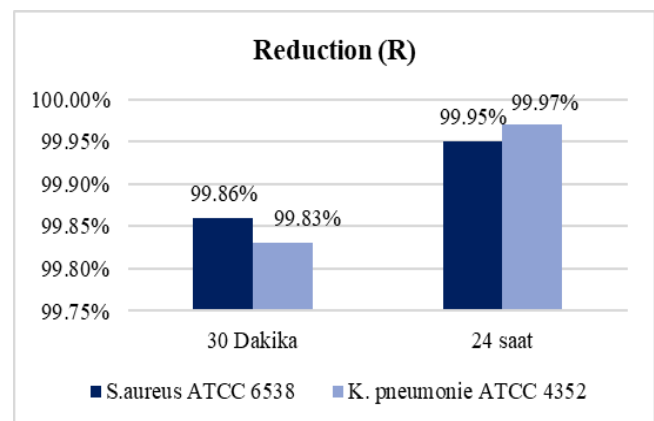

Figure 9. Antibacterial efficacy results for experiment 1 samples (Reduction %)

In Figure 7 and 8, the antibacterial activity increase for Experiment 3 and Experiment 1 is given. Microorganism reduction rate (%) was determined after 30 minutes and 24 hours in Experiment 3. When the results are examined, the reduction (R) % values for 30 minutes were obtained as 58.00% in *S. aureus* ATCC 6538 bacteria and *K. pneumonie* ATCC 4352 bacteria 67.89% in *K. pneumonie* ATCC 4352 bacteria in Experiment 3. For 24 hours, the reduction (R) % of *S. aureus* ATCC 6538 and *K. pneumonie* ATCC 4352 were 99.89% and 99.92%, respectively in Experiment 3. When the amount of increase between 30 minutes and 24 hours was examined for Experiment 3, it was determined as 0.41% in *S. aureus* ATCC 6538 bacteria and 0.32% in *K. pneumonie* ATCC 4352 bacteria. For Experiment 1, the bacterial increase between 30 minutes and 24 hours was 11% in *S. aureus* ATCC 6538 bacteria and 14% in *K. pneumonia* ATCC 4352 bacteria.

3.2. Hydrophilicity Test Results

Hydrophilicity tests were conducted to determine the usability of the trial towels obtained within the scope of the study. Test results are given in Figure 10.
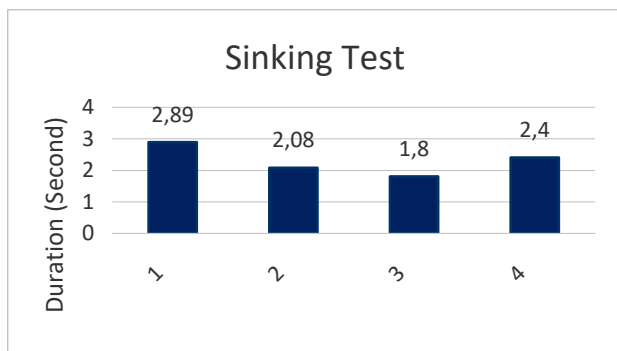

Figure 10. Sinking test results

The sinking test of the optic dyed towel without antibacterial chemical treatment was measured as 2.8 seconds. When the results are examined, it is seen that the hydrophility values of all of the experiments are close to the hydrophilicity value of the optic dyed towel sample without antibacterial treatment. Özmen (2010) stated in his master's thesis that the hydrophilicity value of the towel produced from bamboo fiber is better in the sinking test than the towel produced from cotton fiber [16]. In this study, it is seen that the sinking test value of the towels obtained with bamboo is lower.

3.3. CIELab Results

In the study, it is predicted that silver will create differences on the color due to its own color. For this reason, color differences were measured with reference to the chemical antibacterial finishing experiment. Berger values are given in Figure 11. L * a * b * values of the reference are given in Table 5. Color difference results are given in Table 6.
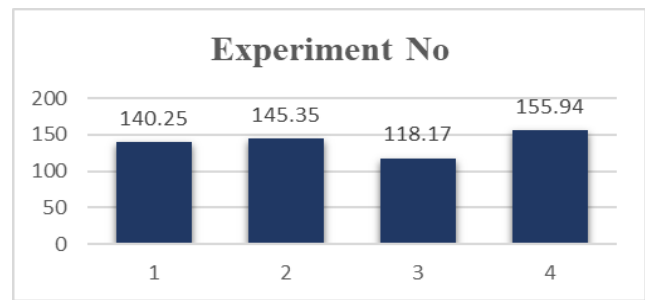

Figure 11. Berger values

Table 5. Reference L * a * b * values

Experiment No	L*	a*	b*
4	96,59	2,97	-11,96

Table 6. Results for CIELab color difference

Experiment No	ΔL*	Δa*	Δb*	ΔC*	ΔH*	ΔE
1	-3,44	0,2	1,62	-1,51	0,63	1,83
2	-3,79	0,81	-1,41	1,57	0,42	1,84
3	0,55	-0,36	0,7	-0,77	-0,19	0,66

In the color difference results, the desired limit values are expected to be below 1 in ΔE. When the color results are examined, it is seen that the color difference value of the Experiment 3 is within the desired limit values, while it is seen that there are color differences in the Experiments 1 and 2 due to the color of the silver itself. When Berger values are examined, it is seen that experiment 3 are lower than other studies.

4. CONCLUSION

Within the scope of the study, different methods were examined to obtain antibacterial towels. Antibacterial chemical finishing process is applied as the classical method for obtaining antibacterial towels. As an alternative to this method, bamboo fiber, which is widely used today, is also an alternative. However, it is supported by the literature that the rate of bamboo used in the towel has an effect on antibacterial activity. When all experiments are compared with antibacterial chemical finish, it is seen that the experiments performed as an alternative in the study show antibacterial efficacy. It has been observed that antibacterial activity does not change with 50% reduction in the use of silver fiber, and it is predicted that antibacterial effectiveness can be achieved by using lower amounts of silver. With the use of bamboo fiber and silver yarn in the towel fabric, antibacterial efficiency with high washing resistance can be achieved, while antibacterial activity with limited washing resistance will be achieved with chemical antibacterial finishing.

The classical method, antibacterial finishing application, has been carried out in experiments using silver and when

the results are examined, it is seen that there is an increase in bacterial decreases depending on the time. In the experiments made from bamboo yarn, it is seen that the rate of bacterial reduction in 30 minutes is lower than other experiments.

It is predicted that alternative methods can be used in these trials to the antibacterial finishing application, which is used as the classical method.

REFERENCES

1. Çukul D. 2013. Examples for the recent developments in technical yarns. *Journal of Textiles and Engineer* 20(91), 50-63.

2. Beşen BS. 2019. Production of disposable antibacterial textiles via application of tea tree oil encapsulated into different wall materials. *Fibers and Polymers* 20(12), 2587-2593.

3. Abedi D, Mortazavi SM, Mehrizi MK, Feiz M. 2008. Antimicrobial properties of acrylic fabrics dyed with direct dye and a copper salt. *Textile Research Journal* 78, 311.

4. Gao Y, Cranston R. 2008. Recent advances in antimicrobial treatments of textiles. *Textile Research Journal* 78(1), 60–72.

5. Üreyen ME, Çavdar A, Koparalı AS, Doğan A. 2015. Antibacterial efficacy and laundering durability of textile fabrics treated by newly developed silver doped nano scaled bio-antimicrobial finishing agent. *Journal of Textiles and Engineer* 69, 26-31.

6. Ibrahim NA, Gouda M, Husseiny M, El-Gamal AR, Mahrous F. 2008. UV-protecting and antibacterial finishing of cotton knits. *Journal of Applied Polymer Science* 112, 3589–3596.

7. Rimbu C, Cerempei A, Muresan R, Guguianu E, Ursache M, Borhan O, Muresan A. 2015. Eco-friendly antibacterial finish for natural knitted fabrics. *Tekstil ve Konfeksiyon* 25(4), 359-364.

8. Joshi M, Ali SW, Purwar R, Rajendran S. 2009. Ecofriendly antimicrobial finishing of textiles using bioactive agents based on natural products. *Indian Journal of Fibre&Textile Research* 34, 295.

9. Filipowska B, Rybicki E, Walawska A, Matyjas-Zgondek E. 2011. New method for the antibacterial and antifungal modification of silver finished textiles. *Fibres & Textiles in Eastern Europe* 19, 4 (87), 124-128.

10. Varesano A, Vineis C, Aluigi A, Rombaldoni F, Tonetti C, Mazzuchetti G. 2013. Antibacterial efficacy of polypyrrole in textile applications. *Fibers and Polymers* 14(1), 36-42.

11. Saengkiettiyut K, Rattanawaleedirojn P, Sangsuk S. 2008. A study on antimicrobial efficacy of nano silver containing textile. *Special Issue on Nanotechnology* 7(1), 33-36.

12. Dzhimak SS, Malyshko VV, Goryachko AI, Sokolov ME, Moiseev AV, Basov AA. 2019. Adsorption of silver nanoparticles on mono- and polyfilament fibers. *Nanotechnologies in Russia* 14 Nos. 1–2, 48–54.

13. Gülgönül M. 2018. Including silver complex production of nanofibers and use in textile, (Master's Thesis). Namık Kemal University Institute of Science.

14. Cruz J, Leitão A, Silveira D, Pichandi S, Pinto M, Fangueiro R. 2017. Study of moisture absorption characteristics of cotton terry towel fabrics. *Procedia Engineering,* 200, 389–398

15. Kakde MV, More H, Magarwadia B, Kejkar V. 2017. Effect of pile density on physical properties of terry towel fabric. *International Journal on Textile Engineering and Processes* 3(1).

16. Özmen B. 2010. Comparison of terryclothes which are made up with bamboo and cotton fiber in point of usag, (Master's Thesis). Gazi University Institute of Education Sciences.

17. Sekerden F. 2012. Effect of pıle yarn type on absorbency, stiffness, and abrasion resistance of bamboo/cotton and cotton terry towels. *Wood and Fiber Science* 44(2), 189-195.

18. Erdumlu N, Ozipek B. 2008. Investigation of regenerated bamboo fibre and yarn characteristics. *FIBRES & TEXTILES in Eastern Europe* 16, 4 (69), 43-47.

19. Mahish SS, Patra AK, Thakur R. 2012. Functional properties of bamboo/polyester blended knitted apparel fabrics. *Indian Journal of Fibre & Textile Research* 37, 231-237.

20. Yasin S, Liu L, Yao J. 2013. Biosynthesis of silver nanoparticles by bamboo leaves extract and their antimicrobial activity. *Journal of Fiber Bioengineering and Informatics* 6(1), 77-84.

21. Tusief MQ, Amin N, Mahmood N, Ahmad I, Abbas M. 2015. Antimicrobial studies of knitted fabrics from bamboo, soybean and flax fibers at various blends. *Journal of Textile Science & Engineering* 5(3).

22. Unango FJ, Ramasamy KM. 2019. A review on the investigation of biologically active natural compounds on cotton fabrics as an antibacterial textile finishing. *International Research Journal of Science and Technology* 1(1), 49-55.

23. Perelshtein I, Applerot G, Perkas N, Guibert G, Mikhailov S, Gedanken A. 2008. Sonochemical coating of silver nanoparticles on textile fabrics (nylon, polyester and cotton) and their antibacterial activity. *Nanotechnology 19,* 245705.

24. Yüksek İÖ. 2008. An investigation into the factors affecting the properties of bamboo yarns, (Master's Thesis). Uludağ University Institute of Education Sciences.

25. Smiechowicz E, Niekraszewicz B, Strzelinska M, Zielecka M. 2020. Antibacterial fibers containing nanosilica with immobilized silver nanoparticles. AUTEX Research Journal 20(4), 441-448.

26. Xu Q, Xie L, Diao H, Li F, Zhang Y, Fu F, Liu X. 2017. Antibacterial cotton fabric with enhanced durability prepared using silver nanoparticles and carboxymethyl chitosan. *Carbohydrate Polymers* 177, 187–193.

27. Sabır EC, Ünal BZ. 2017. The using of nettle fiber in towel production and investigation of the performance properties. *Journal of Natural Fibers,* 14(6), 781–787.

Comparison of Poisson's Ratio Measurement Methods: The Extensometer and the Universal Tensile Testing Devices

Mehmet TIRITOĞLU[1] 0000-0002-2316-0782
Serkan TEZEL[2] 0000-0003-4078-8210
Yasemin KAVUŞTURAN[2] 0000-0002-9919-564X

[1]Bursa Uludag University/ Graduate School of Natural and Applied Sciences/ Department of Textile Engineering, Bursa, Turkey
[2]Bursa Uludag University/ Faculty of Engineering/ Department of Textile Engineering, Bursa, Turkey

Corresponding Author: Mehmet Tiritoğlu, mtiritoglu@uludag.edu.tr

ABSTRACT

Auxetic materials with a negative Poison's ratio (PR) have the potential to meet the demand for different materials, especially technical textiles. Universal Tensile Test (UTT) devices and various experimental setups developed by researchers have been used in PR measurements. This study aims to investigate the PR of knitted fabrics with UTT and extensometer devices comparatively by using the same measurement parameters according to ASTM E132. Knitted fabrics with zigzag and foldable patterns were produced in the study because of their auxetic behaviour. It has been determined that the extensometer device can be used as an alternative to the UTT device for PR measurements. While the PR of foldable fabrics cannot be measured with the UTT device because of the fabrics' folding on themselves, it has been observed that it can be easily measured with the extensometer device thanks to the horizontal axis principle.

1. INTRODUCTION

Poisson's ratio (PR) is a mechanical property representing the lateral behavior of materials under an axial load [1]. The Poisson's ratio (v) is defined as;

$$v = -\frac{\varepsilon_{Trans}}{\varepsilon_{Load}} \qquad (1)$$

Where ε_{Load} is the strain in the loading direction while ε_{Trans} is the perpendicular strain or transverse to the loading direction. Typical natural materials possess a positive Poisson's ratio, which means they contract when they are stretched in one direction (Figure 1). Unlike standard natural materials, auxetic materials are defined as solids with negative PR [1, 2]. PR is an important parameter for numerical simulation of garment pressure distribution, and garment dressing system [3].
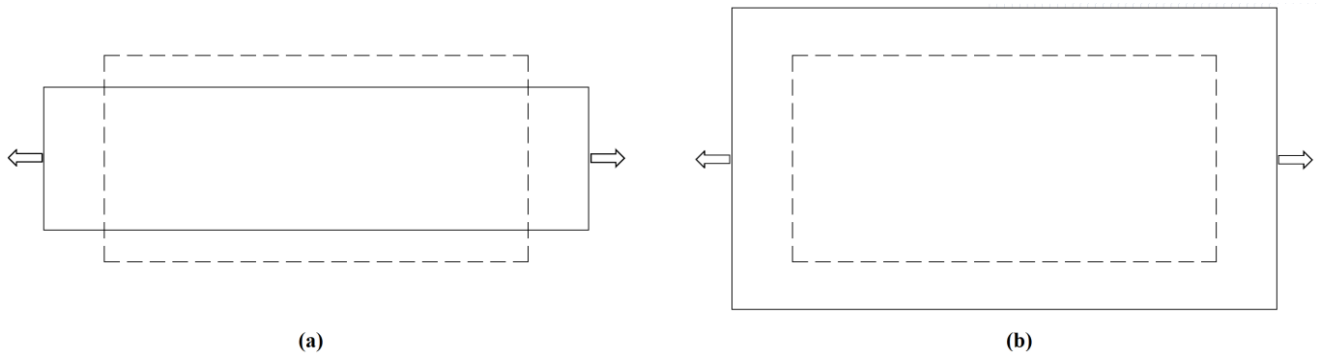
Figure 1. Schematic view of (a) conventional materials (positive PR) and (b) auxetic materials (negative PR)

Auxetic materials have the potential to meet the demand for different materials, especially in technical textiles. Properties associated with the PR can be listed as follows: friction resistance, better tensile strength, synclastic curvature (dome-shaped), increased fracture toughness and enhanced indentation resistance, increased shear stiffness, fiber pull out strength, variable permeability, extra friction resistance, acoustic behavior, superior energy absorption (impact, ultrasonic and sonic), adhesion (interface/matrix) strength, thermal impact resistance, improved drape, increased fracture toughness, tensile strength [4–7]. Potential applications include filter fabrics, geotextiles, reinforcements in advanced composites for aerospace and automotive sectors, and personal and sporting protective garments such as bulletproof vests and batting gloves [8].

In the literature, there are many studies on yarn [1,9–20], woven fabric [21–26], knitted fabric [8, 27–37], composite [38–41] production related to low PR or auxetic textile materials. Auxetic fabrics can also be produced with auxetic yarns or conventional yarns. Researchers changed the yarn properties and/or fabric patterns in literature to achieve low PR values [8,21–37]. These studies show that the researchers used Re-entrant (zigzag), Rotating, Chiral, Fibril-Nodule, and Foldable mesh structures [2,42,43]. Poisson's ratio and different methods for measuring this property have been the subject of many previous research studies due to their significant influence on fabric performance [44]. Reviews on the measurement of the PR of fabrics are as follows.

1.1 Studies with a Universal Tensile Tester (UTT)

In the studies of the PR of fabrics with UTT, many measurement points were marked on the sample placed between two (one fixed and the other movable) jaws vertically. While the samples were forced to elongate in one direction, images are taken at regular intervals to observe the other direction changes. The distances between the marked points were measured with the image processing program, and the PR is calculated [3,4,8,22,27,29,35, 36,43,45-48]. Literature survey on PR of knitted fabrics shows that researchers prepared the fabric samples in

different sizes (170x150, 150x50, 200x50, 50x180, 40x100 mm), stretched at different speeds (30-50-60-200 mm/min) by using different jaw distances (100-150 mm) [3,8,22,35, 43,47-49].

1.2 Studies with other Measuring Methods

These studies are carried out by applying force to the fabric with various test equipment and then calculating the PR from the images obtained. Glazzard (2014) fixed 100 mm wide fabric samples in a 100 mm jaw distance (Figure 2). Markings were made on the sample with 10 mm intervals. The clamps on the frame are moved 10 mm and fixed into place. After each movement, a photograph was taken. The images are then analyzed using digital image analysis software [28]. Steffens (2016) developed a testing device for the evaluation of PR. The specimens were marked at specific two points in both course and wale directions. The fabrics were clamped at their two ends in the testing device and extended manually along the course direction. Steps of 1 cm deformed the knitted fabric, and the distance between the reference points along the course and wale directions at each deformation step was measured [49]. Liu (2010) clamped the knitted fabrics at both ends with a gauge length of 150 mm and then extended manually along the course direction. A digital camera photographed the fabric under each deformation step, and the distances between the markers along the course and wale directions were calculated [29].

Apart from these studies, Jinyun (2010) examined the relationship between PR and the materials' elastic modulus. PR of knitted fabrics was obtained by calculating the ratio between elastic modulus values. He studied the dimensional change of the samples under biaxial force by placing the knitted fabrics produced in the Kawabata Evaluation System (KES) [3]. Boakye (2018) also measured PR values of knitted fabrics using cylinders with different diameters. Different tension was applied to the samples by dressing the fabrics produced in a tubular form on cylinders of 5 different diameters. As a result of the tension, the fabrics' length direction changes were measured, and PR at different elongation values was calculated [30].
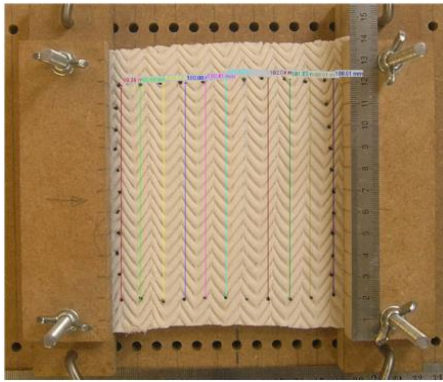
Figure 2. PR measurement equipment [28]

Former studies in this subject show that UTT devices were commonly used in PR measurements. Also, there are some other studies in the literature with self-designed measurement equipments. In these studies, an intermittent force-elongation test procedure was applied. Basically, PR measurement is a force-elongation test. Morton and Hearl (2008) indicate that the experiments' results will be affected by the time allowed and how the load is applied" [50]. In other words, the force-elongation test procedure acts continuously (not intermittently), and test parameters directly affect the test results. Therefore, it is thought that the studies that performed with intermittent test procedure do not simulate the force-elongation test accurately.

Fabrics with highly auxetic properties have a tendency to curl downwards positioned vertically in the UTT devices. While the fabric structures are susceptible to a small amount of force, gravity force acts as a pretension and deforms the fabrics' relaxed position. However, PR determination was calculated on minimal dimensional changes, and this deformation prevents the test accuracy for such kinds of fabrics that tend to curl downwards. This problem can be solved by using an extensometer. The materials are positioned horizontally in the extensometer devices. Extensometer devices are cost-friendly and easy to use compared to UTT devices. Therefore, this study investigates the extensometer devices' usability as an alternative to the UTT device in PR measurement of knitted

fabrics. Zigzag and foldable pattern fabrics were knitted in the study because of their low PR (auxetic behavior).

This study aims to investigate the Poisson's ratio of knitted fabrics with UTT (Shimadzu AG-X HS) and extensometer (SDL ATLAS-Fryma Dual Extensiometer) devices comparatively by using the same measurement parameters according to ASTM E132 "Standard Test Method for Poisson's Ratio at Room Temperature." The extensometer device that was used in this study can apply continuous force and gives more accurate results. Morton and Hearl (2008) also indicate that "The dimensions of the specimen have a direct effect on the results of tensile tests" [50]. Therefore, in this study PR was measured with both UTT and extensometer devices with the same measurement parameters. The comparison of measurement results by these two methods was statistically evaluated.

2. MATERIAL AND METHOD

2.1 Material

Auxetic knitted fabrics with different knitting structures were produced, such as zigzag and foldable patterns knitted fabrics. Besides, plain knitted (RL) fabric was made with the same yarns for control purposes. Double-covered spandex yarn was added for increasing auxetic properties. The samples were knitted on a Stoll CMS 530 Hp E6.2 Multi gauge flat knitting machine using 60% cotton-40% acrylic, Ne 20/1 number yarns. The fourfold yarn was fed into the knitting machine. 240 dtex polyamide elastane texturized yarn was used as spandex yarn. The fabric samples were subjected to dry relaxation by laying samples on a smooth and flat surface in atmospheric conditions (20±2 ^{0}C, 65±4% relative humidity) for 48 hours. The following properties of the fabrics were measured in accordance with relevant standards: course and wale per cm, ISO 7211-2; fabric weight (g/m^2), ISO 3801; fabric thickness (mm), ISO 5084. Measurements were performed five times in a relaxed state of the fabrics (unextended). Dimensional properties of the produced fabrics are presented in Table 1, and knitted structures are shown in Figure 3.

Table 1. Dimensional properties of the samples

Sample Code	Courses per cm	Wales per cm	Thickness (mm)	Weight (g/m²)
Zigzag structure				
4x6	8.2	6.1	3.1	410.6
4x6 - G	8.6	6.4	2.8	392.2
4x8	8.2	6.3	3.1	403.9
4x8 - G	9.0	6.5	3.1	399.6
Foldable structure				
Foldable	9.6	13.5	9.2	1203.7
Foldable - G	9.75	13.0	9.8	1173.6
Plain Knit				
RL	8.6	5.1	1.59	427.1

-G: Shows the use of double-covered spandex yarn in the sample. (with gimped)
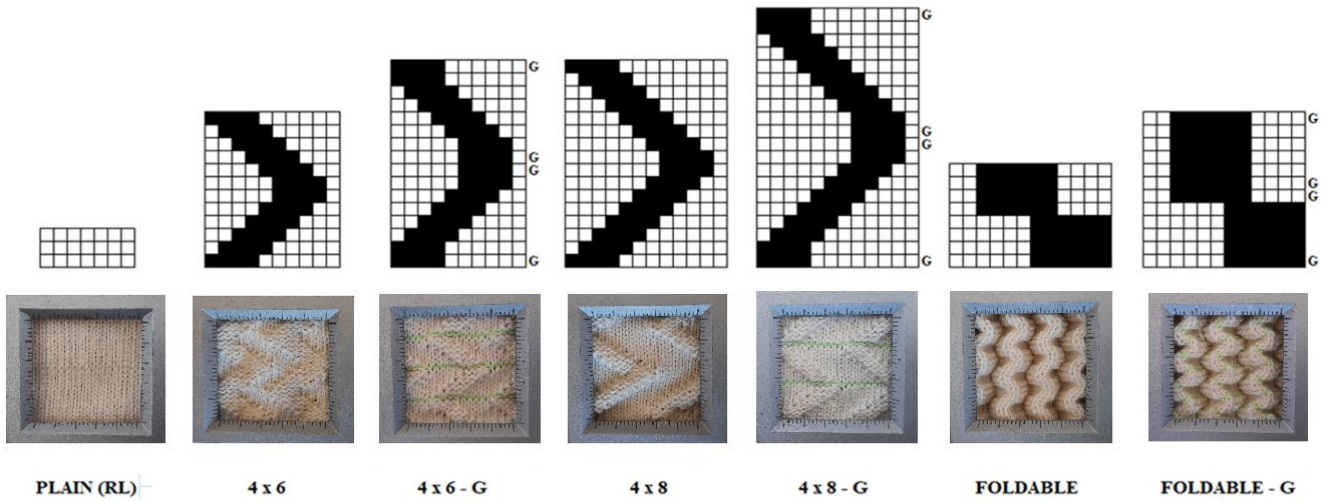
Figure 3. Patterns and images (25.4 mm x 25.4 mm) of the knitted fabrics (*In the unit cell of the knit pattern, the white square "□"represents the face loop and the black square"■"represents the reverse loop. "G" represents double-covered spandex yarn usage.*)

2.2 Method

Two different methods were performed for Poisson's ratio (PR) measurements under ASTM E132 standard test method parameters using Shimadzu AG-X HS universal tensile tester (Figure 5.a) and SDL ATLAS M031 Fryma Fabric Extensometer (Figure 5.b).

ASTM E132 standard defines the test method as "the tested length of the specimen should be at least five times the tested width, and the length between the grips should be seven times the tested width." [51]. Within the scope of the study, samples were cut in 50 mm width, and markings were made at 30 mm intervals on the horizontal and 150 mm on the vertical. The distance between the jaws is 210 mm. PR measurements were performed in the course and wale directions for three fabrics. Course-wise measurements (A1-B1, A2-B2, A3-B3) and wale-wise measurements (C1-D1, C2-D2, C3-D3) were performed three times in each fabric sample. Average values of the measurements were calculated. Markings made on samples are shown in Figure 4.
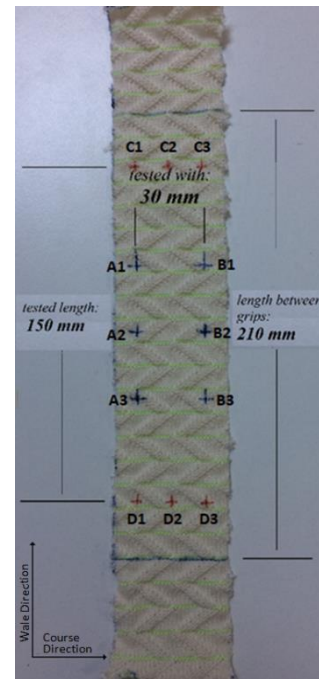

Figure 4. Markings on the sample

Figure 5. Placement of samples in (a) UTT device (zigzag pattern) and (b) Fryma extensometer (foldable pattern)

The ASTM E132 test standard recommends low operating speed, but an exact value is not specified. Sloan (2011) defined low working speed at approximately 1/10 of jaw distance per minute [14]. Based on this, the force was applied at a rate of 20 mm/min for both measurement techniques. The images recorded during the test were transferred to the ImageJ image processing program. Changes in width and length in specific elongation values (1%, 2%, 3%,…, 20%) were measured, and the PR values were calculated (Figure 6).
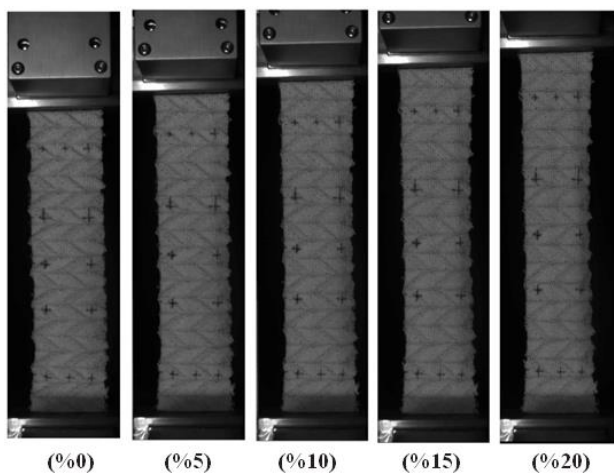

Figure 6. Images of samples at certain elongation rates (UTT)

A two-factor completely randomized ANOVA model was used with SPSS 22 for pattern type (RL, 4x6, 4x6-G, 4x8, 4x8-G) and % elongation (1%, 2%,…. 20%) values for both UTT and extensometer devices in order to demonstrate the significance of pattern type and % elongation on the PR of fabrics. In addition, a three-factor completely randomized

ANOVA model was also used for measurement method (UTT, extensometer), pattern type, and % elongation in order to demonstrate the significance of measurement methods.

3. RESULTS AND DISCUSSION

PR measurements were performed in both UTT and extensometer devices with the same parameters according to ASTM-E132. The changes in width and length in specific elongation values were measured, and PR values were calculated.

3.1 Universal Tensile Test (UTT) Results

Poisson's ratio measurements were made in the UTT device for plain (RL) and zigzag structured (4x6, 4x6-G, 4x8, 4x8-G) knitted fabrics are presented in Figure 7. It is seen that as the % elongation increases in the samples, the PR increases. Plain knitted (RL) fabric has the highest, 4x8 zigzag structure fabric with double-covered spandex yarn (4x8-G) has the lowest Poisson's ratio values.

Two-factor variance analysis was applied for pattern type (RL, 4x6, 4x6-G, 4x8, 4x8-G) and % elongation (1%, 2%,…. 20%) values using the SPSS 22 program for the results of Poisson's ratio measurements made on the UTT device. According to variance analysis, the knitting structure (p:0) and % elongation (p:0) values were statistically effective on the Poisson's ratio of the fabrics. SNK analysis results for knitting structure and % elongation values are presented in Table 2.
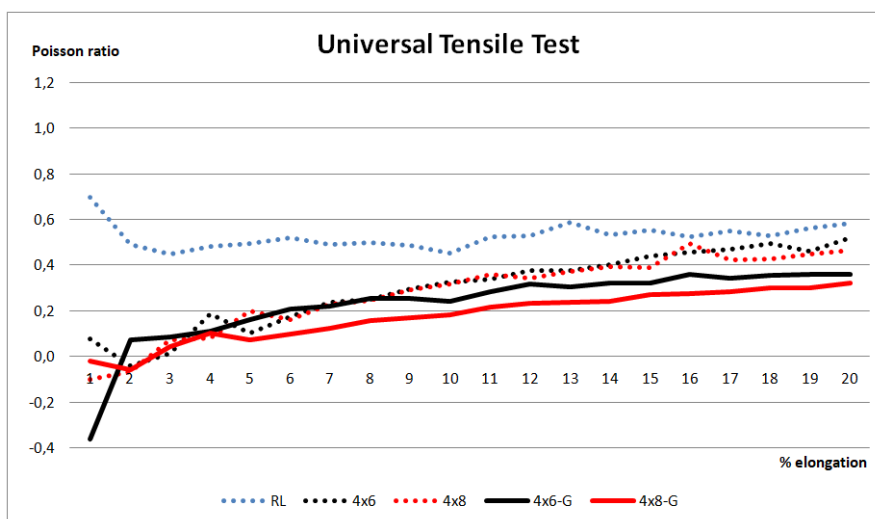

Figure 7. Graph of the Poisson's ratio obtained in the UTT

Table 2. SNK ranking at 5% significance level after at ANOVA model. (UTT)

Knitting Structure		Poisson's Ratio (%)		
4x8 - G	0.18 (a)			
4x6 - G	0.23 (a)			
4x8	0.28 (a)			
4x6	0.30 (a)			
RL		0,53 (b)		

Elongation (%)		Poisson's Ratio (%)		
%1	-0.04 (a)			
%2	0.02 (a)	0.02 (b)		
%3	0.08 (a)	0.08 (b)	0.08 (c)	
%4	0.15 (a)	0.15 (b)	0.15 (c)	0.15 (d)
%5	0.16 (a)	0.16 (b)	0.16 (c)	0.16 (d)
%6	0.19 (a)	0.19 (b)	0.19 (c)	0.19 (d)
%7	0.23 (a)	0.23 (b)	0.23 (c)	0.23 (d)
%8		0.25 (b)	0.25 (c)	0.25 (d)
%9		0.27 (b)	0.27 (c)	0.27 (d)
%10		0.28 (b)	0.28 (c)	0.28 (d)
%11		0.32 (b)	0.32 (c)	0.32 (d)
%12			0.33 (c)	0.33 (d)
%13			0.34 (c)	0.34 (d)
%14			0.35 (c)	0.35 (d)
%15			0.37 (c)	0.37 (d)
%17			0.39 (c)	0.39 (d)
%18			0.40 (c)	0.40 (d)
%19			0.41 (c)	0.41 (d)
%16			0.41 (c)	0,.41 (d)
%20				0.43 (d)

Note that lower case a,b,c,d indicate a significant difference between the values. "a" shows the lowest value, and "d" shows the highest value.

The SNK test results show that zigzag pattern fabrics (4x6, 4x6-G, 4x8, 4x8G) affect the PR values in a similar way. The PR of the zigzag patterned fabrics was lower than the RL. 4x8 and 4x8-G samples have a lower PR than the 4x6 and 4x6-G. The zigzag angle with the horizontal axis for 4x8 and 4x8-G is lower than 4x6 and 4x6-G fabrics. In other words, when the angle with the horizontal axis decreases, PR decreases. This result is consistent with Liu [29] and Boakye [30].

4x8-G and 4x6-G coded samples containing spandex yarn have a lower PR than the 4x8 and 4x6. This result can be explained by the increase of the wales per cm values by the usage of spandex yarn.

3.2 Extensometer Measurement Results

Poisson's ratio measurement results of RL, zigzag (4x6, 4x6-G, 4x8, 4x8-G) fabrics with extensometer are presented in Figure 8. Similar to the UTT device results, it has been determined that while RL fabrics have the highest values, 4x8-G coded fabrics (with spandex yarn) have the lowest PR values.

Two-factor variance analysis was applied for the pattern type (RL, 4x6, 4x6-G, 4x8, 4x8-G) and % elongation (1%, 2%,…. 20%) values using the SPSS 22 program for the results of Poisson's ratio measurements made with the extensometer device. According to this, knitting structure and % elongation were statistically effective in the fabrics' PR. The SNK analysis results for knitting structure and % elongation values are presented in Table 3.
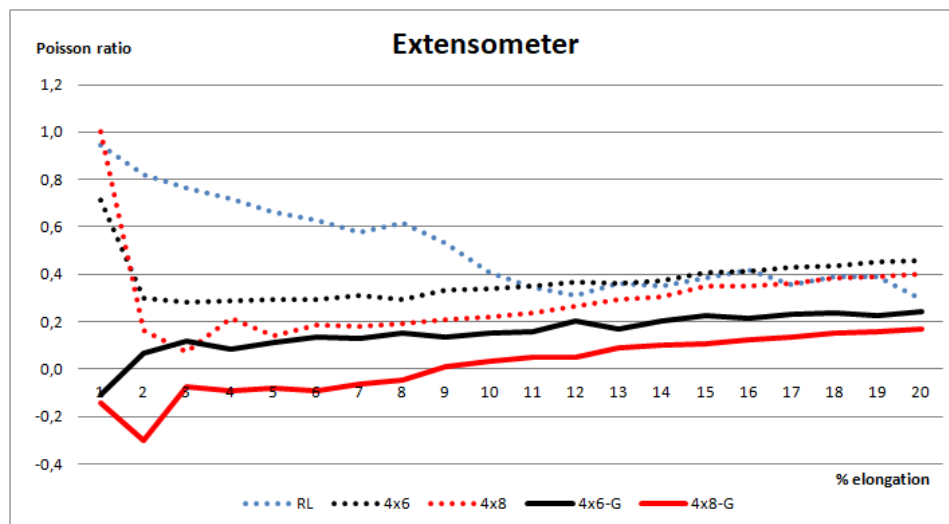

Figure 8. Graph of the Poisson's ratio obtained from the extensometer device

Table 3. SNK ranking at 5% significance level after at ANOVA model. (Extensometer)

Knitting Structure			Poisson's Ratio (%)		
4x8 - G	0.01 (a)				
4x6 - G		0.15 (b)			
4x8			0.30 (c)		
4x6				0.37 (d)	
RL					0.51 (e)

Elongation (%)		Poisson's Ratio (%)
%2	0.12 (a)	
%3	0.15 (a)	
%5	0.16 (a)	
%4	0.17 (a)	
%6	0.17 (a)	
%7	0.17 (a)	
%8	0.18 (a)	
%9	0.20 (a)	
%10	0.20 (a)	
%11	0.21 (a)	
%12	0.23 (a)	0.23 (b)
%13	0.24 (a)	0.24 (b)
%14	0.25 (a)	0.25 (b)
%15	0.28 (a)	0.28 (b)
%16	0.29 (a)	0.29 (b)
%17	0.29 (a)	0.29 (b)
%18	0.31 (a)	0.31 (b)
%19	0.31 (a)	0.31 (b)
%20	0.31 (a)	0.31 (b)
%1		0.41 (b)

Note that lower case a,b,c,d,e indicate a significant difference between the values. "a" shows the lowest value, and "e" shows the highest value.

The results of the variance analysis reveal that PR of the zigzag patterned samples was lower than the RL pattern. 4x8 and 4x8-G coded samples have a lower PR than the 4x6 and 4x6-G. 4x8-G and 4x6-G coded samples containing spandex yarn have lower PR than the 4x8 and 4x6 fabrics without spandex yarn.

3.3 Comparison of UTT and Extensometer Test Device Measurement Results

The results of the PR measurements of RL and zigzag knitted fabrics with UTT and extensometer devices are parallel to each other. The PR values of the knitted fabrics were ordered from low to high is 4x8-G, 4x6-G, 4x8, 4x6, RL for both measurement techniques. In addition to this, as the % elongation increases, PR values also increase for both measurement techniques, except % 1 elongation of the extensometer device measurement result. PR measurement is a measurement technique that needs to be done very precisely. The changes in % elongation values are measured by counting pixels on the computer and calculating the distance. Relatively small changes in positioning the samples onto the device can affect the results. Therefore, some irregular results can be obtained especially at low % elongation values.

Comparing PR test results of RL and zigzag knitted fabrics with UTT and extensometer device was performed by applying a 3-factor variance analysis using the SPSS 22 program. When the variance analysis results were examined, it's seen that there were no statistically significant difference (p:0.101) between measurement methods. This result shows that the both methods can be used as alternatives to each other (Table 4).

3.4 Poisson's Ratio Measurement Results of Foldable Fabrics

The fabric sample is placed vertically between the jaws in the UTT device. Foldable fabrics have a tendency to curl downwards when positioned vertically. The gravity force acts as a pretension and deforms the fabrics' relaxed position while the fabric structures are susceptible to a small amount of force. In other words, the foldable fabric elongates, and its original form changes. While marks on the fabrics with zigzag patterns could be seen clearly (Figure 9.a and 9.b), marks on the fabrics with foldable structure (Foldable and Foldable-G) could not be seen because of the buckling (Figure 9.c and 9.d). Since some of the markings on the fabric cannot be seen due to buckling, PR cannot be measured for the Foldable and Foldable-G fabrics with UTT.

Table 4. SNK ranking at 5% significance level after at ANOVA model (comparison UTT and extensometer).

| Source	Type III Sum of Squares	df	Mean Square	F	Sig.
Corrected Model	18,486[a]	199	0,093	2,372	0,000
Interception	35,123	1	35,123	896,916	0,000
Method	*0,106*	*1*	*0,106*	*2,697*	*0,101*
Fabric Pattern	7,206	4	1,802	46,004	0,000
% Elongation	1,863	19	0,098	2,503	0,001
Method * Fabric Pattern	1,000	4	0,250	6,386	0,000
Method * % Elongation	1,774	19	0,093	2,384	0,001
Fabric Pattern* % Elongation	2,761	76	0,036	0,928	0,646
Method * Fabric Pattern * % Elongation	1,454	76	0,019	0,488	1,000
Error	12,531	320	0,039		
Total	63,593	520			
Corrected Total	31,017	519			
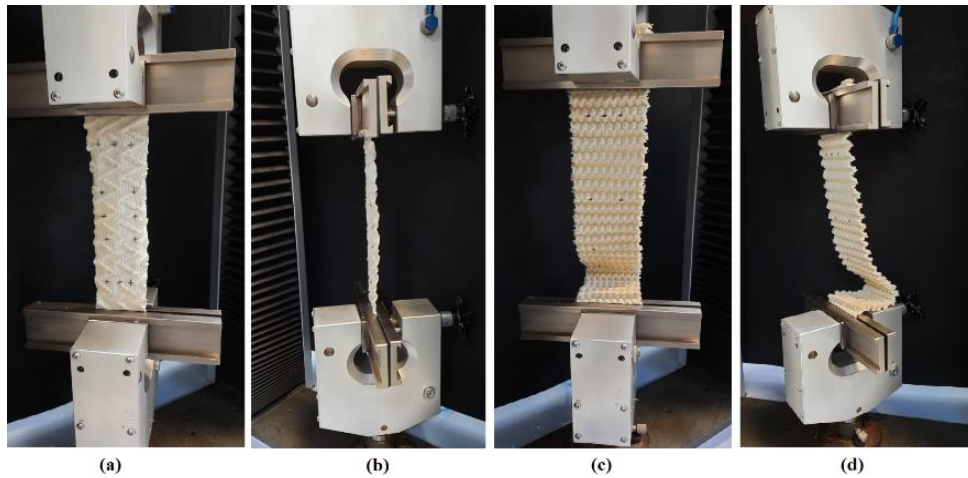
Figure 9. Zigzag pattern fabrics' (a) front view, (b) side view and foldable fabrics' (c) front view, (d) side view at UTT device

PR measurements of the foldable fabrics were measured with SDL ATLAS M031 Fryma Fabric Extensometer (Figure 4.b). The materials are positioned horizontally in the extensometer device. The results are presented in Figure 10. When the measurement results are examined, it is seen that the PR of foldable fabrics is below "0," and Foldable-G is negative after 5% elongation. This result shows that Foldable and Foldable-G have auxetic properties, unlike RL and zigzag fabrics. This result can be explained by the high thickness of the foldable fabrics. As it is also seen from Table 1, while RL and zigzag fabrics have a thickness of 1,59-3,1 mm, foldable fabrics have a thickness of 9,2- 9,8 mm. Because of their unique pattern, these fabrics fold on themselves and generate a 3D structure. By extending the fabric, these folds flatten, and fabrics' course-wise dimensions increase contrary to conventional fabric structures.

A two-factor variance analysis was applied for pattern type and % elongation values for the results of PR measurements made on the extensometer device for all the fabrics examined within the scope of the study. SNK analysis results are presented in Table 5.
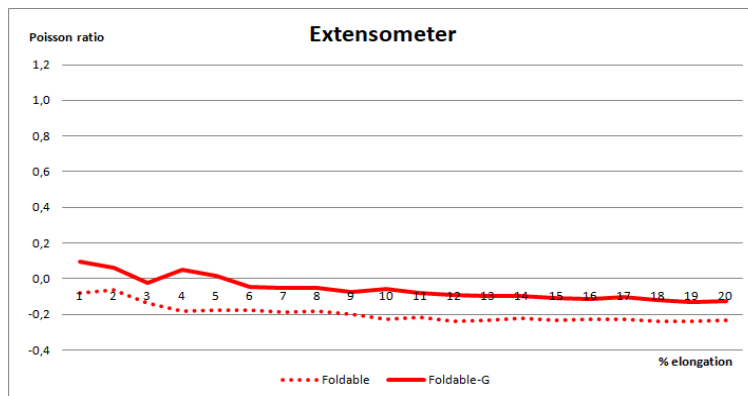

Figure 10. Poisson's ratio of foldable fabrics obtained from the extensometer device

Table 5. SNK ranking at 5% significance level after at ANOVA model.

Knitting Structure	Poisson's Ratio (%)					
Fold.	-0.20 (a)					
Fold-G		-0.06 (b)				
4x8-G			0.01 (c)			
4x6-G				0.15(d)		
4x8					0.30 (e)	
4x6						0.37 (f)
RL						0.51 (g)

Note that lower case a,b,c,d,e,f,g indicate a significant difference between the values. "a" shows the lowest value, and "g" shows the highest value.

It is seen that Foldable fabrics without spandex yarn (Fold) have a lower PR compared to foldable fabrics containing spandex yarn (Foldable-G). This is the opposite of the zigzag fabrics due to the wales per cm values. While zigzag fabrics with spandex yarn (4x6-G and 4x8-G) have higher wales/cm than zigzag fabrics without spandex yarn (4x6 and 4x8), foldable fabric with spandex yarn (Fold-G) has lower wales/cm than foldable fabrics without spandex yarn (Fold).

4. CONCLUSION

The main objective of this study was to investigate the usability of the extensometer devices as an alternative to the UTT device in PR measurement of knitted fabrics. Poisson's ratio of the fabrics were measured with UTT (Shimadzu AG-X HS) and extensometer (SDL ATLAS-Fryma Dual Extensiometer) devices comparatively by using the same measurement parameters according to ASTM E132 "Standard Test Method for Poisson's Ratio at Room Temperature."

RL and zigzag pattern knitted fabrics' PR were measured with both UTT and extensometer devices. Variance analysis results of UTT and extensometer devices reveal that there were no statistically significant differences between the measurement methods. This result shows that these methods can be used as alternatives to each other. The Extensometer device is a practical and cost-friendly device that is widely used in the sector compared to UTT devices.

It was observed that the fabrics with zigzag and foldable pattern structure have lower PR than RL knitted fabrics. As the force is applied to the RL knitted fabric in the wale direction, the shape of the loops changes. While the loop height increases, the loop width decreases. The decrease of the loop's width makes the RL fabric narrow. This behavior is also common for most conventional knitted fabric structures. Zigzag pattern fabrics have R and L loops in diagonal positions. The position of R and L loops conduce to increase the fabrics wales per cm values and make the fabric thicker. Essentially, a foldable fabric pattern is also a type of zigzag pattern. The diagonal position of the R and L loops make the foldable fabrics much thicker and conduce the fabrics to fold on themselves and generate a 3D

structure. When the force is applied to the fabric, firstly fabrics get smooth and lose their 3D shape. While RL fabrics have a thickness value of 1.59 mm, zigzag pattern fabrics have 2.8-3.1 mm, and foldable pattern fabrics have 9.2-9.8 mm thickness values. Therefore, while the foldable pattern fabrics have the minimum PR values, zigzag pattern fabrics have lover PR values than RL fabrics.

4x8 zigzag pattern knitted fabrics have lower PR than 4x6 zigzag pattern fabrics. For the zigzag samples, when the angle with the horizontal axis decreases, PR decreases. This result is consistent with the study of Liu [29] and Boakye [30]. Zigzag pattern fabrics containing spandex yarn (4x6-G, 4x8-G) have lower PR than the fabrics without spandex yarn (4x6, 4x8). This result can be explained by the increase of the wales per cm values by using spandex yarn.

Foldable fabrics have a tendency to curl downwards when positioned vertically in the UTT device. Since some of the markings on the fabric cannot be seen due to buckling, PR cannot be measured for the Fold and Fold-G fabrics with UTT. PR test results of foldable fabrics measured by extensometer device reveal that foldable fabrics without spandex yarn (Fold) have a lower PR compared to containing spandex yarn (Foldable-G). This result is the opposite of the zigzag fabrics due to the wales per cm values. While zigzag fabrics with spandex yarn (4x6-G and 4x8-G) have higher wales/cm than zigzag fabrics without spandex yarn (4x6 and 4x8), foldable fabric with spandex yarn (Fold-G) has lower wales/cm than foldable fabrics without spandex yarn (Fold).

Consequently, it is observed that the extensometer device can be used for PR measurement as an alternative to the UTT device and made possible to measure the PR of fabrics that have a tendency to curl downwards when positioned vertically.

REFERENCES

1. Lim TC. 2015. *Auxetic materials and structures*. New York: Springer.

2. Chen S, Chawla KK, Chawla N. 2019. *Handbook of mechanics of materials*. Springer. New York: Springer.

3. Jinyun Z, Yi L, Lam J, et al. 2010. The poisson ratio and modulus of elastic knitted fabrics. *Textile Research Journal* 80(18), 1965–1969.

4. Miller W, Hook PB, Smith CW, et al. 2009. The manufacture and characterization of a novel, low modulus, negative poisson's ratio composite. *Composite Science and Technology* 69, 651–655.

5. Alderson A, Evans KE. 1995. Microstructural modelling of auxetic microporous polymers. *Journal of Materials Science* 30, 3319–3332.

6. Scarpa F, Patorino P, Garelli A, et al. 2005. Auxetic compliant, flexible PU foams: static and dynamic properties. *Basic Solid State Physics* 242(3), 681–694.

7. Uzun M. 2010. Negatif poisson oranına sahip (Auxetic) malzemeler ve uygulama alanları. *Tekstil ve Mühendis* 17(177), 13–18.

8. Alderson K, Alderson A, Anand S, et al. 2012. Auxetic warp knit textile structures. *Basic Solid State Physics* 249(7), 1322–1329.

9. Hook P. 2011. Patent No: US 8.002.879 B2 Uses of auxetic fibres. United States: Patent Application Publication.

10. Ng WS, Hu H. 2017. Tensile and deformation behavior of auxetic plied yarns. *Basic Solid State Physics* 254(12), 1–11.

11. Shen Y, Adanur S. 2019. Mechanical analysis of the auxetic behavior of novel braided tubular structures by the finite element method. *Textile Research Journal* 89(23-24), 5187–5197.

12. Jiang N, Hu H. 2019. Auxetic yarn made with circular braiding technology. *Basic Solid State Physics* 256, 1–12.

13. Sibal A, Rawal A. 2015. Design strategy for auxetic dual helix yarn systems. *Materials Letters* 161(2015), 740–742.

14. Sloan MR, Wright JR, Evans KE. 2011. The helical auxetic yarn - A novel structure for composites and textiles; Geometry, manufacture and mechanical properties. *Mechanics of Materials* 43(2011), 476–486.

15. McAfee J, Faisal NH. 2017. Parametric sensitivity analysis to maximise auxetic effect of polymeric fibre based helical yarn. *Composite Structures* 162(2017), 1–12.

16. Zeng J, Cao H, Hu H. 2018. Finite element simulation of an auxetic plied yarn structure. *Textile Research Journal* 89(16), 3394–3400.

17. Chen J, Du Z. 2020. Structural design and performance characterization of stable helical auxetic yarns based on the hollow-spindle covering system. *Textile Research Journal* 90(3-4), 271–281.

18. Lee W, Lee S, et al. 2011. Patent No: US 2011/0039088 Moisture sensitive auxetic material. United States: Patent Application Publication.

19. Zhang GH, Ghita O, Evans KE. 2015. The fabrication and mechanical properties of a novel 3-component auxetic structure for composites. *Composites Science and Technology* 117, 257–267.

20. Ge Z, Hu H, Liu S. 2016. A novel plied yarn structure with negative poisson's ratio. The *Journal of Textile Institute* 107(2015), 578–588.

21. Ali M, Zeeshan M, Ahmed S, et al. 2018. Development and comfort characterization of 2D-woven auxetic fabric for wearable and medical textile applications. *Clothing and Textile Research Journal* 36(3), 199–214.

22. Cao H, Zulifqar A, Hua T, et al. 2018. Bi-stretch auxetic woven fabrics based on foldable geometry. *Textile Research Journal* 89(13), 2694-2712.

23. Zulifqar A, Hu H. 2019. Geometrical analysis of bi-stretch auxetic woven fabric based on re-entrant hexagonal geometry. *Textile Research Journal* 89(21-22), 4476–4490.

24. Zulifqar A, Hua T, Hu H. 2019. Single and double-layered bistretch auxetic woven fabrics made of nonauxetic yarns based on foldable geometries. *Basic Solid State Physics* 257(10), 1–13.

25. Kamrul H, Dong W, Zulifqar A, et al. 2020. Deformation behavior of auxetic woven fabric made of foldable geometry in different tensile directions. *Textile Research Journal* 90(3-4), 410-421.

26. Chen Y, Zulifqar A, Hu H. 2020. Auxeticity from the folded geometry: A numerical study. *Basic Solid State Physics* 257, 1–9.

27. Hu H, Wang Z, Liu S. 2011. Development of auxetic fabrics using flat knitting technology. *Textile Research Journal* 81(14), 1493–1502.

28. Glazzard M, Breedon P. 2014. Weft-knitted auxetic textile design. *Basic Solid State Physics* 251(2), 267–272.

29. Liu Y, Hu H, Lam JKC, et al. 2010. Negative poisson's ratio weft-knitted fabrics. *Textile Research Journal* 80(9), 856–863.

30. Boakye A, Chang Y, Rafiu KR, et al. 2018. Design and manufacture of knitted tubular fabric with auxetic effect. The *Journal of Textile Institute* 109(5), 596–602.

31. Luan K, West A, DenHartog E, et al. 2020. Auxetic deformation of the weft-knitted miura-ori fold. *Textile Research Journal* 90(5-6), 617–630.

32. Ugbolue SC, et al. 2011. Patent No: US 2011/0046715 A12011 Auxetic fabric structures and related fabrication methods. United States: Patent Application Publication.

33. Xu W, Sun Y, Lin H, et al. 2020. Preparation of soft composite reinforced with auxetic warp-knitted spacer fabric for stab resistance. *Textile Research Journal* 90(3-4), 323–332.

34. Zhao S, Hu H, Kamrul H, et al. 2020. Development of auxetic warp knitted fabrics based on reentrant geometry. *Textile Research Journal* 90(3-4), 344–356.

35. Wang Z, Hu H. 2013. 3D auxetic warp-knitted spacer fabrics. *Basic Solid State Physics* 251(2), 281–288.

36. Wang Z, Hu H. 2017. Tensile and forming properties of auxetic warp-knitted spacer fabrics. *Textile Research Journal* 87(16), 1925–1937.

37. Blaga M, Ciobanu AR, Cuden AP, Rant D. 2013. Production of foldable weft knitted structures with auxetic potential on electronic flat knitting machines. *Melliand International* 19(4), 220-223

38. Herakovich CT. 1984. Composite laminates with negative through the thickness poisson's ratios. *J Compos Mater* 18, 447–455.

39. Evans KE, Donoghue JP, Alderson KL. 2004. The design, matching and manufacture of auxetic carbon fibre laminates. *Journal of Composite Materials* 38(2), 95–106.

40. Skertchly D. 2011. Patent No: US 2011/0214560 A1 Composite auxetic armour. Place: United States Patent Application Publication.

41. Alderson KL, Simkins VR, Coenen VL, et al. 2005. How to make auxetic fibre reinforced composites. *Basic Solid State Physics* 242(3), 509–518.

42. Grimmelsmann N, Meissner H, Ehrmann A. 2016, May. 3D printed auxetic forms on knitted fabrics for adjustable permeability and mechanical properties. *IOP Conference Series: Materials Science and Engineering*. Hangzhou, China.

43. Chang Y, Ma P. 2018. Fabrication and property of auxetic warp-knitted spacer structures with mesh. *Textile Research Journal* 88(19), 2206–2213.

44. Ezazshahabi N. 2020. A Review on the poisson's ratio of fabrics. *Journal of Textiles and Polymers* 8(1), 53–63.

45. Lolaki A, Shanbeh M. 2019. Variation of poisson's ratio of fabrics woven with helical composite auxetic weft yarns in relation to fabric structural parameters. *Journal of Industrial Textiles* 50(2),1-21.

46. Nazir MU, Shaker K, Hussain R, et al. 2019. Performance of novel auxetic woven fabrics produced using helical auxetic yarn. *Materials Research Express* 6(2019), 1-12.

47. Chang Y, Ma P, Jiang G. 2017. Energy absorption property of warp-knitted spacer fabrics with negative possion's ratio under low velocity impact. *Composite Structures* 182(2017), 471–477.

48. Xu W, Sun Y, Raji KR, et al. 2019. Design and fabrication of novel auxetic weft-knitted fabrics with Kevlar yarns. The *Journal of Textile Institute* 110(9), 1257–1262.

49. Steffens F, Rana S, Fangueiro R. 2016. Development of novel auxetic textile structures using high performance fibres. *Materials and Design* 106(2016), 81–89.

50. Morton WE, Hearle JWS. 2008. *Physical properties of textile fibres.* England: Woodhead Publishing.

51. ASTM-E132. 2010. Standard testmethod for poisson's ratio at room temperature.

Precision of Measurement of Water Vapor Resistance of Fabrics with Different Surface Roughness by a Skin Model

Lubos HES[1] 0000-0002-0734-8603
Vinay Kumar MIDHA[2] 0000-0002-1630-9382

[1]Technical University of Liberec, Faculty of Textile Engineering, Liberec, Czech Republic
[2]Dr B R Ambedkar National Institute of Technology, Jalandhar, India

ABSTRACT

Skin models are used for determination of water and thermal resistance of fabrics. Measurement in these instruments starts with determination of water vapour resistance of a boundary layer above the sweating hotplate. In the second step, the hotplate is covered by the tested fabrics and the instrument measures WV resistance of the fabric and that of boundary layer. Afterwards, the difference between these measurements presents the required WV resistance of the measured fabric, provided that WV resistance of the boundary layer is in both measurements identical. However, fabric surface roughness may change WV resistance of the boundary layer in the second measurement. In the paper, the effect of the fabric surface on measurement precision is theoretically analysed and experimentally verified by procedure, which provides same air surface friction during both steps of the measurement. Experiments confirmed certain but small effect of the fabric surface roughness on the measurement precision.

1. INTRODUCTION

In last decades, lot of attention is paid to measurement of parameters of thermo-physiological comfort of textile fabrics, namely fabrics with high added value used for sport and protection. The most important standard for testing of thermal and water vapour resistance of fabrics R_{ct} and R_{et} is the ISO 11092, which present most important parameters for characterisation of thermophysiological comfort of clothing [1-3].

The original related instrument called "Skin Model" consists of heated metallic plate surrounded on most of its surface by a thermal insulation layer kept electronically at the same temperature. Due to this isothermal arrangement, no heat is transferred out of this plate, except the heat passing through the only free surface. Free surface of this measuring plate covered by the porous layer is exposed to parallel air flow of 1 m/s velocity moving in the special wind channel (Figure 1).
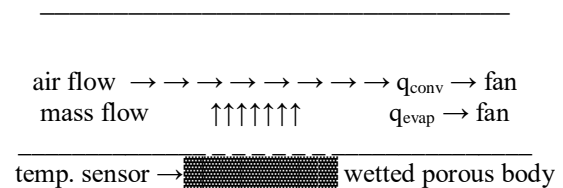
Figure 1. Heat and mass transfer in a skin model

When measuring the fabric thermal resistance R_{ct}, the air temperature in the channel is kept at 20ºC, and the measuring plate is dry. First, the power H supplied to the hotplate in order to heat the measuring system to temperature 35ºC is measured. Then, the tested fabric is placed on the porous layer of the measuring plate and the electric power expressing heat passing through the system to outer air is measured again. Edges of the tested sample are placed on the mentioned surrounding isothermal envelope, in order to avoid heat loses from the sample in

the enviroment of different temperature.

When evaluating the water vapour resistance R_{et}, both the measuring plate and the air are kept at the temperature 35°C (to achieve the isothermal conditions) and the porous layer is continuously filled with water. Then, again the heating power H without and with the specimen is measured and saved. In the second step, the specimen is inserted between the measuring plate and the wind channel and the steady-state and the heating power H is recorded again. All the power values then serve for the calculation of thermal and water vapour resistance values according to the simple formulas presented in the ISO 11092.

The small Skin model PERMETEST used in this study works on the same principle, just the amount of heat power passing through the measuring surface is measured directly by a special calibrated sensor. Other details about the device are presented elsewhere [4].

2. MATERIAL AND METHOD

2.1 Principal Disadvantage of the ISO 11092 Testing Method

The proper principle of this method for determination of both thermal and water vapour resistance levels is based on subtracting the boundary layer resistance R_{ct} or (corresponding to smooth free measuring plate) from the total resistance consisting of fabric resistance and fabric boundary layer resistance. However, the fabric boundary layer resistance can differ from the resistance of boundary layer adhered to instrument measuring plate. This difference can result from different air friction against the fabric surfaces with different surface profiles (sweaters, blankets), which affects the degree of turbulence and hence the thickness of the boundary layer. As the boundary layer thickness divided by a diffusion coefficient (or by a thermal conductivity) presents approximately its water vapour resistance (or thermal resistance), the measured levels values of these principal comfort parameters can differ from the real ones. Certain effect of the fabric surface roughness on the measured thermal and evaporation resistances caused by varying fabric structure was observed in [5,6].

Thus, these uncertainties in the determination of water vapour resistance and thermal resistance of boundary layers adhered to the free measuring surface and to surface of the tested fabrics may theoretically cause certain measurement imperfection. In next research we will investigate, whether these imperfections are substantial or not. From large practical use of the ISO 11092 follows, that in most cases the possible reduction of the measurement precision does not prevent the successful application of the ISO 11092 in many textile areas [5].

2.2. Reynolds Analogy for Boundary Layers

This analogy correlates the air friction coefficient f, Reynolds dimensionless number Re and dimensionless numbers Nu and Sh, which serve for calculations of heat and mass transfer coefficients. The analogy applicable for laminar flow of fluids has the following form [7]:

$$Re.f = 2 Nu = 2 Sh \qquad (1)$$

The abovementioned Reynolds number is given by relationship

$$Re = u.d/\nu, \qquad (2)$$

where u is the air velocity above the tested sample, which in all Skin models reaches 1 m/s, d is the hydraulic diameter of the air channel (0,068 m in the used PERMETEST instrument) and ν is kinematic viscosity of air ($1,71.10^{-5}$ Pa.s). Thus, from the calculations executed in the study[5] follows, that Reynolds number in a measuring channel reaches the value Re = 5780, which confirms the turbulent character of the air flow in this instrument. The limit RE number for laminar flow is 2300. However, all these calculations are based on a presumption, that the velocity profile is fully developed. The commonly known Bussinesq relation which requires a length (distance) D of a flow in a channel longer than D > 0,065. d.Re for the development of a full laminar velocity profile is applicable for the laminar flow only. According to the source [7], for the above confirmed turbulent flow the full velocity profile in a channel can be developed much earlier, within a distance D longer than 10 multiple of the hydraulic diameter d of the channel, in means here 0,68 m.

However, the distance d between a pressured air outlet (perforated plate) and a measuring hotplate in the measuring cannel (zone) of Skin models, where the air runs parallely along the tested fabric surface, is lower than 0,5 m. Thus, within the short distance between the air outlet and a tested sample, only the laminar boundary layer is developed, as it can be seen on the ~~below picture~~ Figure. 2.

Thus, the above principle of the effect of air friction f, by which the dimensionless heat transfer coefficient Nu and mass transfer coefficient Sh depend on this air friction coefficient f, which is proportional to the fabric surface roughness, is applicable here:

$$Nu = Re.f/2, \; Sh = Re.f/2 \qquad (3)$$

As already mentioned, Nusselt and Sherwood numbers Nu and Sh present dimensionless forms of heat and mass transfer coefficients α and β_c, given by equations (4):

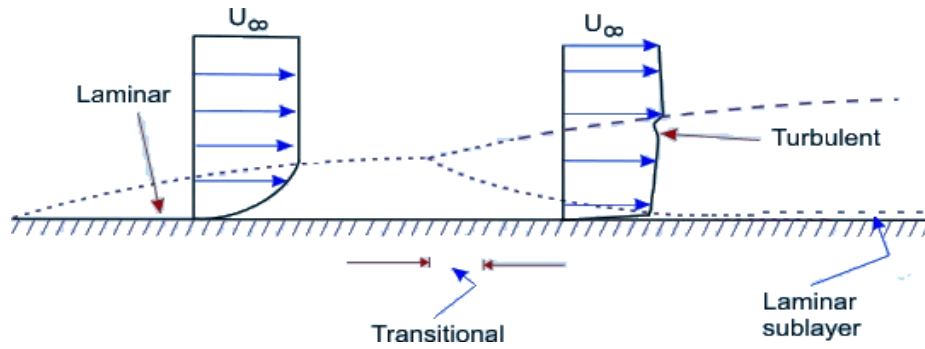$$Nu = \alpha d /\lambda \text{ and } Sh = \beta_c d/D_a \qquad (4)$$

Figure 2. Development of boundary layer above the bottom of the measuring channel in Skin models
(https://nptel.ac.in/content/storage2/courses/112104118/lecture-32/32-3_lami_turb_trans.htm)

where λ is the coefficient of thermal conductivity and D_a means the coefficient of water vapour diffusion in air (in this case). Here, the mass transfer coefficient β_c is destined for driving force expressed in water vapour concentration difference. When driving force is expressed as a difference of water vapour partial pressures, a transformation coefficient (based on the common gas equation) must be used:

$$\beta p = \beta_c / (r.T) = Sh.D_a/(d.r.T) = f. Re. D_a/(2.d.r.T) \qquad (5)$$

Here, r means gas constant for air having value 461, $Jkg^{-1}K^{-1}$, T is mean temperature of the mass transfer process in K.

Now, it should be explained, why the correlation between the air friction and the heat and mass transfer coefficients important. That is because the R_{eto} and R_{cto} resistances created by boundary layer on the fabric surface are inverted values of heat and mass transfer coefficients α and β_c, as given in Equation (6):

$$R_{cto} = 1/\alpha \text{ and } R_{eto} = 1/\beta_p \qquad (6)$$

Thus, the fabric surface roughness, which strongly influences the air friction coefficient f, theoretically influences the R_et and R_ct levels also and in this way affects the measurement precision. For the purpose of next extension of this study (determination of evaporation resistances R_{eto} and R_{et}, mass transfer coefficient β_p [kg/m²/s] can be determined from the following experimental equation applicable for a laminar flow along a flat plate [6] instead of the Equation (6), as it is quite uneasy to measure the air friction coefficient:

$$Sh = 0{,}664 \cdot Re^{0,5} \cdot Sc^{0,33} \qquad \beta_c = Sh. D_a/d \qquad (7)$$

$$\beta_p = 0{,}664 \cdot Re^{0,5} \cdot Sc^{0,33}. D_a. d^{-1} r^{-1}.T^{-)1}$$

$$R_{eto} = 1{,}51 \, Re^{-0,5} \cdot Sc^{-0,33}. D_a^{-1} d. r.T \qquad (8)$$

The Sc dimensionless number used in the above equations characterize the boundary layer, in which mass (here water vapour) is transferred by diffusion and convection [7]. From a study [8] follows, that for conditions used in the PERMETEST tester the R_{eto} reaches approx. 6,5 m²Pa/W.

In the next part of the study, the effect of the surface roughness on the determined values of evaporation resistance of selected fabrics [8-10] will be verified experimentally.

2.3. Modified Method of Determinatıon of Fabrıics Water Vapour Resistance

In the first step of this new method, the porous layer (measuring surface) of the skin model instrument is covered by <u>one tested fabric</u> characterized by its thermal resistance R_{ct} and water vapour resistance $_{Ret}$. Then, heating power H (in Watts in standard Skin models) or cooling flow $q_{cool,f+bl}$ (W/m² in the Permetest skin model) are used for calculation of the complex "boundary layer", $R_{et} + R_{eto}$:

$$R_{et} + R_{eto} = (p_{parc, sat} - p_{parc, air}) /q_{cool 1} \qquad (9)$$

In the second step, the measuring surface of the Skin model is covered by <u>two layers of the tested fabric:</u>

$$2R_{et} + R_{eto} = (p_{parc, sat} - p_{parc, air}/q_{cool 2} \qquad (10)$$

In the third step, the instrument calculates the difference between both measurements:

$$_{et} = (p_{parc, sat} - p_{parc, air}/(q_{cool 2} - q_{cool 1})$$
$$= (2R,2_{et} + R_{eto}) - (R_{et} + R_{eto}) \qquad (11)$$

Formally, water vapour resistance and thermal resistance values, were determined according to the ISO 11092 procedure, but this time, the air flow passes along the same measuring surface (textured fabric surface), therefore, same boundary value resistance R_{eto} and R_{cto} appear in the determination of the R_{et} and R_{ct} levels. It is expected, that this procedure excludes all the boundary layer effects, thus being scientifically correct.

2.4. Tested Samples

In order to confirm the above findings, R_{et} values [m²Pa/W] of 7 various commercial woven fabrics differing in their surface structure were determined by means of the PERMETEST Skin model. The fabrics consisted of 100% cotton, 100% polyester and 100% polypropylene [8] – see the Table 1

The use of cotton in this research is given by general importance of cotton fabrics in clothing. The other used

fabric, consisting of synthetic polypropylene, exhibits low moisture sorption, which increases the measurement repeatability. The requirement of high repeatability also avoids the selection of knitted structures, as knits suffer from higher mass variation. Before testing, samples were washed at 60° C with a detergent. Their surface roughness was determined by the KES instrument – see the example of these measurements on the Figure 5. First measurements step followed the ISO 11092 Standard, the second series of measurements was based on the new 1+2 layers method. In the last series of measurements multiple layers of the polypropylene fabrics were used, in order to verify the linearity of the new method.

Table 1. Parameters of the tested woven samples

Sample code	Composition	Structure	Square mass [g/m²]	Roughness [µm]
1.1	cotton structured	waffle weave	240	5,0
1.2	cotton structured	corduroy	190	1,9
1.3	cotton smooth	plain	270	1,8
2.1	polyester smooth	plain	300	1,9
2.2	polyester structured	plain	300	3,3
3.1	polypropylene smooth	twill	230	2,0
3.2	polypropylene smooth	plain	220	2,0

Figure 3. Samples No. 1.1, 1.2 and 2.2 with surface texture with increased friction against the air flow

Figure 4 Samples No. 1.3, 2.1 and 3.1 with smooth surface with low friction against the air flow
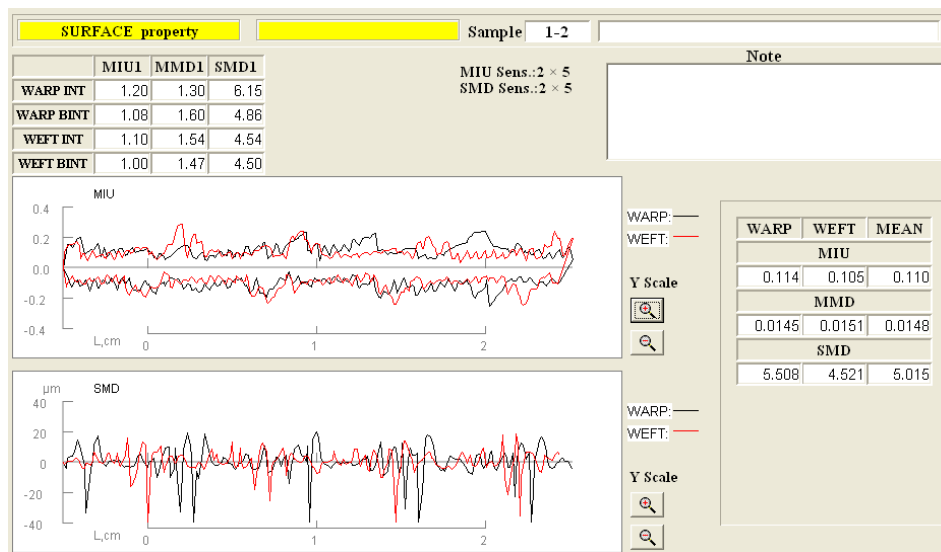

Figure 5. Diagrams of surface roughness and friction coefficients of the sample 1.1. from the KES tester
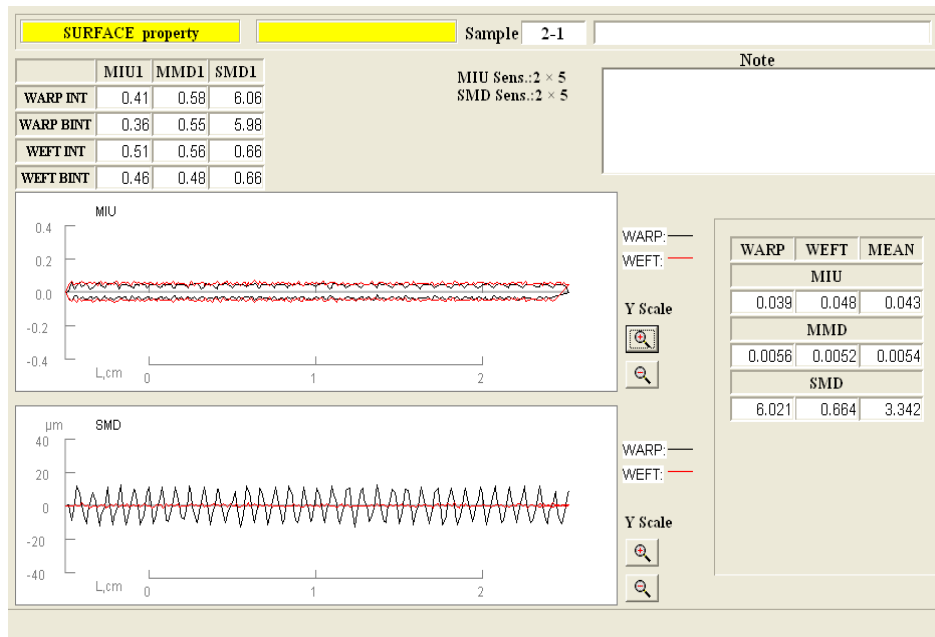
Figure 6. Diagrams of surface roughness and friction coefficients from the KES tester of the sample 2.2.
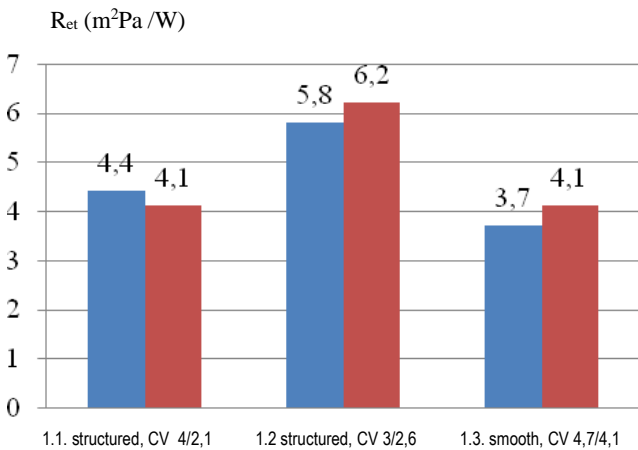
3. RESULTS AND DISCUSSION

Figure 7. R_{et} of cotton samples. Simple sample is in blue, double one is in red. CV is Variation Coef. in (%).
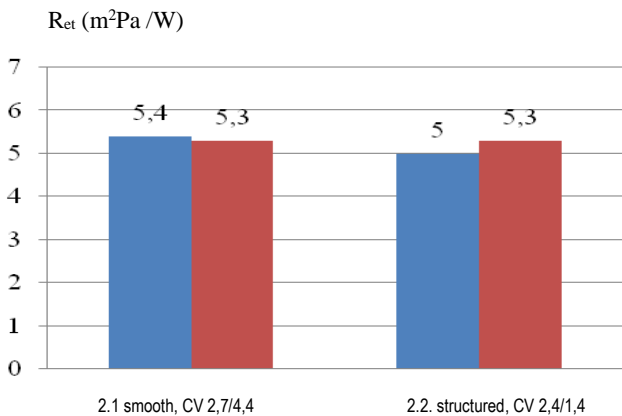
Figure 8. R_{et} of polyester samples. Simple sample is in blue, double sample is red.
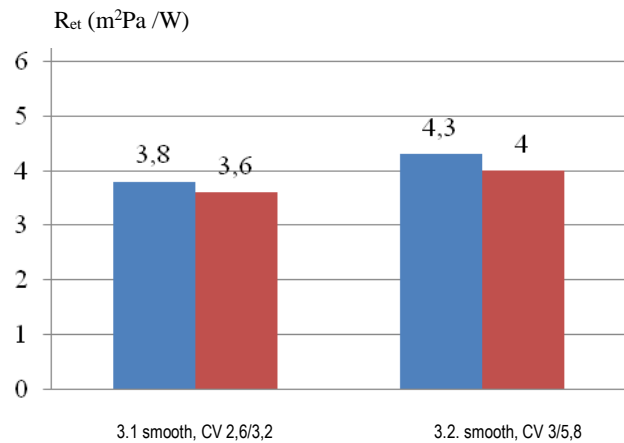
Figure 9. R_{et} of polypropylene samples. Simple sample is in blue, double sample is red.

It was found, that for smooth samples, the new 1+2 method provides lower levels (2-7%) of the evaporation resistance R_{et}, whereas for the structured samples with higher surface friction higher levels (6-10%) of R_{et} are determined. Thus, the theoretical considerations, which indicate certain imperfections of the ISO 11092 Standard, are probably correct.

The objective of the last research step is to verify, whether the linear increase of the total thickness of multilayer fabric system would cause the corresponding linear increase of evaporation resistance of the fabric system. In order to exclude the possible effect of moisture accumulated in fabrics and the effect of surface hairiness, smooth hydrophobic polypropylene fabrics were used in the testing. The use of smooth fabrics without texture would also avoid the creation of hollow places between the multilayer fabrics, which might provide additional uncontrolled thermal resistance. The results are displayed on the Figure 10.

Figure 10. R_{et} of smooth polypropylene samples No. 3.2. Simple sample is in blue, multiple sample is in red. CV was always lower then 5,0 %. The 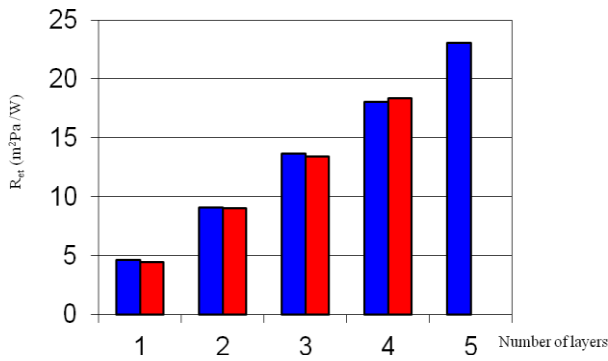linear increase of the evaporation Ret resistance with the number of layers confirms the correctness of the presented method of measurement and the linearity of the used testing instrument [10].

The results shown on the Figure 10 indicate first, that the contact resistances between the fabric layers do not reduce the measurement precision substantially – if the resistance values are linked with the line, in both cases the lines pass through the initial point x=0, y=0. More important result is, that for smooth fabrics, the differences between the classical and new method are almost negligible [8].

5. CONCLUSION

In the study, the effect of the surface roughness of selected textile fabrics tested by a Skin model on the determined water vapour resistance of these fabrics. Firstly, the fabrics were tested according to the ISO 11092 standard. In the second series of measurement, modified testing method was used, where the measuring surface of the Skin model was covered by one layer of the tested fabric and then by double layered fabric, in order to avoid the effect of the fabric surface on the determined values of fabric water vapour resistance. It was found, that when testing the structured samples by a new method, the Ret values were 6-10% higher than at the standard testing. For smooth samples, new method displayed lower Ret values (from 2% to 7%). However, from the large practical use of the ISO 11092 follows, that in most cases the possible reduction of the measurement precision does not prevent the successful application of the ISO 11092 in textile areas [11]. It can be concluded, that at fabrics with common surface roughness, the boundary layer thickness is probably higher than the surface unevenness, thus making the evaporation resistance of boundary layer practically independent on the level fabric surface roughness. However, this preliminary conclusion should be confirmed by next systematic research.

REFERENCES

1. Mukhopadhyay A, Midha VK. 2008. A review on designing the waterproof breathable fabrics part I: Fundamental principles and designing aspects of breathable fabrics. *Journal of Industrial Textiles* 37(3), 225-262.

2. Ertekin G, Marmaralı A. 2011. Heat, air and water vapor transfer properties of circular knitted spacer fabrics. *Tekstil ve Konfeksiyon* 21(4), 369–373.

3. Matusiak M. 2006. Thermal insulation properties of single and multilayer textiles. *Fibres & Textiles in Eastern Europe* 14, 5(59), 98-112.

4. Hes L, Araujo M. 2010. Simulation of the effect of air gaps between the skin and a wet fabric on resulting cooling flow. *Textile Research Journal* 80(14), 1488–1497.

5. Özdemir H. 2017. Thermal comfort properties of clothing fabrics woven with polyester/cotton blend yarns. *AUTEX Research Journal* 17(2), 135-141.

6. Özdemir H. 2017. Permeability and wicking properties of modal and lyocell woven fabrics used for clothing. *Journal of Engineered Fibers and Fabrics* 12(1), 7-21.

7. Incropera FP, DeWitt PD. 2002. *Fundamentals of heat and mass transfer.* Cornell University, Willey.

8. Hes L. 2008, May. Comments to Heat and Mass Transfer in Skin models Testers of Water Vapour Permeaility of Fabrics. In E.E. D. Adolphe (Ed.) Proceedings of Spring Fiber Society International Conference (110-112). ENSITM Mulhouse, France.

9. Rekova M. 2010. The effect of the fabric structure on its measurement of water vapour permeability according to the ISO 11092 (in Czech, unpublished BSc Thesis). Technical university of Liberec, Liberec.

10. Hes L, Baczek-Boguslawska M. 2018, November. The effect of surface rough ness on determination of water vapour resistance of fabrics tested by a skin model. In E.E. S. Msahli (Ed.) Proceedings of International conference on applied research on textile CIRAT 8 (13-14). Monastir, Tunisia.

11. Ahmad HS, Jamshaid H. 2019. Development of thermo-physiologically comfortable knit structure for sports applications. *Tekstil ve Konfeksiyon* 29(2), 105-112.

Optimization of Draft and Twist Values for Improvement of Breaking Strength and Elongation Properties of Dual-Core Yarns

Sümeyye ÜSTÜNTAĞ   0000-0002-2625-4063

Faculty of Engineering, Department of Textile Engineering, Erciyes University, 38039, Kayseri, Turkey

Corresponding Author: Sümeyye Üstüntağ, sumeyyeustuntag@erciyes.edu.tr

ABSTRACT

Dual-core yarns, which are developed to have high elasticity and strength properties at the same time in the yarn structure, have been the focus of interest in yarn sector. Considering the purpose of developing dual-core yarns, it is obvious that the breaking strength and elongation performances expected from these yarns are very important. In this paper, the twist coefficient and PET (Polyethylene terephthalate)/Elastane draft ratios of dual-core yarns were optimized by Taguchi Method for improved of breaking strength and elongation performance. The signal to noise ratio (SNR) was calculated for each output and optimum levels were determined over these ratios. As a result of the study, it was determined that PET draft was the most effective parameter for both outputs. Considering the individual optimum levels determined for each output, common factor-level combinations covering both outputs were determined. Consequently, optimal common combination for the multi-performances was found as 4.2 twist coefficient, 1.15 PET draft ratio and 3.8 elastane ratio.

1. INTRODUCTION

Elastic materials that impart stretch and recovery capability to fabrics or garments are widely used for fashionable and functional apparel products such as denim fabrics, medical textiles and sportswear [1]. Core-spun yarn spinning technology is a widely preferred method for placing elastic materials in fabric structure, especially in the denim industry. The elastic core-spun yarn which is a multicomponent textile structure, consists of elastane core (lycra®, creora® etc.) covered by natural or man-made fibers with a certain twist. The elastic core part ensures the yarn to have better stretch and recovery properties; besides, the sheath fibers improve physical and comfort properties of fabrics. In addition to the use of elastic core-spun yarn, core-spun yarns containing PET, PA, PBT and T400® filament are often preferred in order to enhance some characteristics of fabric i.e. mechanical and functional properties. Lately, dual-core yarns have been developed in order to produce fabrics having better recovering, durability and lower shrinkage as compared to the traditional single-core yarns containing only elastane in the core and cotton in the sheath. The dual core-spun yarns are composed of two core components; filament (PET, PA etc.) and elastane or semi-elastic core [2, 3]. Dual-core yarns can be manufactured on modified conventional ring spinning machine in two different methods. In the first method, previously combined two core yarns are fed simultaneously, whereas in the second method, two core yarns are fed separately into the center of sheath fiber bundle. Dual-core yarns produced with the first method are called as pre-treated dual-core yarns (PDC) while the yarns

To cite this article: Üstüntağ, S. 2021. Optimization of draft and twist values for ımprovement of breaking strength and elongation properties of dual-core yarns. Tekstil ve Konfeksiyon, 31(3), 220-227.

obtained with the second method are named as dual-core (DC) yarns.

In recent years, dual-core yarns are highly preferred for high quality fabrics and therefore, works on dual-core yarns are increasing, day by day. Aydoğdu and Yılmaz studied the effects of dual-core yarn production parameters (different sheath fiber types, yarn counts, and core filament linear densities) on some yarn and fabric properties. They found that dual-core yarns with cotton sheath fibres had significantly higher yarn unevenness, hairiness, thick places, neps, and lower tenacity and breaking elongation values, when compared to cotton/Tencel fibre and viscose sheath fibers [4]. Erbil et al. investigated the structure and properties of plain, elastane containing, and elastane + filament containing hybrid yarns, produced by using cotton as sheath fibers. They found that the elastic behaviour of dual-core yarns was higher when compared to elastane core and 100% carded cotton yarns [5]. Ute worked on influence of the weft density and weft yarn type on mechanical and dimensional properties of denim fabrics for dual-core and core-spun. At the end of the study, it was determined that growth values of the fabrics with elastic core-spun weft yarns were generally higher than the growth values the fabrics with elastic dual-core weft yarns [6]. Ertaş at al. evaluated some properties of denim fabrics produced with different weft densities by using elastane containing dual-core yarns. They found that as weft density increased, permanent elongation decreased [7]. Babaarslan at al. investigated the air permeability of denim fabrics made from dual-core spun weft yarns with different filament fineness and elastane draft, by comparing them with PET filament core-spun yarns and 100% cotton yarns. They revealed that the elastane draft ratio had a significant effect on the denim fabric air permeability whereas filament fineness had no effect on air permeability [8]. Jabbar at al. studied the effects of PET and elastane linear density on the physical and mechanical properties of dual-core cotton yarns. They revealed that yarn tenacity, elongation, uniformity, and hairiness was significantly affected by the linear densities of both the PET and elastane filaments in the core [2]. Türksoy and Yıldırım investigated the influence of some production parameters such as twist level, wool draft and elastane draft on the properties of dual-core yarns containing wool/elastane. The results indicated that the twist level was significantly effective parameter for the unevenness, hairiness, tenacity and elongation values of dual-core yarns. In addition, it was also observed that variation of elastane draft level affected tenacity and elongation values of dual-core yarns [9].

Breaking strength and elongation are among the most important and widely measured property of core-spun yarns. Yarn strength and elongation, like other yarn properties, is mainly influenced by fibre properties, yarn twist, and yarn count. Since these properties are strongly correlated with loom efficiency and usage performance, it would be very useful to estimate the optimum yarn strength and elongation, accurately. When we look at the literature in general, the effects of the production parameters of dual-core yarns on the yarn strength and elongation were examined separately. While examining the factors affecting the strength and elongation of multicomponent yarns, considering all outputs together will provide more accurate results. In this study, firstly, the optimum draft and twist values of dual-core yarns were determined separately for maximum breaking strength and elongation value. Then, common optimum factor levels were determined for both outputs. Taguchi method was used for the analysis of input factors selected and the optimization of this factors.

1.1 Taguchi Method

The full factorial design considers all possible combinations of a certain set of factors. As most of the industrial experiments normally include a considerable number of factors, a full factorial design results in a great number of experiments. Contrary to the full factorial design, Taguchi method provides the utility in terms of cost and time by reducing the number of experiments [10]. The Taguchi method is a statistical off-line quality control method that purposes to minimize product or process variation at the design phase. In Taguchi method, there are three design stages, which are system, parameter and tolerance designs. In system design, scientific and engineering knowledge is utilized to detect the basic arrangement of the process. With the parameter design, the settings that minimize the variation change in performance characteristics and adjust its mean to an ideal value are determined. Parameter design is a methodology used to determine the best tolerances for parameters, between system design and tolerance design [11].

The orthogonal array (OA) and the signal to noise ratio (SNR) are two important tools utilized in the Taguchi method [12]. Orthogonal arrays are utilized to organize the factors that influence the process and the levels where they should vary [13]. OA is a matrix of numbers arranged in rows and columns. Each row represents the level of factors in each run and each column represents a specific level for a factor that can be changed for each run [12].

The general purpose of the Taguchi design is to detect factor levels that maximize the SNR is a measure of the performance variability of processes in the presence of noise factors. In that, S stands for mean and that is called signal and also N stands for standard deviation and that is called noise [11]. The higher the S/N ratio, the better the quality; in general, the S/N ratio is classified into three modes where smaller is better, nominal is better or larger is better [10].

Nominal-the-better:

$$S/N = -10 \log \left[\frac{1}{n} \sum_{i=1}^{n} (y_i - m)^2 \right] = -10 \log \left[(\bar{y} - m)^2 + S^2 \right] \tag{1}$$

Larger-the-better

$$S/N = -10 \log \left[\frac{1}{n} \sum_{i=1}^{n} \frac{1}{y_i^2} \right] \tag{2}$$

Smaller-the-better

$$S/N = -10 \log \left[\frac{1}{n} \sum_{i=1}^{n} y_i^2 \right] = -10 \log (\bar{y}^2) \tag{3}$$

where S denotes the standard deviation; y_i the data obtained from experiments; n represents the number of experiments.

2. MATERIAL AND METHOD

2.1 Design of experiment

The selection of control factors is the most important step in the Taguchi method. By controlling these factors, the standard deviation of the process can be reduced. In this study, three factors, namely, twist coefficient, PET draft ratio and elastane draft ratio were determined as the parameters affecting breaking strength and elongation of dual-core yarns. The range of parameters was determined from the preliminary experiments. In order to examine the non-linear effect of process parameters, each parameter was examined at three levels. The identified process parameters and their levels are summarized in Table 1.

Table 1. The factors and their levels

| Levels | Factors | | |
	Twist coefficient	PET draft ratio	Elastane draft ratio
1	3.9	1.05	3.4
2	4.2	1.10	3.6
3	4.5	1.15	3.8

The selection of orthogonal matrix is the step after the determination of factors and levels. The orthogonal array allows for the gathering of the requisite data to set which factors affect product quality the most, with a minimum amount of trial, thus saving time and resources [14]. In this paper, L9 orthogonal array was chosen to determine experimental plan because it is the most suitable for the conditions being investigated; three factors with three levels. Factor levels were selected from the operable values. Minitab 16.0 software package was utilized for obtaining the orthogonal matrix given in Table 2. This matrix provides to adjust the group specification during sample production. According to orthogonal matrix, experimental layout given in Table 2 was arranged.

2.2 Preparation of test specimens

At this stage, dual-core yarns were produced depending on the experimental layout. Nine cotton-wrapped dual-core yarn samples were prepared using different twist coefficient, draft ratios of elastane and PET filaments as input variables. 100 % ABD cotton fibers were used to produce yarn samples and the cotton fibre specifications (Table 3) were measured by Uster® High Volume Instrument (HVI 1000). The cotton fibers were processed through blow room line (Trützschler Blendomat, Trützschler BOA, Trützschler AFC, Trützschler mixer, Trützschler CVT-4 and Trützschler DX), carding machine (Trützschler DK803), drawing frame (Rieter RSB D45), roving frame (Marzoli FT7D), ring frame (Marzoli MDS1) with special core filament insertion device and winding machine (Sauro) to produce dual-core yarn of linear density Ne 18.0. The schematic representation of dual-core yarn production is given in Fig. 1.

Table 2. The orthogonal matrix and the experimental layout

| Experiment no. | Factors and their levels | | | Experimental layout | | |
	A	B	C	Twist coefficient	PET draft ratio	Elastane draft ratio
1	1	1	1	3.9	1.05	3.4
2	1	2	2	3.9	1.10	3.6
3	1	3	3	3.9	1.15	3.8
4	2	1	2	4.2	1.05	3.6
5	2	2	3	4.2	1.10	3.8
6	2	3	1	4.2	1.15	3.4
7	3	1	3	4.5	1.05	3.8
8	3	2	1	4.5	1.10	3.4
9	3	3	2	4.5	1.15	3.6

Table 3. The cotton fibre specifications

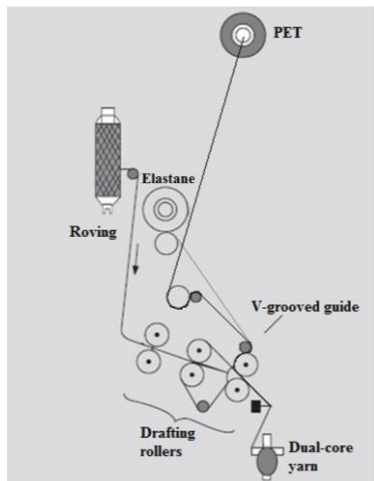| Specifications	Values
Spinning Consistency Index	112
Microner index	4.5
Maturity index	0.87
UHML- fibre length, mm	28.19
UI- Uniformity index, %	80.2
Short Fiber, %	8.2
Fibre strength, g/tex	28.5
Fibre elongation, %	5.8

Figure 1. The schematic representation of dual-core yarn

50 denier PET (36f) and 78 dtex Lycra® filaments were used as the core components for dual-core yarns. In dual-core spun yarn production, the core components of PET and Lycra filaments were fed to the nip point of the front rollers by means of V-grooved guide roller. PET and Lycra elastane core filaments were covered by cotton on conventional ring spinning machine with 760 turns/m.

2.3 Yarn Testing

All dual-core yarn samples were conditioned at 20 ± 1 ºC and 65 ± 2% relative humidity according to ISO 139 before the test. The quality specifications of the sample yarns (unevenness, hairiness, thin/thick place, Neps) were tested on Uster Tester 5 at 400 m/min test speed. Mechanical properties (breaking strength and elongation) of the yarns were measured on Uster Tensojet tester at 500 m/min in accordance with ISO 2062 standard.

2.4 Analysis Method

Test results were analyzed by the parameter design of the Taguchi method using Minitab 16 statistical software. After testing the yarns produced according to the experimental design, the following steps were used to optimize process with multiple performance characteristics: (1) analysis of the experimental results using the S/N and ANOVA analyses; (2) selection of the optimal levels of design parameters; (3) prediction of output results through the optimal design parameters; and (4) calculation of improving rate using optimum factor levels.

3. RESULTS AND DISCUSSION

Because the S/N ratio can reflect both the mean and variation of the quality characteristics, the Taguchi method uses the S/N ratio instead of the mean value to interpret experimental results [15]. In this paper, the performance statistics of the larger-the-better (Eq. 2) was used to define the optimal process conditions of dual-core yarns for both outputs. Because, the high strength and elongation at break of the yarns are known to affect the production efficiency of denim fabrics positively. The orthogonal matrix, the quality parameters and S/N ratios for breaking strength and elongation of the dual-core yarns are given in Table 4.

Taguchi method presents the response table and response graph for each output. The table and the graph show mean of S/N ratios at different levels for each factor. The factor levels corresponding to the maximum mean S/N ratio are selected as the optimum levels. In response table, the delta value is calculated by subtracting the largest value from the lowest from among the values in each column. A higher delta value amounts that the difference at the selected level for a given factor is highly pronounced. Further, rank value in the response table shows the influence degree of factors on the examined output.

Fig. 2 illustrates the main effects plot for S/N of the breaking strength output. It is seen that the optimum levels of the production parameters for breaking strength are 4.2 twist coefficient, 1.1 PET draft ratio and 3.6 elastane draft ratio (A2B2C2). In other words, the dual-core yarns produced at intermediate levels have been found to show higher breaking strength values than others. As can be seen from Table 5, the most effective input parameter is PET draft ratio (B). When the PET draft value is 1.1 from 1.05, it is seen that there is a significant increase in the strength value of the yarn. However, when the PET draft value is increased to 1.15, a slight decrease is observed in the strength value of dual-core yarns. For core-spun yarns containing elastane, it has been proven in many studies that as the core filament is getting finer, the number of sheath filaments increases and thus its contribution to strength increases [16-19]. However, PET core is generally used to prevent the bagging problem in the dual-core yarn structure as well as to increase the decreasing

Table 4. The orthogonal matrix, the quality parameters and S/N ratios of the dual-core yarns

| No.	A	B	C	CVm	IPI	H	B. Strength cN/tex	B. Strength S/N ratio, dB	B. Elongation %	B. Elongation S/N ratio, dB
1	1	1	1	13.07	229.50	7.36	13.20	22.38	9.17	19.24
2	1	2	2	13.20	207.50	7.27	15.42	23.75	12.21	21.72
3	1	3	3	13.76	261.00	7.05	14.56	23.24	14.92	23.46
4	2	1	2	13.31	215.50	7.31	14.30	23.03	11.32	20.87
5	2	2	3	13.24	183.00	7.48	14.92	23.37	12.46	21.89
6	2	3	1	13.84	288.50	7.63	15.19	23.63	15.07	23.56
7	3	1	3	13.28	226.00	6.97	13.48	22.58	9.37	19.41
8	3	2	1	13.37	225.50	7.02	15.48	23.78	11.59	21.27
9	3	3	2	13.69	250.50	7.41	15.28	23.62	14.82	23.41
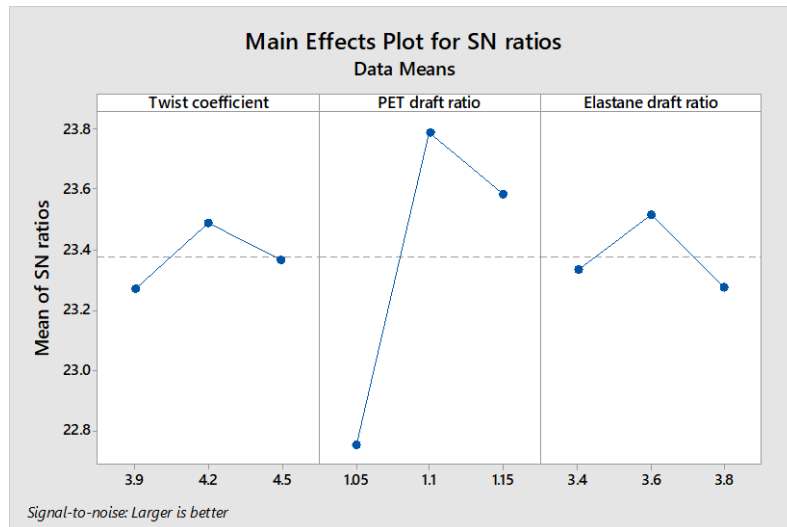
Figure 2. Main effects plot for S/N of the breaking strength output

Table 5. Response Table for the S/N ratio of the breaking strength output

Factors	Average S/N, dB			Delta	Rank
	Level 1	Level 2	Level 3		
A	23.27	23.49*	23.37	0.22	3
B	22.75	23.79*	23.59	1.04	1
C	23.34	23.52*	23.28	0.24	2

* Optimum parameter level

Table 6. ANOVA Table for S/N ratio of the breaking strength output

Factor	df	Sum of squares	Mean square	F-value	P	Percentage contribution (%)
A	2	0.07008	0.035042	9.86	0.092	3.52
B	2	1.82156	0.910779	256.23	0.004	91.44
C	2	0.09341	0.046704	13.14	0.071	4.69
Residual	2	0.00711	0.003555			0.36
Total	8	1.99216				1.00

strength with the presence of elastane in the structure. Therefore, it is clear that the sheath fibers and PET filament greatly effect of strength the dual-core yarns. Depending on the increase of draft values in the study, nonlinear strength tendency may be related to this situation. It is thought that the sheath fiber number in the cross section and the molecular chain structure of the PET filament affect the strength of produced dual-core yarns with 1.1 PET draft value at the same time.

The statistically significant input parameters are determined by conducting ANOVA test. Contribution value which is a percentage value for the process effect is calculated using the sum of squares values in the ANOVA table. The bigger this value on the output of that parameter is understood to be effective at that rate. As shown in Table 6, only the PET draft ratio is statistically effective on the breaking strength value and the contribution rate of this input parameter is calculated as 91.44%. As can be understood from this result, the breaking strength value of the dual-core yarns varies greatly with the PET draft ratio. In addition, the contribution rates of the twist coefficient and elastane draft ratio are 3.52% and 4.69%, respectively. It is estimated that the low contribution of variations of these factors to the strength is due to the presence of a durable component such as PET in the yarn structure. With this result, it can be concluded that the selected ranges for the elastane draft ratio and twist coefficient are suitable values for the breaking strength values of dual-core yarns and all these values can be used depending on the other properties expected from the yarns upon customer request. Furthermore, it is seen that the error contribution due to interaction effect is around 0.36%. This ratio is quite small and therefore, the factors can be evaluated independently.
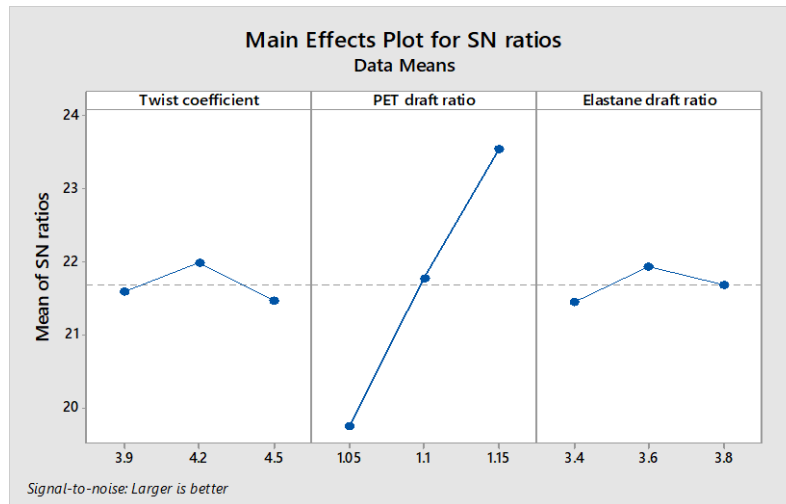
Figure 3. Main effects plot for S/N of the breaking elongation output

Table 7. Response Table for the S/N ratio of the breaking elongation output

Factors	Average S/N, dB				
	Level 1	Level 2	Level 3	Delta	Rank
A	21.59	21.98*	21.46	0.52	2
B	19.73	21.76	23.54*	3.81	1
C	21.44	21.92*	21.67	0.48	3

* Optimum parameter level

As can be seen from Figure 3 and Table 7, the optimum levels of the production parameters for breaking elongation are 4.2 twist coefficient, 1.15 PET draft ratio and 3.6 elastane draft ratio (A2B3C2). Depending on Table 7, it is seen that the most effective input parameter is PET draft ratio (B) and as the PET draft ratio increases, the breaking elongation value of dual-core yarns increases. When the core-spun containing filament is subjected to a force, the fibers of both components will be elongated as the force increases, until the fibers with smaller elongation break and so transfer the entire load to other fibers [20]. As can be understood, the proportion of sheath cotton fibers in the yarn cross-section mainly affects the elongation time and thus the breaking elongation value. Basically, with the increasing the draft ratio, PET% ratio in the yarn structure decreases, which means more number of sheath fibers. In this case, the contribution of staple fibers to strength and elongation is thought to increase [21]. However, this situation was not observed for the elastane filament draft ratio. From this result, it is understood that the presence of PET filament with higher strength than elastane in the structure makes the effect of the draft change of the

elastane filament on the strength and elongation values of the yarn insignificant.

Similar to the breaking strength results, only PET draft ratio is found statistically significant on the breaking elongation values of dual-core yarns and the contribution rate is 96.32% (Table 8). At the same time, the effect of the other two factors is very low. Furthermore, it is clear that the ANOVA test has resulted in around 1.54% of error contribution owing to interaction effect.

3.1 Optimization

The arrays corresponding to optimum factor levels determined by Taguchi method may not be available in experimental design. In such cases, the performance values corresponding to optimum factor levels can be predicted by utilizing the balanced characteristic of orthogonal arrays [22]. Since the optimum factor-level combinations obtained for both outputs in the study were not included in the experimental design, the predicted S/N ratios were calculated using Eq. 4. The predicted S/N ratios were placed in Eq. 2, and the predicted breaking strength and elongation values were achieved.

Table 8. ANOVA Table for S/N ratio of the breaking elongation output

Factor	df	Sum of squares	Mean square	F-value	P	Percentage contribution (%)
A	2	0.4462	0.2231	11.59	0.079	1.97
B	2	21.7844	10.8922	565.70	0.002	96.32
C	2	0.3476	0.1738	9.03	0.100	2.94
Residual	2	0.0385	0.0193			1.54
Total	8	22.6167				1.00

$$\eta_0 = \eta_m + \sum_{i=1}^{j} (\eta_i - \eta_m) \tag{4}$$

where, η_m is total mean of S/N ratio, j is the number of factors, and η_i are the multiple S/N ratios corresponding to optimum factor levels.

Table 9 shows the S/N ratios and results obtained according to the predicted and experimental optimal combinations. According to the experimental results given in Table 4, the highest value for the breaking strength (15.48 cN/tex) was reached with the combination of A3B2C1 and the S/N ratio of this result was calculated as 23.78 dB. As a result of the prediction made for the optimal combination obtained with TM, the value and S/N ratio of breaking strength were calculated as 15.98 and 24.04, respectively. In the experimental analysis for the breaking elongation, the highest values (15.07% and 23.56 dB) were reached with the A2B3C1 combination. However, it was predicted that 15.70% breaking elongation and 24.09 dB S/N ratio would be reached, with the combination suggested by TM. As can be seen, it is seen that there is a slightly increase in output results with the combinations obtained as a result of optimization.

The improvement rates to be seen with the predicted optimum combinations determined by TM for both outputs were calculated by Equation 5. The improvement rate is calculated from the "d" value obtained by subtracting the predicted S/N ratio of the predicted optimum combination (S/N_0) from the S/N ratio of the experimental optimum combination (S/N_i) (Table 9). Through the equation given below [23], the breaking strength of dual-core yarns under predicted optimum conditions was found to be increased

1.06 times according to the experimental optimum combination. It was also observed the breaking elongation increased 1.13 times.

$$d = \frac{S}{N_i} - \frac{S}{N_o} = -10 \log L_i - (-10(\log L_o))$$

$$\frac{L_o}{L_i} = 10^{\frac{d}{10}} \tag{5}$$

For dual-core yarns, both breaking strength and elongation properties are expected to be at ideal levels. It becomes very important to combine these effects in order to get an idea over the total optimization by making a sensible comparison of each output. First, the optimum levels for each output were determined separately. Taking into account the levels of all outputs, the combination of optimum levels was determined (Table 10). Here, coefficients a, b and c symbolize the importance level of each factor and indicate the first, the second and the third effective parameter, respectively.

Table 10 shows the common optimum twist coefficient and draft ratio values for both outputs. For PET draft ratio, the alteration of S/N ratio depending on the level ranges were examined on separate graphs for each output. 3rd level (1.15) of PET draft ratio was selected for combination since a greater alteration was observed with the optimum level determined for the breaking elongation, compared to breaking strength. Consequently, the levels determined according to the combination of all outputs were found to be the same as the optimum levels determined for breaking elongation of dual-core yarns.

Table 9. Experimental and predicted optimal S/N ratios and results

	Experimental Optimal Combinations		Predicted Optimal Combinations	
	B. Strength	B. Elongation	B. Strength	B. Elongation
Optimal Level	A3B2C1	A2B3C1	A2B2C2	A2B3C2
Results	15.48	15.07	15.98	15.70
S/N ratio	23.78	23.56	24.04	24.09

Table 10. The combination of optimum levels for all outputs

		Factors		
		A	B	C
Breaking strength	Optimum Level	2[c]	2[a]	2[b]
	Optimum Value	4.2	1.1	3.8
Breaking elongation	Optimum Level	2[b]	3[a]	2[c]
	Optimum Value	4.2	1.15	3.8
Combination	Optimum Level	2	3	2
	Optimum Value	4.2	1.15	3.8

[a] The first effective parameter, [b] The second effective parameter, [c] The third effective parameter

4. CONCLUSION

In this paper, the twist coefficient and the draft ratios of the PET and Elastane components of dual-core yarns were optimized by Taguchi Method for improvement of their breaking elongation and strength performances. Among the factors examined for both outputs, it was determined that only PET draft ratio had a statistically significant effect. For both outputs, the optimum S/N ratios were achieved with the median level of elastane draft ratio and twist coefficient. However, different optimum PET draft ratio levels were obtained for each output. While reaching the optimum S/N ratio with median PET draft ratio level for breaking strength, it was observed that the breaking elongation increased with the increase of PET draft ratio value. It was observed that the difference between the S/N ratios of the breaking elongation of the dual-core yarns produced with the 2nd level (1.1) and 3rd level (1.15) PET draft values was bigger compared to the breaking strength. As a result, it was decided that the common optimum levels

for both outputs were 4.2 twist coefficient, 1.15 PET draft ratio and 3.8 elastane draft ratio.

The predicted maximum breaking strength and elongation values that can be reached with the optimum levels determined by TM were calculated based on the experimental results. Based on these predicted values, the expected improvement rates in both outputs were calculated thanks to the determined optimum levels. It was concluded that with the factor-level combinations determined and not included in the experimental design in the study, the breaking strength would increase 1.06 times and the breaking elongation would increase 1.13 times compared to the experimental optimum combination.

REFERENCES

1. Hua T, Wong NS, Tang WM. 2018. Study on properties of elastic core-spun yarns containing a mix of spandex and PET/PTT bi-component filament as core. *Textile Research Journal* 88(9) 1065-1076.

2. Jabbar A, Tariq U, Hussain T, Basit A, Hai A, Zubair M. 2020. Effect of polyester and elastane linear density on the physical and mechanical properties of dual-core-spun cotton yarns. *Journal of Natural Fibers* 17 (4), 463-471.

3. Babaarslan O, Sarioğlu E, Çelik Hİ, Avci ME. 2018. Denim fabrics woven with dual core-spun yarns. *Engineered Fabrics*. Licensee IntechOpen, 19-39.

4. Aydoğdu SH, Yılmaz D. 2020. Effect of yarn fineness and core/sheath fibre types on the physical properties of dual-core yarns and fabrics. *Cellulose Chemistry and Technology* 54(3-4), 381-394.

5. Erbil Y, Islam R, Babaarslan O, Sırlıbaş S. 2020. Effect of structural changes on the cotton composite yarn properties *Journal of Natural Fibers*, doi: 10.1080/15440478.2020.1788687© 2020 Taylor & Francis.

6. Ute TB. 2019. Analysis of mechanical and dimensional properties of the denim fabrics produced with double-core and core-spun weft yarns with different weft densities. *The Journal of The Textile Institute* 110(2), 179-185.

7. Ertaş O G, Ünal BZ, Çelik N. 2016. Analyzing the effect of the elastane-containing dual-core weft yarn density on the denim fabric performance properties. *The Journal of The Text Institute* 107(1), 116-126.

8. Babaarslan O, Sarioğlu E, Kaynak HK, Avcı ME. 2018, June. Air permeability analysis of denim fabrics from dual-core spun yarns. 18thAUTEX World Textile Conference (20-22), İstanbul, Turkey.

9. Turksoy HG, Yildirim N. 2018. Effect of process variables on the properties of dual-core yarns containing wool/elastane. *Industria Textila* 69(5), 352-356.

10. Fazeli F, Tavanai H, Hamadani AZ. 2012. Application of Taguchi and full factorial experimental design to model the color yield of cotton fabric dyed with six selected direct dyes. *Journal of Engineered Fibers and Fabrics* 7(3), 34-42.

11. Zeydan M. 2007. Modelling the woven fabric strength using artificial neural network and Taguchi methodologies. *Inter Journal of Clothing Science and Technology* 20(2), 104-118.

12. Khosla A, Kumar S, Aggarwal KK. 2006. Identification of strategy parameters for particle swarm optimizer through Taguchi method. *J Zhejuchi Univ Science A* 7(12), 1989-1994.

13. Khanlou HM, Ang BC, Talebian S, Afifi AM, Andriyana A. 2015. Electrospinning of polymethyl methacrylate nanofibers: optimization of processing parameters using the Taguchi design of experiments. *Textile Research Journal* 85(4), 356-368.

14. Khan KR, Hossain MM, Sarker RC. 2015. Statistical analyses and predicting the properties of cotton/waste blended open-end rotor yarn using Taguchi OA design. *International Journal of Textile Science* 4(2), 27-35.

15. Gaitonde VN, Karnik SR, Davim JP. 2008. Taguchi multiple-performance characteristics optimization in drilling of medium density fibreboard (MDF) to minimize delamination using utility concept. *Journal of Materials Processing Technology* 196, 73-78.

16. Dhuib AB, El-Ghezal S, Cheikhrouhou M. 2006. A study of the impact of elastane ratio on mechanical properties of cotton wrapped elastane-core spun yarns. *The Journal of the Textile Institute* 97(2), 167-172.

17. Örtlek HG, Ülkü Ş. 2007. Effects of spandex and yarn counts on the properties of elastic core-spun yarns produced on Murata vortex spinner. *Textile Research Journal* 77(6), 432-436.

18. Das A, Chakraborty R. 2013. Studies on elastane-cotton core-spun stretch yarns and fabrics: Part I-Yarn characteristics. *Indian Journal of Fibre &Textile Research* 38, 237-243.

19. Aydoğdu SH, Yılmaz D. 2019. Analyzing some of the dual-core yarn spinning parameters on yarn and various fabric properties. *Tekstil ve Konfeksiyon* 29(3), 197-207.

20. Baykal PD, Babaarslan O, Erol R. 2006. Prediction of strength and elongation properties of cotton/polyester-blended OE rotor yarns. *Fibres & Textiles in Eastern Europe* 14, 1 (55), 18-21.

21. Qadir MB, Hussain T, Malik M, Ahmad F, Jeong SH. 2014. Effect of elastane linear density and draft ratio on the physical and mechanical properties of core-spun cotton yarns. *The Journal of The Textile Institute* 105 (7), 753-759.

22. Çopur M, Özmetin C, Özmetin & Kocakerim MM. 2004. Optimization study of the leaching of roasted zinc sulphide concentrate with sulphuric acid solutions. *Chemical Engineering and Processing: Process Intensification* 43(8), 1007-1014.

23. Park CK, Ha JY. 2005. A process for optimizing sewing conditions to minimize seam pucker using the Taguchi Method. *Textile Research Journal* 75(3), 245-252.

Design of an Impact Absorbing Composite Panel from Denim Wastes and Acrylated Epoxidized Soybean Oil based Epoxy Resins

Janset OZTEMUR ⬛ 0000-0002-7727-9172
Hande SEZGIN ⬛ 0000-0002-2671-2175
Ipek YALÇIN-ENIS ⬛ 0000-0002-7215-3546

Istanbul Technical University / Textile Technologies and Design Faculty/Textile Engineering Department/Istanbul, Turkey

Corresponding Author: Janset Oztemur, oztemurj@itu.edu.tr

ABSTRACT

The focus of this work is to make a significant contribution to solid waste management by designing impact-absorbing bio-composite panels using bio-resin and denim wastes. In this context, composite panels are produced by vacuum infusion technique using both epoxy and acrylated epoxidized soybean oil (AESO) based hybrid resins while denim wastes are utilized as reinforcement materials in fiber and fabric forms. Both physical (fiber density and fiber weight ratio) and mechanical analyses (drop-weight impact resistance and dynamic mechanical analysis (DMA)) of the composites are performed. The outcomes of the study prove that the increase in the AESO ratio of the resin system improves the ductility of the composite and consequently the impact resistance. On the other hand, dynamic mechanical analysis results indicate that the AESO plug-in reduces the storage module and increases the damping factor.

1. INTRODUCTION

The textile industry is a significant threat to the environment, especially due to the processing of raw materials, fabric preparation and finishing processes, as well as post-consumer waste, and it accounts for 5% of the world's pollutants [1]. It is estimated that the waste volume, which was only 92 million tons of global fashion waste in 2015, will increase to 148 million tons in 2030. In addition, a much larger amount is encountered when upholstery, bedding, mattresses, packaging, rugs and carpets and automotive interiors are added to this volume [2]. However, it is a fact that only 15% of the textile wastes is recycled and the rest is buried in landfills [3-4]. This situation encourages the search for alternative products that can turn this risky waste group into an advantage as a raw material, and bio-composites have an important share at this point.

Bio-composites generally consist of petroleum-based matrix and natural reinforcement materials [5]. Bio-composites containing natural fibers have become increasingly important considering the difficulties in plastic disposal and the overuse of petroleum resources [6]. The use of recycled natural fiber reinforcement takes this issue one step further. For instance, denim fabrics are particularly harmful to the environment in both pre-consumer and post-consumer stages, and unfortunately, most of the denim waste cannot be recycled. For this reason, non-recyclable denims, which have strong and stiff structure, can be used in composite constructions to minimize environmental impact [7-8]. There are many other bio-composite studies of petroleum-based matrix reinforced with different recycled natural fibers in the literature [9-11].

On the other hand, when petroleum-based polymers are used with natural reinforcement in a composite structure,

this composite cannot be said to be completely "bio" since the resins have serious environmental impacts besides their benefits such as availability and low cost [12-13]. Thus, considering the sustainability and environmental concerns, matrix materials as well as reinforcement materials used during composite production becomes crucial. This leads to the emergence of the term "green composites". Green composites can be defined as composite structures in which both the reinforcement and matrix materials are obtained from renewable resources [14].

Although petroleum-based epoxy resin is widely preferred in composite materials due to its low cost, ease of use and high mechanical properties, uncertainties about petroleum resources, prices and environmental effects necessitate reducing the use of epoxy and replacing it with biomaterials [15]. The most common bio-resins used in green composites are vegetable oils such as soybean oil, castor oil, palm oil, linseed oil, and sunflower oil [16]. Among them, acrylated epoxized soybean oil (AESO) which is produced by the epoxidation and acrylization of soybean oil, is commercially available choice and it has benefits such as non-volatile and non-toxic structure. However due to its high viscosity at room temperature and low crosslinking capacity, it is mostly used in hybrid resin systems [17-18].

In the literature, many studies are conducted with composite production including AESO resin and natural fiber reinforcements. In a study conducted by Temmink et al. (2018), it was seen that composites reinforced with four-plied denim fabric, containing bio-epoxy and AESO have very acceptable tensile strength (approximately 50 MPa for bio-epoxy and 20 MPa for AESO) and impact resistance (approximately 25 kJ/m^2 for bio-epoxy and 30 kJ/m^2 for AESO) values in comparison to polyester resin systems that serve alternatives for application areas such as automotive interior parts, furniture, interior construction, and leisure equipment [19]. In a similar way, a research on hybrid bio-based composites developed by vacuum infusion technique with reinforcement of woven jute fabric and AESO/epoxy blended matrix was implemented by Ozkur et al (2020). Results indicated that the ascending AESO ratio increased

the impact resistance of the material, but when the AESO ratio was more than 30 wt. %, the tensile strength of the material decreased, thus 30-50 wt. % AESO was stated as optimum hybridization ratio with epoxy [5]. The enhanced plasticity with the addition of AESO to the epoxy resin reinforced with natural fiber composites are also studied by Bakar et al [15] and Kocaman and Ahmetli [20].

On the other hand, it is not possible to see studies on recycled natural based textile wastes with AESO in the literature. In this context, in this study, bio-composite structures with improved impact resistance are produced by reinforcing epoxy resin and AESO with waste denim structures in both fabric and fiber web form. Eight different designs are produced via vacuum infusion method by changing the resin type and/or reinforcement form (fiber/fabric). The drop-weight impact resistance and thermo-mechanical properties of the composite samples are evaluated.

2. MATERIAL AND METHOD

2.1 Materials

Waste denim fabrics utilized in this study are supplied from Calik Denim (Table 1) and used as reinforcement materials in either fabric or fiber web form. Epoxy (F-1564, FIBERMAK) and AESO (Sigma Aldrich) are used as matrix materials while a hardener (F-3486, FIBERMAK) is added to the resin system to initiate the curing process. The properties of the matrix components are listed in Table 2.

2.2 Method

Preparation of reinforcement materials

The waste denim fabrics are shredded two times by rag pulling machine (Balkan Makina, Turkey) for the preparation of fiber webs, and then transferred to the carding machine to obtain smooth surfaces at homogeneous web density. These fiber webs are used either alone or in combination with fabric forms to form sandwich structures. The preparation steps of the reinforcement materials are seen in Figure 1.

Table 1. Physical properties of denim fabric

Warp yarn type / yarn count	ring spun / Ne 9
Weft yarn type / yarn count	core spun / Ne 10
Fiber type	98% cotton 2% elastane
Weave type	3/1 Twill (Z)
Areal density (g/m^2)	289.5 ± 6.36
Count of cloth (ends/cm*picks/cm)	32*20

Table 2. The properties of matrix components

	Epoxy	AESO	Hardener
Viscosity (25°C) (cps)	1200-1400	18000-32000	10-20
Density (25°C) (g/cm³)	1.15	1.40	1.00

Figure 1. Preparation steps of reinforcement materials

Composite Panel Production

The composites are produced by the vacuum infusion technique (Figure 2). With this method, the resin is distributed homogeneously to reinforcement material and the excess resin in the composite is vacuumed [21].

Eight different composite samples are produced by varying reinforcement forms and resin systems. Also, the layers of the panels are created by keeping the weights constant. In structures consisting of different layers, the fabric and the fiber layer have the same weight. The details of the composite designs with sample codes are listed in Table 3.

For physical and mechanical analysis, test samples are cut by CNC milling machine according to the related standards.

Physical Analysis

Average thicknesses, densities and fiber weight ratios of composite samples are calculated based on the measured weights and dimensions, also results are given with standard deviations (SD).

Mechanical Analysis

Drop-weight Impact Resistance

The drop-weight impact resistance analysis is performed via an impact tester (Besmak) with 16 mm diameter striker according to the ASTM D7136 standard. 59*88mm cut composite samples are subjected to 12 Joule impact energy with a standard hemispherical head. Maximum load, absorbed energy and maximum displacement are measured for five samples from each sample group and average results are given with standard deviations.
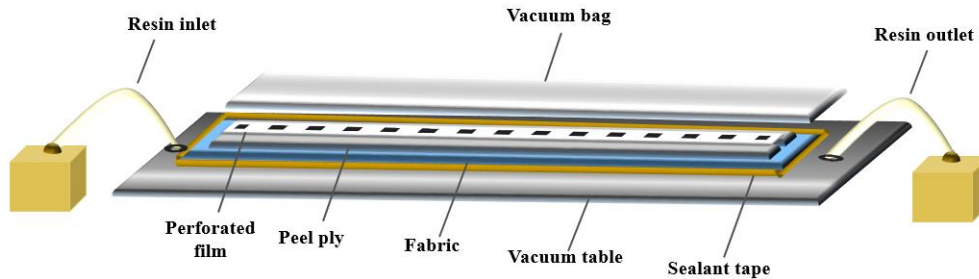

Figure 2. Vacuum infusion set-up.

Table 3. Composite designs

Sample Codes	Reinforcement Type	Resin Weight Ratio (Epoxy:AESO)	Hardener Weight Ratio (%)
DD-30	Two layers of denim fabric	(70:30)	33
DDD-30	Three layers of denim fabric	(70:30)	33
DFD-30	Fiber web between two layers of denim fabric	(70:30)	33
FFF-30	Three layers of fiber web	(70:30)	33
DD-0	Two layers of denim fabric	(100:0)	33
DDD-0	Three layers of denim fabric	(100:0)	33
DFD-0	Fiber web between two layers of denim fabric	(100:0)	33
FFF-0	Three layers of fiber web	(100:0)	33

Dynamic Mechanical Analysis

Dynamic mechanical analysis (DMA) is performed on a DMA testing apparatus (Mettler Toledo, SDTA861) in three-point bending mode by using rectangular samples (10*50mm) in conformity with ASTM D7028 test standard. Experiments are carried out in the temperature range of 20 °C to 100 °C with heating rate of 3°C/min with a constant frequency of 10 Hz.

3. RESULTS AND DISCUSSION

3.1 Physical Analysis

The average thicknesses, densities and fiber weight ratios are listed in Table 4.

It is observed that the average densities of composites containing different resin systems are very similar to each other, and the differences are observed between samples produced with different reinforcement forms such as fabric or fiber webs. For example, DD and DDD samples have almost the same densities with similar fiber weight ratios. Despite the increase in the number of fabric layers, similar values between DD and DDD show that the resins display a homogeneous distribution throughout the fabric and the amount of absorbed resin increases at the same rate due to the increasing number of layers, thus the sample thickness. This can be explained by the advantages of the vacuum infusion technique, which allows production under constant pressure [22].

On the other hand, regardless of resin type, the samples containing fiber web layers (DFD and FFF) have higher densities (1.02-1.03 and 0.95-0.96 g/cm^3, respectively) with lower fiber weight ratios (32-35 and 32%, respectively). This can be clarified by the higher resin absorption due to the loose nature of the fibrous layers compared to denim fabrics, thus allowing the higher amount of resin trapped. In tight structures compared to loose ones, the matrix is more constrained and this leads to various mechanical behavior differences [23]. FFF samples in both resin groups are the thickest samples manufactured under same pressure due to its fluffy fibrous content that results in higher resin absorption levels.

3.2 Drop-weight Resistance

The reinforcement material is very effective in defining the final impact properties of composites [24-27]. For this reason, as can be seen in Table 5, as the layers of reinforcement material in the composite structure change, the impact resistance values of the structure differ. DDD has higher maximum load, absorbed energy, and maximum displacement values than DD as a result of the addition of one more fabric layer. Studies in the literature also support that the increment in the number of fabric layers used as reinforcement material increases the impact resistance [28]. In particular, the impact energies absorbed by DDD samples are more than twice of the impact energies absorbed by DD samples.

Table 4. Average thicknesses, densities and fiber weight ratios of the composites

Sample Codes	Avg. Thickness ± SD (mm)	Avg. Density ± SD (g/cm³)	Avg. Fiber Weight Ratio ± SD
DD-30	1.89±0.05	0.92±0.03	0.45±0.01
DDD-30	2.73±0.22	0.91±0.07	0.47±0.00
DFD-30	2.22±0.12	1.03±0.02	0.32±0.01
FFF-30	3.52±0.19	0.95±0.09	0.35±0.01
DD-0	1.85±0.41	0.98±0.18	0.45±0.02
DDD-0	2.79±0.21	0.97±0.26	0.44±0.07
DFD-0	3.49±0.24	1.02±1.02	0.32±0.02
FFF-0	3.79±0.52	0.96±0.08	0.32±0.03

Table 5. Drop-weight impact resistance test results

Sample Codes	Max Load ± SD (kN)	Absorbed Energy ± SD (J)	Max Displacement ± SD (mm)
DD-30	0.84±0.06	3.48±0.33	10.10±0.02
DDD-30	1.35±0.10	8.77±0.52	13.40±0.17
DFD-30	1.67±0.05	9.03±0.46	9.88±0.44
FFF-30	1.43±0.11	7.36±0.67	9.42±0.92
DD-0	0.83±0.04	3.50±0.13	11.10±0.17
DDD-0	1.22±0.09	7.31±0.39	13.40±0.52
DFD-0	2.15±0.14	7.95±0.60	7.41±0.65
FFF-0	1.63±0.18	5.20±0.61	6.11±0.55

When the FFF and DFD samples that have similar fiber weight ratios are compared with each other, it is seen that the values of maximum load, absorbed energy and maximum displacement are higher for DFD. It is believed that the use of fabric in both the lower and upper layers creates a layer resistant to the falling object, while the fibrous layer acts as an impact-absorbing layer. In sandwich-type composite structures, the core layer provides time and space for high energy absorption when it exposed to an impact loading [29]. In addition, sandwich structures with stiff surface layers and less rigid core structure exhibit improved properties under mechanical loads [30]. When DDD and DFD samples are compared, it can be said that increased impact resistance is obtained by using a fibrous layer in the middle instead of the fabric layer. This can be explained by the high contribution of the fibrous surface in the middle layer to the absorption of impact energy, as explained above.

Comparing resin systems with each other; by adding 30% AESO to the epoxy resin, it has been observed that the absorbed impact energy and maximum displacement are improved in almost all samples. Also, the damage patterns on the composite panels can be seen in Figure 3. As can be seen from the images, while very sharp fractures occur in epoxy-based composites, the fractures in samples with AESO added are much softer. In addition, the fact that AESO additive increases the impact resistance is a situation supported by the literature [5].

On the other hand, the maximum load values of the FFF-30 and DFD-30 samples for the AESO resin system (1.43 and 1.67 kN, respectively) are lower than the same sample groups for pure epoxy resin systems (for FFF-0 and DFD-0; 1.63 and 2.15 kN, respectively). The fiber weight ratios of these samples are relatively lower than that of DDD and DD samples, which means there is more resin in the composite structure. While epoxy resin is preferred for its superior tensile properties in composites, AESO resin is used due to its toughness [31]. For this reason, the increase in the AESO ratio in the increasing resin amount is expected to cause a decrease in the maximum load value.

3.3 Dynamic Mechanical Analysis

Storage Modulus

The storage modulus is an indicator of how much energy the material absorbs and its viscoelastic rigidity [21]. In all sample groups, the storage modulus curves decreases with increasing temperature as seen in Figure 4. At low temperatures, the molecules of the materials are more stable and have a tighter arrangement. However, when the temperature increases from the glassy state to the rubbery state, the mobility of the material improves and its ductile properties increases [32-33]. Figure 4 also shows that AESO-doped structures store less energy in their glassy state compared to epoxy matrix composites and pass through to the rubbery state at relatively lower temperatures due to the lower glass transition temperature (T_g) of AESO resin compared to that of epoxy resin.
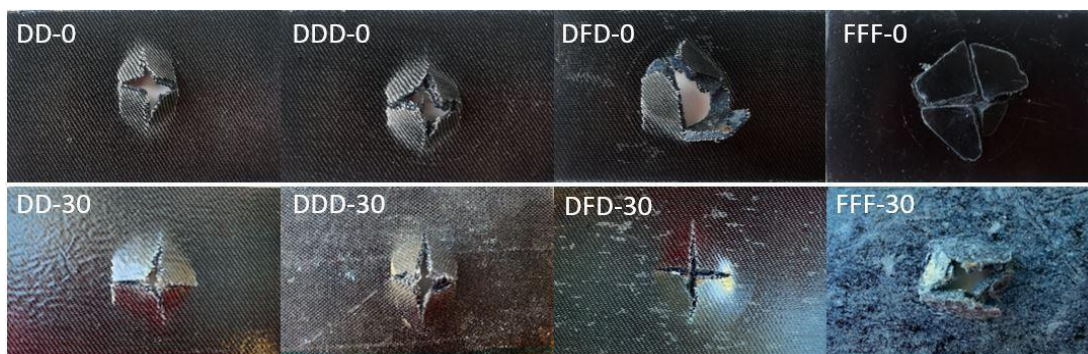

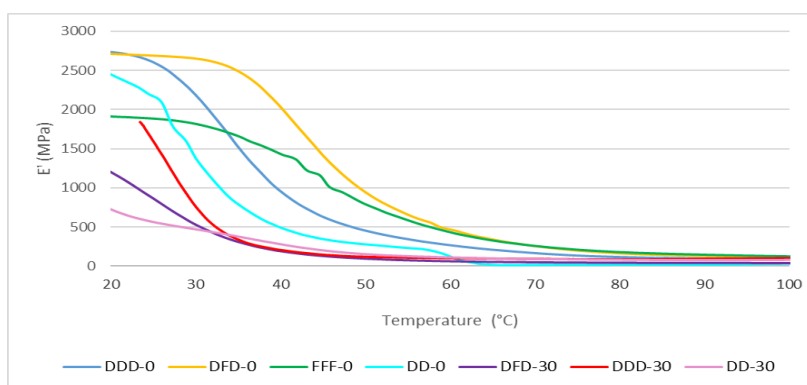**Figure 3.** Damage patterns resulting from drop-weight impact test.

Figure 4. Storage modulus curves of the samples

Dynamic-mechanical measurements of the FFF-30 composite structure could not be performed due to the dimensional limits (up to 5mm in sample thickness is allowed) of the device. Fully fiber reinforced epoxy matrix composite structure (FFF-0) is found to have a lower storage modulus compared to DDD-0 and DFD-0, and this is consistent with drop-weight impact resistance test results. The reason for this behavior, which causes the lower modulus of FFF-0, is the less stiff structure of the fibers in the composite panel and the weaker interaction between the reinforcement and the matrix. Increased interaction between reinforcement and resin decreases the mobility of molecular chains at the interface, improving the composite's rigidity and storage modulus [31]. On the other hand, when examining fabric composite structures with both AESO and epoxy matrix, it is seen that two-layer panels (DD-0 and DD-30) have less storage module compared to three-layer panels.

Damping Factor (Tan delta)

Tan delta represents the damping characteristic of the structures with viscous or elastic phases and is affected by the matrix-reinforcement interface interaction [34]. Low damping value indicates that reinforcement and matrix materials in composite structures adhere well to each other, while materials with high tan delta value tend to dissipate more energy [32]. In composite panels with epoxy matrix, it is observed that the adhesiveness between matrix and reinforcement is better with the lower level of the tan delta peak (Figure 5). On the other hand, this value varies depending on both the type of resin and its ratio in the composite structure. The damping factor peaks point out to the T_g value of the material. After this temperature, the immobility of the structure decreases and the panel begins to turn into a rubbery form. While the T_g values of epoxy based composites are around 45°C, it is seen that the T_g values of AESO/epoxy based composites are around 30°C. Considering that the T_g value of AESO resin is around -20°C [35], the decrease in T_g obtained with the addition of AESO is an expected result. The outcomes of the study conducted by Niedermann (2014) also support that the addition of soybean oil resin to aromatic epoxy resins result in a decreased T_g value [36].

As seen in Figure 5, the T_g value decreases with the addition of AESO to the structure. However, these structures had wider peaks, indicating a mixture of heterogeneous structures providing a wider temperature range to initiate viscous chain motions [31].

4. CONCLUSION

It is thought that this study, which is carried out using waste denim fabrics and bio-resins, will contribute to the solid waste management by serving a greener alternative to traditional composite industry. In the scope of the study, by using different combinations of matrix and reinforcement materials; physical, mechanical and thermo-mechanical properties of the composite samples are investigated. The main results obtained remark that the panels with fiber reinforcement in their structure (FFF-0, FFF-30, DFD-0, and DFD-30) have higher densities with lower fiber weight ratios due to the loose nature of the fibrous structures that allows more resin absorption. In addition, the composites produced with an epoxy:AESO hybrid resin system have higher ductility due to the content of bio-resin and consequently the impact resistance of the composite material increases. On the other hand, regardless of the resin type, the drop-weight impact test results show that three-layer fabric (DDD) and fabric/fiber (DFD) reinforced panels absorb more energy than remaining samples. From the point of dynamic mechanical analysis, the effect of the matrix material is clearly observed. Due to the nature of AESO, the T_g value in AESO doped composites is quite lower compared to the other samples. It is also found that DDD-0 and DFD-0 panels with epoxy matrices have the highest storage moduli and relatively low tan delta values.
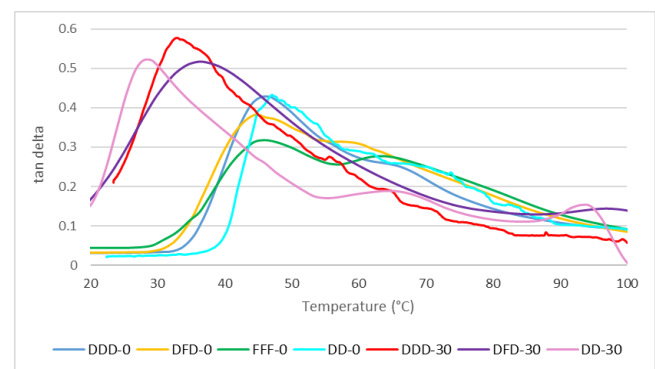

Figure 5. Tan delta curves of the samples

When the results obtained are evaluated holistically, especially AESO-doped fiber/fabric sandwich structured (DFD-30) samples can be used as shock absorbing panels in various end use areas such as construction and automotive, thanks to their improved impact resistance properties. In addition, it can make a significant contribution to solid waste management thanks to the utilization of denim wastes and its bio-resin content.

Acknowledgement

REFERENCES

1. Stanescu MD. 2021. State of the art of post-consumer textile waste upcycling to reach the zero waste milestone. *Environmental Science and Pollution Research* 28, 14253–14270.

2. Echeverria CA, Handoko W, Pahlevani F, Sahajwalla V. 2019. Cascading use of textile waste for the advancement of fibre reinforced composites for building applications. *Journal of Cleaner Production* 208, 1524–1536.

3. Shirvanimoghaddam K, Motamed B, Ramakrishna S, Naebe M. 2020. Death by waste: Fashion and textile circular economy case. *Science of the Total Environment* 718, 137317.

4. Wang Y. 2010. Fiber and textile waste utilization. *Waste and Biomass Valorization 1*(1), 135–143.

5. Ozkur S, Sezgin H, Akay E, Yalcin-Enis I. 2020. Hybrid bio-based composites from blends of epoxy and soybean oil resins reinforced with jute woven fabrics. *Materials Research Express* 7(1), 15335.

6. Gnaba I, Omrani F, Wang P, Soulat D, Ferreira M, Vroman P, Jaouachi B. 2019. Mechanical behavior of flax/polypropylene commingled nonwoven at dry scale: Influence of process parameters. *Textile Research Journal* 89(5), 791–800.

7. Haque MS, Sharif A. 2017. Processing and characterization of waste denim fiber reinforced polymer composites. *International Journal of Innovative Science and Modern Engineering*, 2(4), 24–28.

8. Uncu Akı S, Candan C, Uygun Nergis B, Onder N. 2020. Understanding denim recycling: a quantitative study with methodology. In Korlu A (Ed.) *Waste in Textile and Leather Sectors*. United Kingdom: Intechopen, 1-26.

9. Baccouch W, Ghith A, Yalcin-Enis I, Sezgin H, Miled W, Legrand X, Faten F. 2020. Investigation of the mechanical, thermal, and acoustical behaviors of cotton, polyester, and cotton/polyester nonwoven wastes reinforced epoxy composites. *Journal of Industrial Textiles*. Advance online publication. [https://doi.org/10.1177/1528083720901864]

10. Islam M, Sharif A, Hussain M, Hassan I. 2019. Synergic effect of recycled cotton fabric and wood saw dust reinforced biodegradable polypropylene composites. *Bangladesh Journal of Scientific and Industrial Research* 54(1), 21–30.

11. Wei B, Xu F, Azhar SW, Li W, Lou L, Liu W, Qiu Y. 2015. Fabrication and property of discarded denim fabric/polypropylene composites. *Journal of Industrial Textiles*, 44(5), 798–812.

12. Narewska J, Lassila L, Fardim P. 2014. Preparation and characterization of new mouldable cellulose-AESO biocomposites. *Cellulose* 21(3), 1769–1780.

13. Åkesson D, Skrifvars M, Walkenström P. 2009. Preparation of thermoset composites from natural fibres and acrylate modified soybean oil resins. *Journal of Applied Polymer Science* 114(4), 2502–2508.

14. Pecas P, Carvalho H, Salman H, Leite M. 2018. Natural fibre composites and their applications: a review. *Journal of Composites Science* 2(4), 66.

15. Abu Bakar MB, Masri MN, Amini MMH, Thirmizir MMZ, Salim MS. 2018, November. Mechanical, thermal and morphological properties of epoxy resin toughened with epoxidized soybean oil. In Abdullah MMA, Bin Abd. Rahim SZ, Bin Mat Saad MN, Bin Ghazli MF, Ahmad R, Bin Mohd Tahir MF and Binti Jamaludin L. (Eds.), *AIP Conference Proceedings*, (020277). Ho Chi Minh, Vietnam.

16. Grishchuk S. Karger-Kocsis J. 2011. Hybrid thermosets from vinyl ester resin and acrylated epoxidized soybean oil (AESO). *Express Polymer Letters* 5(1), 2-11.

17. Wu Y, Li K. 2017. Replacement of styrene with acrylated epoxidized soybean oil in an unsaturated polyester resin from propylene glycol and maleic anhydride. *Journal of Applied Polymer Science* 134(28), 450456.

18. Liu W, Fei M, Qiu R. 2017, August. Biocomposites from hemp fibers and acrylated epoxidized soybean oil-based resins. *21st International Conference on Composite Materials*, Xi'an, China.

19. Temmink R, Baghaei B, Skrifvars M. 2018. Development of biocomposites from denim waste and thermoset bio-resins for structural applications. *Composites Part A: Applied Science and Manufacturing* 106, 59–69.

20. Kocaman S, Ahmetli G. 2016. Eco-friendly natural filler based epoxy composites. *World Academy of Science, Engineering and Technology International Journal of Chemical, Molecular, Nuclear, Materials and Metallurgical Engineering* 10(4), 471-474.

21. Sezgin H, Mishra R, Militky J, Berkalp OB. 2020. Mechanical, thermo-mechanical and thermal characteristics of multi-walled carbon nanotubes-added textile-reinforced composites. *Journal of Industrial Textiles* 50(5), 692–715.

22. Baccouch W, Ghith A, Yalcin-Enis I, Sezgin H, Miled W, Legrand X, Faten F. 2020. Enhancement of fiber-matrix interface of recycled cotton fibers reinforced epoxy composite for improved mechanical properties. *Materials Research Express* 7(1), 15340.

23. Liang Y, Wang H, Gu X. 2013. In-plane shear response of unidirectional fiber reinforced and fabric reinforced carbon/epoxy composites. *Polymer Testing* 32(3), 594–601.

24. Arpitha GR, Sanjay MR, Senthamaraikannan P, Barile C, Yogesha B. 2017. Hybridization effect of sisal/glass/epoxy/filler based woven fabric reinforced composites. *Experimental Techniques* 41(6), 577–584.

25. Awais H, Nawab Y, Anjang A, Md Akil H, Zainol Abidin MS. 2020. Effect of fabric architecture on the shear and impact properties of natural fibre reinforced composites. *Composites Part B: Engineering* 195, 108069.

26. Ramesh M, Palanikumar K, Reddy KH. 2013. Mechanical property evaluation of sisal-jute-glass fiber reinforced polyester composites. *Composites Part B: Engineering* 48, 1–9.

27. Selver E, Dalfi H, Yousaf Z. 2020. Investigation of the impact and post-impact behaviour of glass and glass/natural fibre hybrid composites made with various stacking sequences: Experimental and theoretical analysis. *Journal of Industrial Textiles*. Advance online publication. [https://doi.org/10.1177/1528083719900670]

28. Shyr TW, Pan YH. 2003. Impact resistance and damage characteristic of composite laminates. *Composite Structures* 62(2), 193-203.

29. Lampeas G. 2020. Cellular and Sandwich Materials. In Pantelakis S and Tserpes K. (Eds) *Revolutionizing Aircraft Materials and Processes*. Cham: Springer, 137-162.

30. Skrifvars M, Dhakal H, Zhang Z, Gentilcore J, Åkesson D. 2019. Study on the mechanical properties of unsaturated polyester sandwich biocomposites composed of uniaxial warp-knitted and non-woven viscose fabrics. *Composites Part A: Applied Science and Manufacturing* 121, 196–206.

31. Sahoo SK, Mohanty S, Nayak SK. 2017. Mechanical, thermal, and interfacial characterization of randomly oriented short sisal fibers reinforced epoxy composite modified with epoxidized soybean oil. *Journal of Natural Fibers* 14(3), 357–367.

32. Jabbar A, Militký J, Wiener J, Karahan M. 2016. Static and dynamic mechanical properties of novel treated jute/green epoxy composites. *Textile Research Journal* 86(9), 960–974.

33. Liu W, Chen T, Fei M, Qiu R, Yu D, Fu T, Qiu J. 2019. Properties of natural fiber-reinforced biobased thermoset biocomposites: Effects of fiber type and resin composition. *Composites Part B: Engineering* 171, 87–95.

34. Shao B, Fang Y, Chen B, Shen J, Xu S, Ou R, Wang Q. 2020. Statistical distribution of mechanical properties and energy absorption of laminated cotton fabric reinforced epoxy composites. *Polymer Composites* 41(7), 2829–2840.

35. Fu L, Yang L, Dai C, Zhao C, Ma L. 2010. Thermal and mechanical properties of acrylated epoxidized-soybean oil-based thermosets. *Journal of Applied Polymer Science* 117(4), 2220-2225.

36. Niedermann P, Szebenyi G, Toldy A. 2014. Effect of epoxidized soybean oil on curing, rheological, mechanical and thermal properties of aromatic and aliphatic epoxy resins. *Journal of Polymers and the Environment* 22(4), 525-536.